

Aus der Klinik und Poliklinik für Augenheilkunde der Universität Rostock

Direktor: Professor Dr. med. R. F. Guthoff

Corneal Imaging By Spectral Domain Optical Coherence Tomography

Inauguraldissertation

zur

Erlangung des akademischen Grades

Doktor der Medizin

der Medizinischen Fakultät

der Universität Rostock

vorgelegt von

Riyam Al-kadhi

geb. Aden, Jemen

Rostock, February 2013

Dekan: Prof. Emil C. Reisinger

1. Gutachter: Prof. Dr. med. R.F. Guthoff
2. Gutachter: Prof. Dr. med. H-W. Pau
3. Gutachter: Prof. Dr. Alexander Heisterkamp

Tag der Einreichung: 26.2.2013

Tag der Verteidigung: 25.9.2013

بسم الله الرحمن الرحيم

وقل ربي زدني علما

صدق الله العظيم

Dedication

This thesis is dedicated to:

My parents, who were a great source of motivational support, unending help and precious treasure to make me live a better life all throughout with continuous encouragement.

My husband for his great patience and generous spirit throughout the PhD study.

My dear sister, who shared my troubles and hardship giving me continuous love during all the years of my PhD.

1 TABLE OF CONTENT

| | | |
|---------|--|----|
| 1 | Table of Content | 5 |
| 2 | Introduction..... | 7 |
| 3 | Anatomy of the cornea..... | 8 |
| 4 | Materials and Methods..... | 16 |
| 4.1 | Subjects..... | 16 |
| 4.1.1 | Healthy Cornea | 16 |
| 4.1.2 | Corneal pathologies..... | 16 |
| 4.2 | Devices..... | 17 |
| 4.2.1 | Spectral domain optical coherence tomography | 17 |
| 4.2.2 | Rotating Scheimpflug camera..... | 19 |
| 4.2.3 | AC Master..... | 20 |
| 4.2.4 | Corneal parameters determined by spectral domain optical coherence tomography, Scheimpflug camera and AC Master | 21 |
| 4.3 | Statistics | 21 |
| 5 | Results..... | 23 |
| 5.1 | Healthy cornea | 23 |
| 5.1.1 | SD-OCT of healthy cornea | 23 |
| 5.1.2 | Corneal layers thickness analysis by SD-OCT | 23 |
| 5.1.3 | Relationship between thickness of different corneal layers and age measured by SD-OCT | 24 |
| 5.1.3.1 | The epithelium | 24 |
| 5.1.3.2 | The Bowman’s membrane | 26 |
| 5.1.3.3 | The stroma | 28 |
| 5.1.4 | Analysis of Central corneal thickness by devices | 30 |
| 5.1.5 | Correlation in CCT measurement between SD-OCT, Scheimpflug and AC Master..... | 31 |
| 5.1.6 | Agreement in CCT measurements between SD-OCT, Scheimpflug and AC Master..... | 31 |
| 5.1.7 | Analysis of the Relationship between the CCT and gender..... | 33 |
| 5.1.8 | Analysis of the relationship between CCT and both eye | 34 |
| 5.1.9 | Analysis of the relationship between the CCT and age | 35 |
| 5.2 | Corneal pathologies | 38 |
| 5.2.1 | Epithelial diseases | 39 |
| 5.2.1.1 | Corneal degeneration unclar dignity | 39 |
| 5.2.1.2 | Perforated corneal ulcer | 40 |
| 5.2.1.3 | Recurrent epithelial erosions..... | 42 |

| | | |
|---------|--|----|
| 5.2.1.4 | Epithelial edema caused by acute angle closure glaucoma..... | 43 |
| 5.2.1.5 | Dry eye syndrome | 44 |
| 5.2.1.6 | Soft contact lens | 45 |
| 5.2.1.7 | Hard contact lens..... | 46 |
| 5.2.2 | Stromal diseases | 47 |
| 5.2.2.1 | Keratitis associated with contact lens wear..... | 47 |
| 5.2.2.2 | Fungal keratitis..... | 48 |
| 5.2.2.3 | Stromal keratitis | 49 |
| 5.2.2.4 | Corneal foreign body | 50 |
| 5.2.2.5 | Corneal scar | 51 |
| 5.2.2.6 | Granular corneal dystrophy..... | 52 |
| 5.2.2.7 | Keratoconus | 53 |
| 5.2.3 | Endothelial diseases | 54 |
| 5.2.3.1 | Keratitis, Endothelitis..... | 54 |
| 5.2.3.2 | Descemet’s membrane detachment..... | 55 |
| 5.2.3.3 | Fuchs’ endothelial dystrophy | 56 |
| 5.2.3.4 | Assessment of wound profile after penetrating keratoplasty (PKP) | 57 |
| 5.2.3.5 | Bullous keratopathy | 58 |
| 6 | Discussion | 59 |
| 6.1 | Healthy cornea | 59 |
| 6.2 | Corneal pathologies | 66 |
| 7 | Conclusion | 74 |
| 8 | Theses | 76 |
| 9 | References..... | 79 |
| 10 | Captions for Figures and Tables | 89 |
| 10.1 | Figure | 89 |
| 10.2 | Table | 91 |
| 10.3 | List of Abbreviations | 92 |
| 11 | Curriculum vitae | 94 |
| 12 | Declaration..... | 95 |
| 13 | Acknowledgments..... | 96 |

2 INTRODUCTION

Cross-sectional imaging techniques are not commonly used for the diagnosis of corneal abnormalities. Ultrasonic biomicroscopy is used as a diagnostic tool for the anterior segment of the eye and laser confocal microscopy can provide higher resolution images that delineate corneal cellular structures *in vivo*.¹ Ultrasonic biomicroscopy requires an immersion technique while laser confocal microscopy requires direct contact to the cornea. It exhibits limited practicality in patients with corneal epithelial problems, infectious disorders, and postoperative patients whereby the non contact method becomes more advantageous.¹

Recent advances in optics and laser technology enabled the development of a novel optical imaging modality optical coherence tomography (OCT), which is a non invasive and non contact technique that provides high-resolution cross-sectional images of weakly absorbing and scattering objects.² Currently, this technique is used mainly for the evaluation of the macular and optic disc diseases.³ Izatt *et al* (1994) first reported the application of OCT to normal human corneas in volunteers.⁴ Hoerauf *et al* used a slit-lamp–adapted OCT to study normal corneas and a cornea that had undergone phototherapeutic keratectomy or laser thermokeratoplasty.⁵ Based on their reports, one of the principal advantages of OCT is its use *in vivo* microscopic cross-sectional imaging system providing precise measurements of ocular structures.^{4,5} The main disadvantage of conventional time domain OCT (TD-OCT) is the requirement of a long acquisition time, which causes a decrease in image quality.⁶ With the recent advances of technology, a new variant of OCT has been developed, the spectral domain OCT (SD-OCT), which is characterized by the provision of tomograms of outstanding quality based on their high sensitivity and short acquisition time.⁷

The aim of the study:

1. To measure the central corneal thickness (CCT) and the thickness of the different corneal layers by spectral domain optical coherence tomography (SD-OCT) in 100 healthy Eyes.
2. To compare the accuracy of SD-OCT with the established measurement methods (Scheimpflug camera and AC Master).
3. To describe the application of the high-resolution SD-OCT to cross-sectional imaging of different corneal pathologies.

3 ANATOMY OF THE CORNEA

Macroscopic anatomy

The cornea is a clear transparent tissue that joins the opaque sclera at the corneoscleral limbus.⁸ The anterior corneal surface is covered by tear film while the posterior corneal surface is bathed directly by the aqueous humor.⁸ Externally, the cornea appears elliptical with its vertical diameter of about 11.7 mm shorter than the horizontal diameter of about 12.6 mm, being flatter in the periphery and steeper centrally.⁹ It is approximately 0.5 mm thick at the center with a gradual increase towards the periphery having 0.7 mm thickness.⁹ The refractive power of the cornea is 40-44 diopters and constitutes about two-thirds of the refractive power of the eye.⁸ The optical properties of the cornea are determined by its transparency, surface smoothness, contour, and refractive index. The corneal transparency is mostly attributable to the arrangement of the collagen fibers in the stroma.⁹

Microscopic anatomy

The cornea can be divided into five layers: (1) epithelium, (2) Bowman's membrane layer, (3) stroma, (4) Descemet's membrane, and (5) endothelium (Fig.1).⁹ The cell types that constitute the cornea include epithelial cells, keratocytes, and endothelial cells. Epithelial cells are derived from the epithelial ectoderm, whereas keratocytes and endothelial cells are of neural crest origin.⁹ The cornea is suffused anteriorly by the tear film and posteriorly by the aqueous humor.⁸

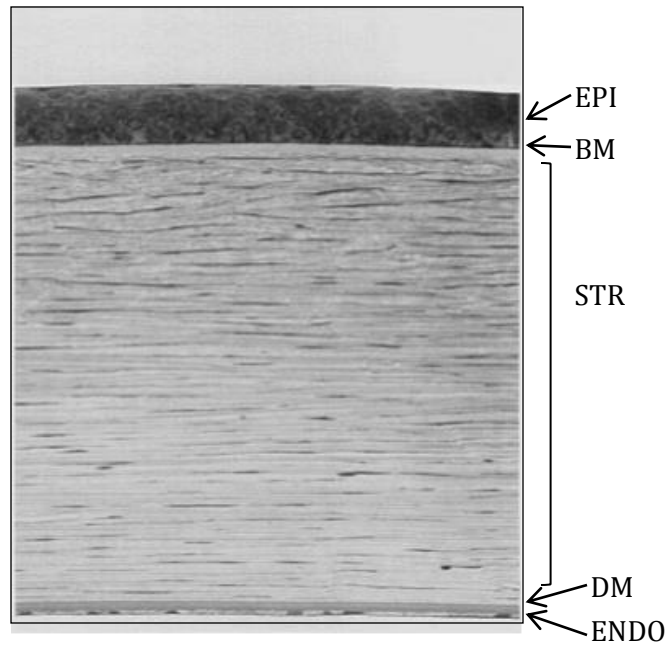


Fig. 1: Light micrograph of a human cornea showing the corneal layers: epithelium (EPI), Bowman's membrane layer (BM), stroma (STR), Descemet's membrane (DM), and the endothelial cell layer (ENDO).¹⁰

(1) Epithelium

The epithelium is composed of nonkeratinized, stratified squamous epithelium which represents 10 % of the corneal thickness. The epithelium is divided morphologically into three layers: the superficial or squamous cell layer, the middle or wing cell layer, and the deep or basal cell layer (Fig. 2).^{11, 12}

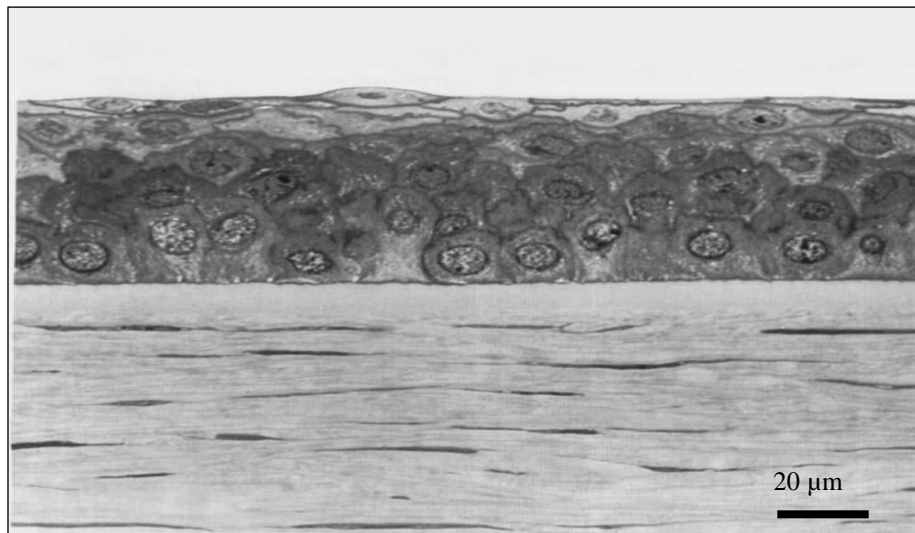


Fig. 2: Light microscopy of the central corneal epithelium shows the maturation of the basal cells forming wing and superficial cells.¹⁰

The basal cells are the only epithelial cells that undergo mitosis. The daughter cells thus formed push interiorly and change their shape, conforming to the contiguous wing cells. As the cells continue to move interiorly, they become the superficial cells, after which they disintegrate and are shed into the tear film in a process known as desquamation. Complete turnover of corneal epithelial cells occurs in about 7-10 days.¹³ Corneal epithelium acts as a barrier to external biological and chemical insults. The presence of junctional complexes between adjacent corneal epithelial cells prevents passage of chemical substances into the deeper corneal layers. Defects in the corneal epithelium allow the penetration of tear fluid into the stroma, resulting in stromal oedema that interferes with the light transmission through the cornea. Rapid renewal and formation of intercellular junctions between corneal epithelial cells also help to protect the cornea from microbial attack. Both cell-cell and cell-matrix interactions are important for maintenance of the normal stratified structure and physiological functions of the corneal epithelium. Tight junctions are present mostly between cells of the superficial cell layers which together with the interdigitation of cell membranes provide a highly effective barrier to prevent the tear fluid penetration and its chemical constituents. Adherent's junctions and desmosomes are present in all corneal epithelial layers, whereas gap junctions, that allow the passage of small molecules between cells, are present in the wing cells and basal cells of the epithelium (Fig. 3).¹⁴

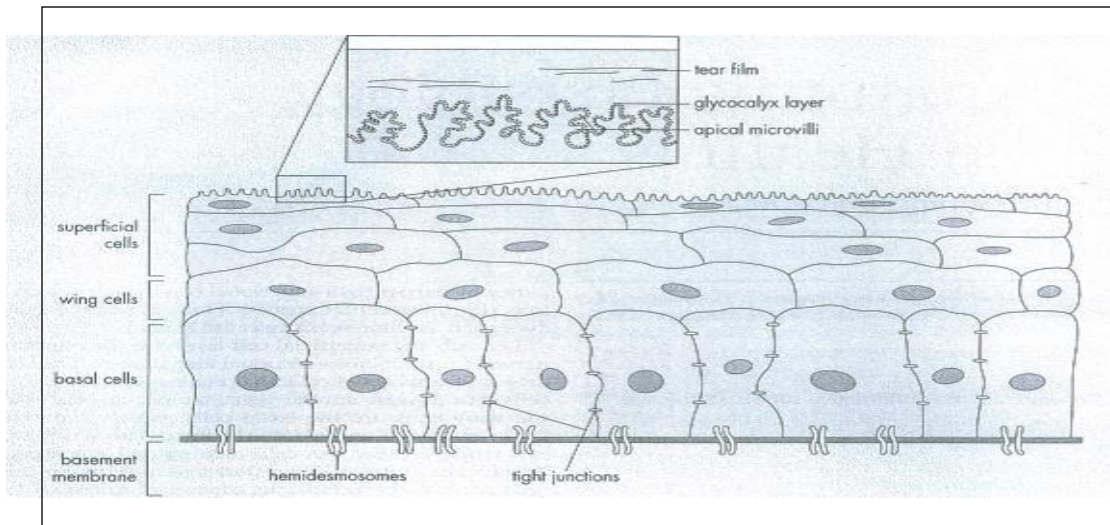


Fig. 3: Schematic representation of the localization of tight junctions and hemidesmosomes.⁹

The basement membrane is an extracellular secretory product of the basal epithelial cells produced not only during embryonic development but also throughout adult life though with a

slow rate of secretion. It is 40- 60 nm thick. Transmission electron microscopy reveals that the basement membrane is composed of an anterior clear zone, (lamina lucida), and a more obvious posterior dense zone, (lamina densa) (Fig.4).¹⁵

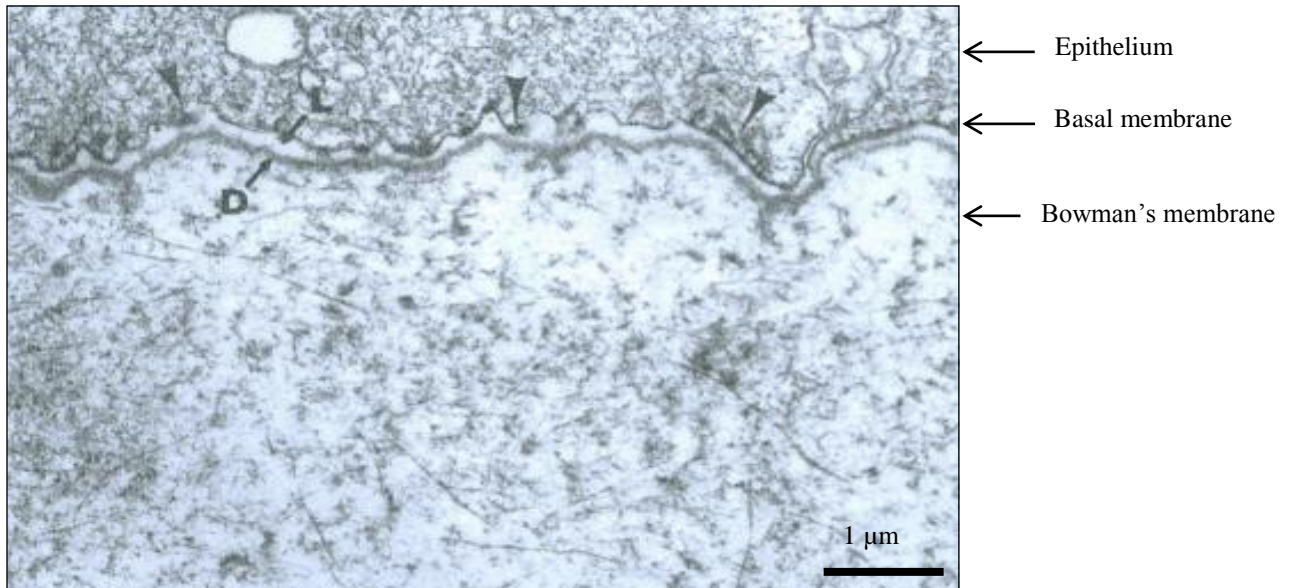


Fig. 4: Electron microscopic graph illustrates the two layers of basement membrane (L) lamina lucidam (D) lamina densa.⁹

The absence of the basement membrane can result in the ingrowth of epithelial cells into Bowman's layer or the anterior stroma.²³ The basement membrane provides a matrix on which cells can migrate and is thought to be important for maintenance of the stratified and well-organized corneal epithelium. It thus appears to play a prominent role in epithelial wound healing.^{15, 16}

(2) Bowman's membrane

A cellular membrane-like zone known as Bowman's membrane (BM), is 12 μm thick. It is not membrane but rather a random arrangement of collagen fibers.¹⁷ Bowman's layer is considered to be the anterior portion of the corneal stroma. It can not be stripped away from stroma as a continuous sheet as the descemet's membrane can.²⁵ The anterior surface of this layer, which faces the basement membrane, is smooth.¹⁶ Bowman's layer does not regenerate after injury and is attached to the stroma by collagen fibrils that insert into Bowman's layer becoming part of the anterior stromal lamellae (Fig. 5).¹⁷

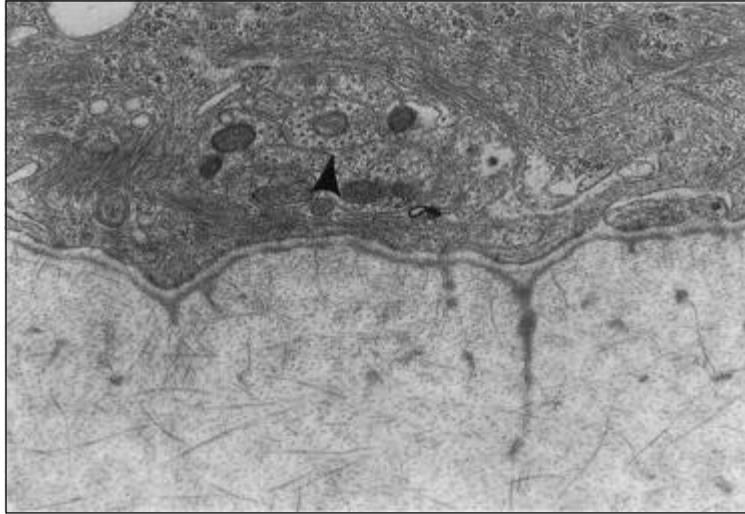


Fig. 5: Electron micrograph illustrate the fibrillar network which formed of type I collagen fibers of the Bowman's membrane. X 30000.¹⁰

(3) Stroma

The stroma constitutes the largest portion, more than 90%, of the cornea. Corneal characteristics including its physical strength, stability of shape, and transparency, are largely attributable to the anatomic and biochemical properties of the stroma.¹⁸ The uniform arrangement of collagen fibers in the stroma is essential for corneal transparency.¹⁸ The layered arrangement is more regular in the posterior stroma than in the anterior stroma, where the lamellae are narrow and interleaved (Fig. 6).¹⁹ The collagen fibrils packed in parallel arrays from 300 to 500 lamellae of the stroma.^{20, 21} They are surrounded by a polyanionic extracellular matrix, which may be important in maintaining the fairly constant separation distance of 60 nm between the fibril centres.²² Keratocytes in the normal cornea usually lie between collagen lamellae and their function is to maintain the collagen fibrils and extracellular matrix by a constant synthetic activity (Fig. 7).²³

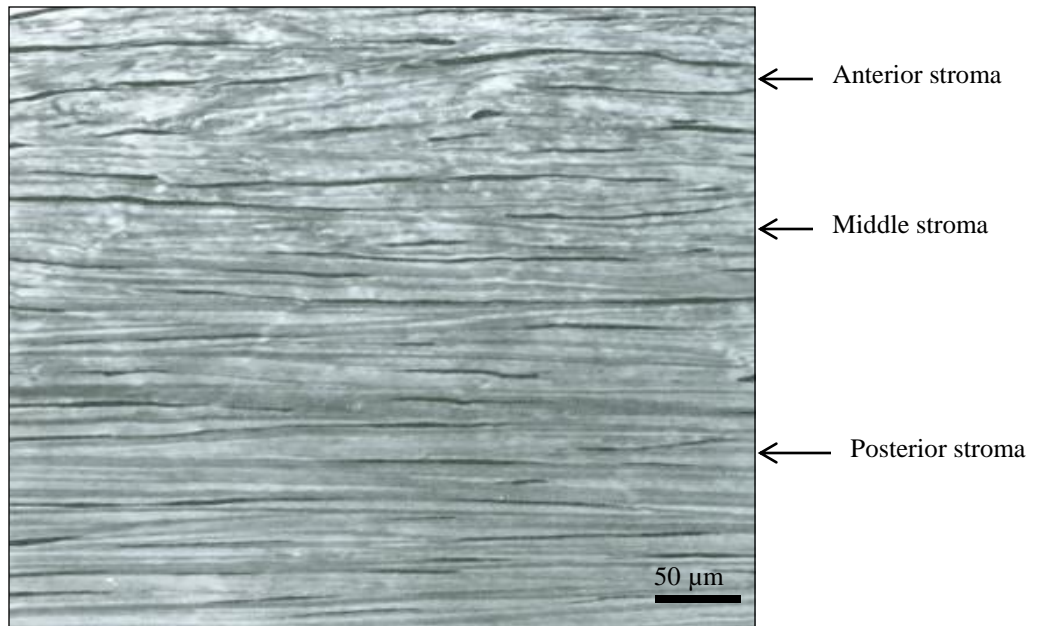


Fig. 6: Light micrograph illustrates the organization of the stromal lamellae. Interiorly, the lamellae are interleaved, in the middle and posterior third of the stroma the lamellae are more compact. ¹⁰

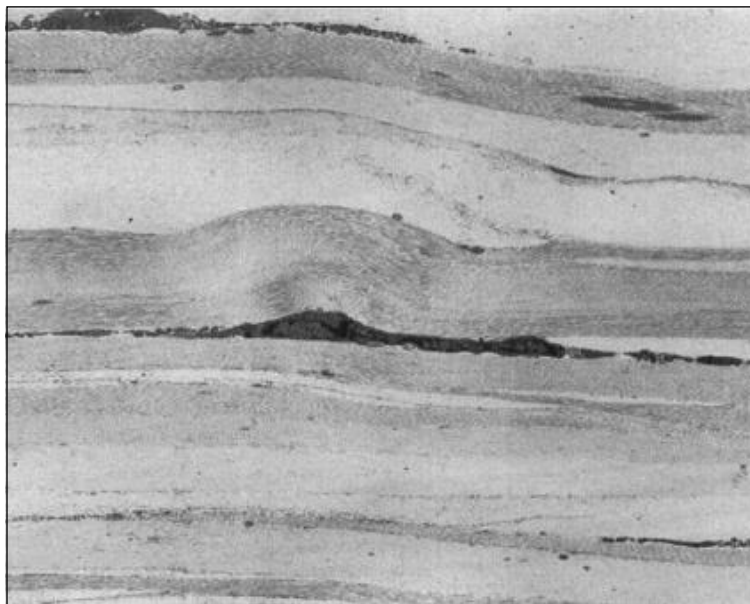


Fig. 7: Electron micrograph illustrate The keratocytes, the fibroblasts of the cornea situated between the collagen lamella. X 4200. ¹⁰

(4) Descemet's membrane

Descemet's membrane is the basement membrane of the corneal endothelium. It is composed of anterior banded portion and posterior non banded portion (Fig.8).²⁴ It increases in thickness during life, but this accumulation appears to be limited to the non banded posterior layer.²⁵

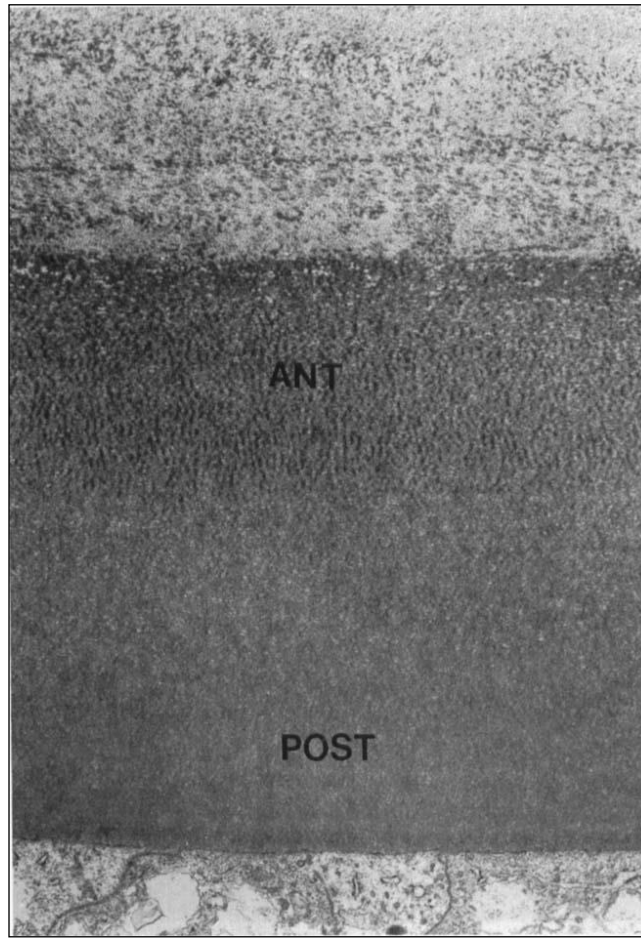


Fig. 8: Electron micrograph illustrates Descemet's membrane which consists of an anterior banded portion (ANT) and a posterior non banded portion (POST).¹⁰ X 9500

Descemet's membrane adheres loosely to the posterior surface of the corneal stroma and reflects any change in the stromal shape. If the corneal stroma swells, the folding of Descemet's membrane can be observed clinically.²⁵ It does not regenerate; however, if endothelial cells migrate over the denuded stroma at the site of a tear, the membrane covers the ruptured area and stromal edema subsides.²⁵

(5) Endothelium

The corneal endothelium forms a single layer of approximately 400,000 cells, 4-6 μm thick, and 20 μm wide which are predominantly hexagonal in shape. (Fig.9). Endothelial cells do not regenerate in any significant fashion in adult.¹⁰

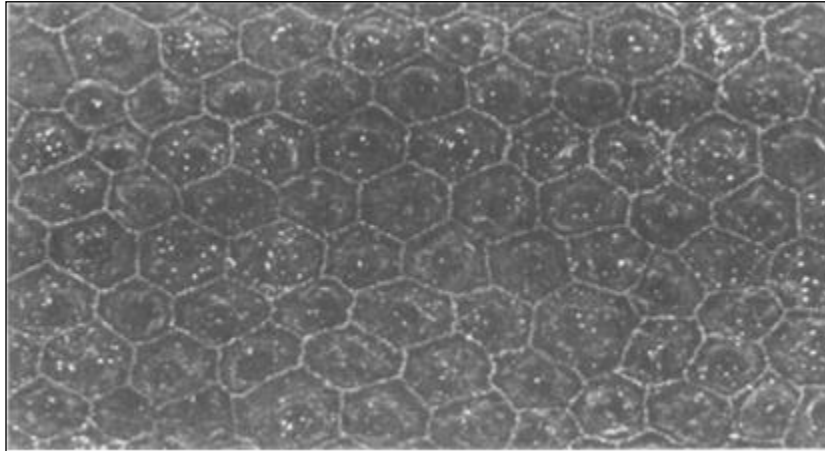


Fig. 9: Electron micrograph illustrates the close hexagonal packing of the endothelial cell layer in a normal individual. X 1200¹⁰

The endothelial cells contain various junctional complexes, including zonula occludens, macula occludens, and macula adherents, but not desmosomes. In addition, gap junctions allow the transfer of small molecules and electrolytes between the endothelial cells.²⁶

Similarly to the central nervous tissue, the cells of the human corneal endothelium are essentially amitotic after birth. However, corneal endothelial cells have a remarkable ability to enlarge and maintain normal function in the face of cellular inadequacies or deficiencies during normal cell loss in the aging process, and after cell loss caused by intraocular surgery and trauma.¹⁷ Endothelial cell density is highest at birth, up to 7500 cells/ mm^2 . Despite a rapid decline during the first year of life; it reaches average values of 2700 cells/ mm^2 in adults. When cell density decreases below the level of 300-500 cells/ mm^2 due to pathological conditions corneal decompensation is likely to occur.²⁷ Corneal endothelial cells do not proliferate in humans, when these cells are subjected to stress particularly when some cells are lost, the remaining cells may lose their regular hexagonal shape and become irregular in shape (pleomorphism) and size (polymegethism). These changes usually occur with age, after trauma, and in long-term contact lens wearers.²⁸

4 MATERIALS AND METHODS

4.1 SUBJECTS

4.1.1 HEALTHY CORNEA

A total number of 100 eyes (50 right eyes and 50 left eyes) from 50 healthy volunteers (20 males and 30 females) were enrolled in this study with inclusion criteria of having no history of ocular disease such as glaucoma or retinal disease. Contact lens wear or ocular surgery including refractive surgery and refractive errors less than or equal to 6.0 D were included as normal. The age of the healthy subjects ranged from 23-83 years with a mean age \pm SD of 53.1 ± 18.6 years. A complete ophthalmological examination was performed including visual acuity, intraocular pressure measurements and anterior and posterior segment evaluation. Central corneal thickness (CCT) of both eyes of every subject was measured by spectral domain optical coherence tomography (CCT-OCT) (Spectralis; Heidelberg Engineering, Germany), a rotating Scheimpflug camera (CCT-SCH) (Pentacam; Oculus, Wetzlar, Germany) and finally AC Master (CCT-ACM) (Zeiss Meditec, Germany). For each subject 5 and each device consecutive measurements were obtained by one examiner on a single occasion were averaged and treated as a single number. Neither topical application of anesthetics nor speculum insertion was used for the examination.

4.1.2 CORNEAL PATHOLOGIES

Seventy patients with various corneal pathologies recruited from department of ophthalmology at Rostock University, Germany were subjected to examination and included this study. Slit-lamp examination followed by SD-OCT scanning was performed for all subjects. All SD-OCT scans were compared with slit-lamp biomicroscopy. A verbal consent was obtained from all subjects after a brief explanation of the nature and purpose of the study. Study procedures were performed in accordance with the ethical standards of Declaration of Helsinki.

4.2 DEVICES

4.2.1 SPECTRAL DOMAIN OPTICAL COHERENCE TOMOGRAPHY

Spectralis OCT (Heidelberg Engineering, Heidelberg, Germany) is a system that combines a spectral domain OCT and a confocal laser scanning ophthalmoscope with an active eye tracking function which used to acquire corneal images. This device enables multiple B-scans to enhance image quality with high scanning speed up to 40000 A-scans per second. Its optical and digital depth resolution is 7 μm and 3.5 μm respectively, and the transverse and axial resolution is 20 μm and 5 μm respectively. The functions of this instrument has been reported previously.² Prior to start of the procedure, an accessory objective lens was attached to the eye piece of SD-OCT system to shift the focal plane from the retinal layer to the cornea. The subject sits in front of the camera and put the chin on a chin rest. The subject is asked to fixate on a target in the camera and the measurement is performed in the centre of the Pupil in normal subjects and in centre of the lesion in corneal pathologies. The SD-OCT scanning beam position was monitored with an infrared camera. An appropriate scanning region was located by changing position of the SD-OCT head or by getting the patient to follow a light fixation. High speed resolution digital images of 768 \times 768 pixels were obtained using a digital zoom at an angle of 30° and exported as RGB image for further image analysis.

Thickness analysis

Corneal layers thickness and corneal lesions parameters were analysed using an executable software program with MATLAB (version 7.0, Mathworks, Inc.) runtime environment that was developed in the department of ophthalmology at Rostock university to display SD-OCT corneal image and to determine point to point distance measurement of the corneal layers and corneal lesions. The principle of MATLAB program was previously described in details in the literature.²⁹

Measurement method

The epithelial thickness (ET) was measured from the inflection point on descending peak of the first maximum and ascending peak of the second maximum, The Bowman's membrane thickness (BMT) measured from the inflection point of ascending peak of the second maximum and the inflection point on descending peak of the second maximum. The stromal thickness (ST) between the inflection point of descending peak of the second maximum and the inflection point on the descending peak of the last maximum. The central corneal thickness (CCT) between the inflection point on descending peak of the first maximum and the inflection point on descending peak of the last maximum. The highly reflective first maximum which represents the precorneal tear film layer was excluded from the measurement. In our study we measured central corneal thickness (CCT-OCT), epithelial thickness (ET-OCT), Bowman's membrane thickness (BMT-OCT) and stromal thickness (ST-OCT) by SD-OCT as shown in Fig. 10.

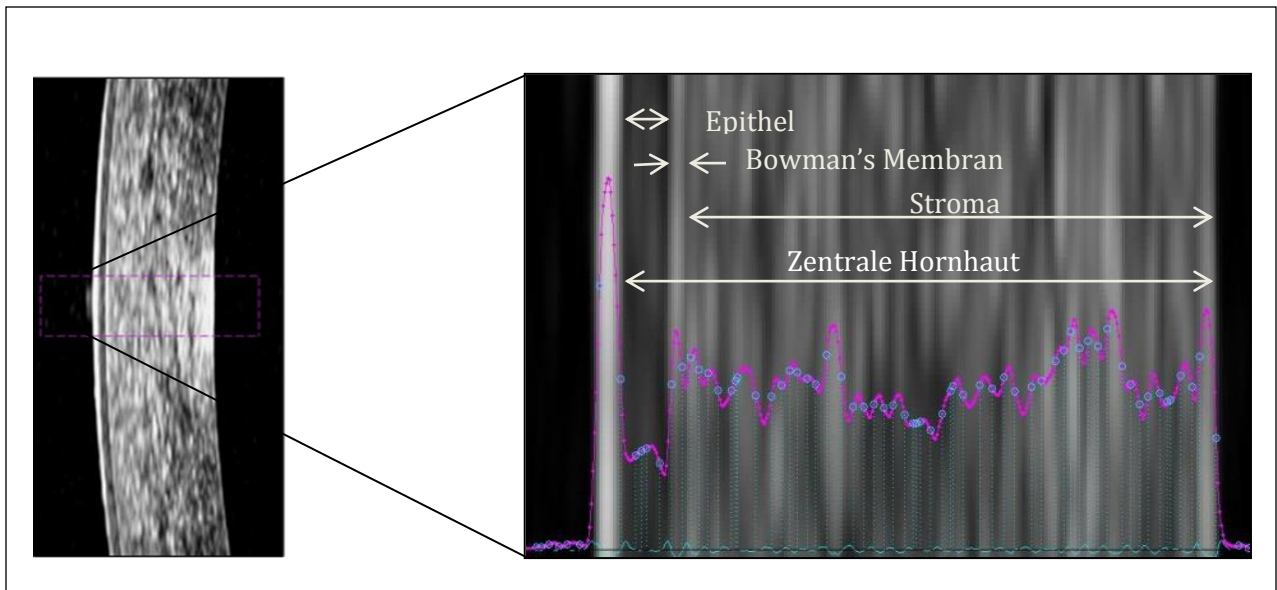


Fig. 10: SD-OCT image and thickness analysis of healthy cornea. Epithelial thickness (ET-OCT), Bowman's membrane thickness (BMT-OCT), stromal thickness (ST-OCT) and central corneal thickness (CCT-OCT) can be determined.

4.2.2 ROTATING SCHEIMPFLUG CAMERA

The rotating Scheimpflug camera (Pentacam; Oculus, Wetzlar, Germany) takes multiple (50) slit images of the anterior eye segment in approximately 2 seconds with 500 true elevation points incorporated in each slit image. The Scheimpflug system consists of Scheimpflug camera itself and a personal computer (Fig. 11). The software is fully automated.³⁰ The subject sits in front of the camera and places the chin on a chin rest. He/she is asked to fixate on target in the center of the camera. The examiner sees a real-time image of the patient's eye on the computer screen. The image must be focused and centered manually by moving the Scheimpflug camera in the respective directions. As soon as the image is perfectly aligned, the patient is asked not to move and to keep the eye open, and the scan is started. After completing a scan, the software calculates a three-dimensional image of the anterior segment, including anterior and posterior corneal surface, lens surface as well as lens opacities. In our study we measured only the central corneal thickness (CCT-SCH) by Scheimpflug camera.

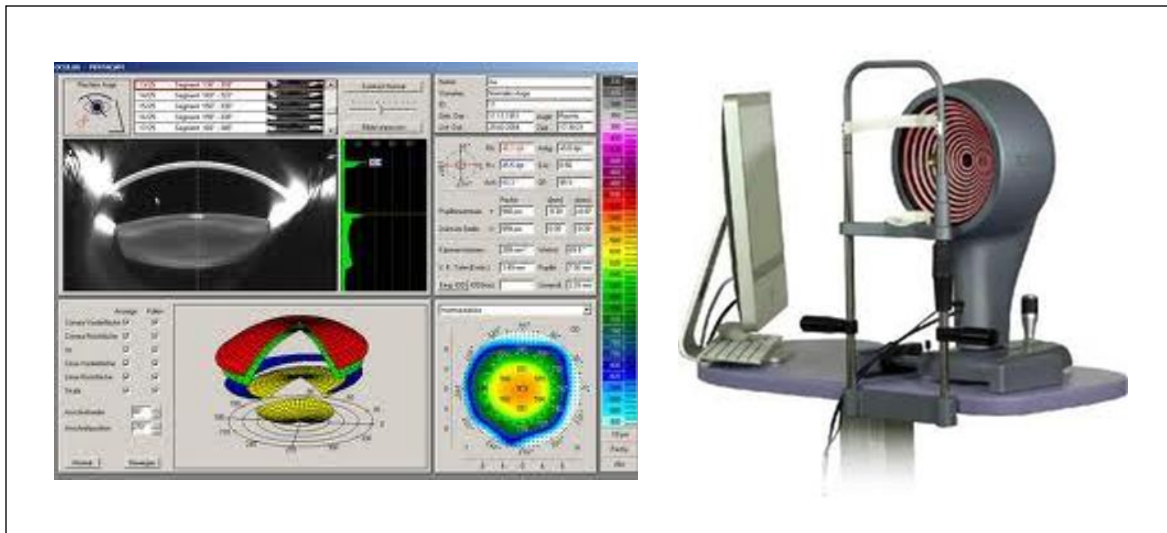


Fig. 11: Rotating Scheimpflug camera HR. (Pentacam; Oculus, Wetzlar, Germany).

4.2.3 AC MASTER

The AC-Master (Zeiss Meditec, Germany) measures central corneal thickness (CCT), anterior chamber depth (ACD) and lens thickness (LT) from a single point of the cornea (usually the center) in one step by the partial coherence interferometry (PCI) principle. The white-to-white distance is determined from an image of the iris before performing biometry.³¹ In AC Master; the patient fixates on a target visible on a liquid crystal display, which serves to control the direction of eye gaze. The ideal position of the fixation target is calculated by AC-Master, but can be adjusted manually. To measure along the optical axis, the four Purkinje images that result from reflections of the intraocular interfaces must be superimposed during the measurement. This can be controlled by the observer on the real-time image of the patient's eye shown on the computer screen and, if necessary, adjusted by moving the fixation target. Each measurement consists of one or more PCI A-scans (approximately 1 second per scan). In our present study we measured only the central corneal thickness (CCT-ACM) by AC Master device.



Fig. 12: AC Master device. (Zeiss Meditec, Germany)

4.2.4 CORNEAL PARAMETERS DETERMINED BY SPECTRAL DOMAIN OPTICAL COHERENCE TOMOGRAPHY, SCHEIMPFLUG CAMERA AND AC MASTER

The following corneal parameters measured by the 3 devices will be discussed in the study as shown in the table 1.

Table 1: Determination of corneal parameters measured by the 3 instruments.

| | SD-OCT | Scheimpflug camera | AC Master |
|--|---------------|---------------------------|------------------|
| Central corneal thickness (CCT) | CCT-OCT | CCT-SCH | CCT-ACM |
| Epithelial thickness (ET) | ET-OCT | – | – |
| Bowman’s membrane thickness (BMT) | BMT-OCT | – | – |
| Stromal thickness (ST) | ST-OCT | – | – |

4.3 STATISTICS

All data were collected and entered into the Statistical Package for Social Sciences (SPSS-PC) version 20.0. Statistical analysis included quantitative descriptive analysis and summary statistics. The data sets were checked for normality using the Kolmogorov-Smirnov test, they showed asymmetric distribution making the appropriate use of non parametric statistical tests. Measurements of central cornea thickness with optical coherence tomography (CCT-OCT), Scheimpflug camera (CCT-SCH) and AC Master (CCT-ACM) were analyzed using correlation and regression analysis. Analysis of Variance Wilcoxon-Test (ANOVA) was used for pairwise comparisons of the difference between measurements of three devices. The mean of CCT in both sexes and both eyes was analyzed using Mann-Whitney-U-Test for the 3 devices. The mean of CCT, ET-OCT, BMT-OCT and ST-OCT in different age groups was analyzed using a Kruskal-Wallis-Test for the 3 instruments.

Bland-Altman plots were used to measure the agreement between the three devices. The mean (a) ± standard deviation (s) of the difference in the central corneal thickness was calculated first between SD-OCT and Scheimpflug camera, then SD-OCT and AC Master and finally Scheimpflug and AC Master. Then the coefficient of agreement (COA) was calculated by multiplying 1.96 between the difference of every two instruments (s) (COA = 1.96 x s). COA is the value below which the difference between 2 measurements from 2 different instruments can be expected to fall with 95% probability. Limits of agreement (LOA) were calculated as (a ±

1.96 x s).³² The magnitude of these limits would determine whether the two instruments could be considered to be in agreement (i.e could be used interchangeably) and therefore if the SD-OCT could be reliably used for central corneal thickness measurement. P values of less than 0.05 were considered to be statistically significant.

5 RESULTS

5.1 HEALTHY CORNEA

5.1.1 SD-OCT OF HEALTHY CORNEA

A healthy 35 years old volunteer with normal findings on clinical corneal examination (Fig. 13 A) was subjected to the SD-OCT examination as an example of a healthy cornea. The SD-OCT image (Fig. 13 B) showed that the epithelium (arrow 1), Bowman’s membrane (arrow 2) and stroma (arrow 3) were visualized as distinct entities. The Descemet’s membrane and the endothelial layer were seen as 1 complex (arrow 4). The precorneal tear film appeared as hyperreflective layer in front of the epithelium (arrow 5). This SD-OCT image was used as a reference for interpreting the results of the other patients with different corneal abnormalities.

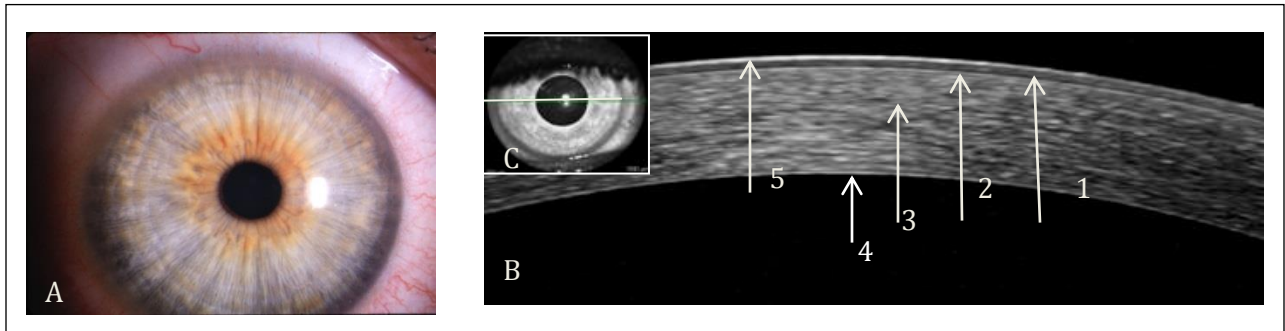


Fig. 13: (A) Slit-lamp photograph of healthy cornea. (B) SD-OCT image of healthy cornea. (C) shows the scan orientation.

5.1.2 CORNEAL LAYERS THICKNESS ANALYSIS BY SD-OCT

The mean thickness values and standard deviation (mean \pm SD) of the corneal layers measured by SD-OCT device for 100 healthy eyes are shown in table 2.

Table 2: Thickness of different corneal layers (Mean \pm SD) measured by SD-OCT (N=100).

| | ET-OCT | BMT-OCT | ST-OCT | CCT-OCT |
|---|----------------|----------------|------------------|------------------|
| Mean \pm SD in μm | 39.9 \pm 6.0 | 11.7 \pm 2.1 | 496.6 \pm 34.8 | 545.6 \pm 35.0 |

5.1.3 RELATIONSHIP BETWEEN THICKNESS OF DIFFERENT CORNEAL LAYERS AND AGE MEASURED BY SD-OCT

5.1.3.1 THE EPITHELIUM

The epithelial thickness values (ET-OCT) mean and standard deviation (mean ± SD) in different age groups measured with SD-OCT in 100 eyes are shown in table 3 and figure 14.

Table 3: Epithelial thickness values (mean ± SD) in µm in different age groups (N ≥ 10) measured by SD-OCT.

| ET-OCT (Mean ± SD) in µm | |
|--------------------------|------------|
| 20-30 y | 38.8 ± 4.8 |
| 31-40 y | 38.6 ± 4.8 |
| 41-50 y | 40.9 ± 6.9 |
| 51-60 y | 38.7 ± 5.4 |
| 61-70 y | 40.3 ± 6.5 |
| 71-80 y | 40.0 ± 7.8 |
| 81-90 y | 42.3 ± 7.5 |

Kruskal-Wallis-Test was used to determine the comparison between the mean ET-OCT in different age groups and revealed no significant statistical difference in the thickness of the epithelium in different age groups (P Value = 0.6).

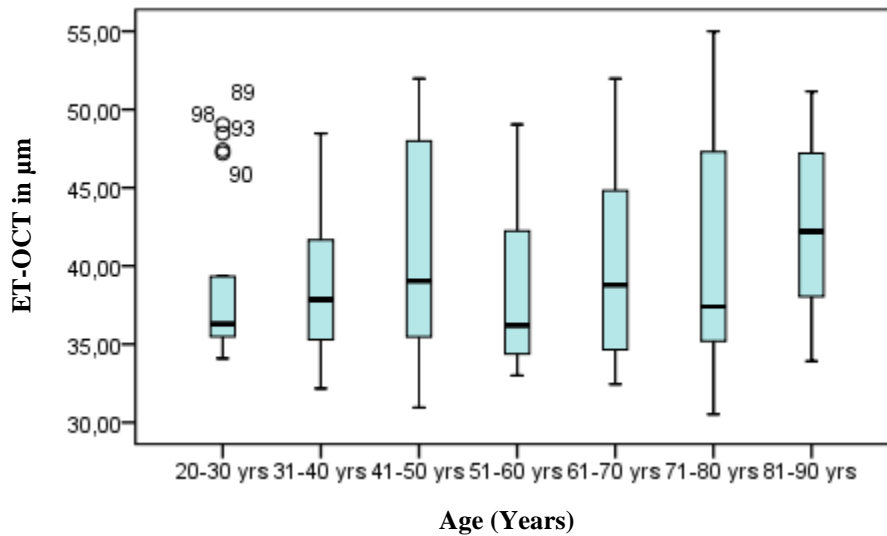


Fig. 14: Box-and-Whisker diagram shows the distributions of ET in different age groups by SD-OCT instrument.

It has been found no correlation between the epithelial thickness measured by SD-OCT (ET-OCT) and the age (Pearson correlation coefficient $r = 0.112$, $P = 0.2$). The mean epithelial thickness (ET-OCT) and standard deviation values (mean \pm SD) in male/female and right eye/left eye measured with SD-OCT shown in the table 4 and figures 15 and 16.

Table 4: Epithelial thickness (mean \pm SD) in μm in both sexes and both eyes measured by SD-OCT.

| | Male | Female | Right eye | Left eye |
|--|----------------|----------------|----------------|----------------|
| ET-OCT in μm (mean \pm SD) | 39.6 ± 6.0 | 40.1 ± 6.1 | 40.1 ± 6.4 | 39.7 ± 5.8 |

It has been found no association between the ET-OCT and sex ($r = 0.042$, $P = 0.6$) and right or left eye ($r = 0.038$, $P = 0,7$).

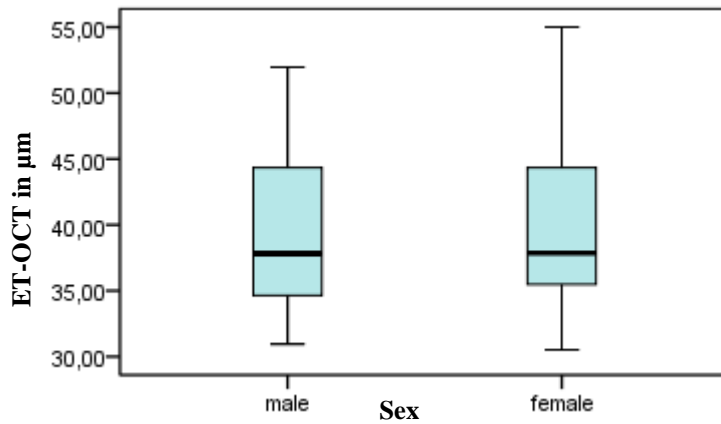


Fig. 15: Box-and-Whisker diagram shows the ET-OCT distributions of ET both sexes

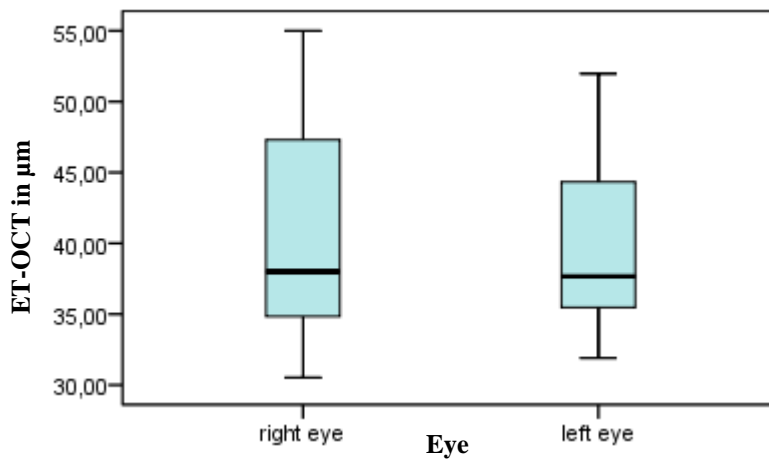


Fig. 16: Box-and-Whisker diagram shows the ET-OCT distributions of ET both eyes.

5.1.3.2 THE BOWMAN’S MEMBRANE

Bowman’s membrane thickness (BMT-OCT) mean and standard deviation (mean ± SD) values measured with SD-OCT in 100 eyes in different age groups are shown in table 4 and figure 17.

Table 5: Bowman’s membrane thickness values (mean ± SD) in µm in different age groups (N ≥ 10) measured by SD-OCT.

| BMT-OCT (Mean ± SD) in µm | |
|----------------------------------|------------|
| Age group (20-30 y) | 11.9 ± 2.1 |
| Age group (31-40 y) | 11.5 ± 1.7 |
| Age group (41-50 y) | 11.2 ± 2.3 |
| Age group (51-60 y) | 12.1 ± 2.3 |
| Age group (61-70 y) | 11.7 ± 2.7 |
| Age group (71-80 y) | 10.7 ± 0.6 |
| Age group (81-90 y) | 12.5 ± 2.8 |

Kruskal-Wallis-Test showed no significant statistical difference in the thickness of the Bowman’s membrane between the mean BMT-OCT in different age groups (P Value = 0.5).

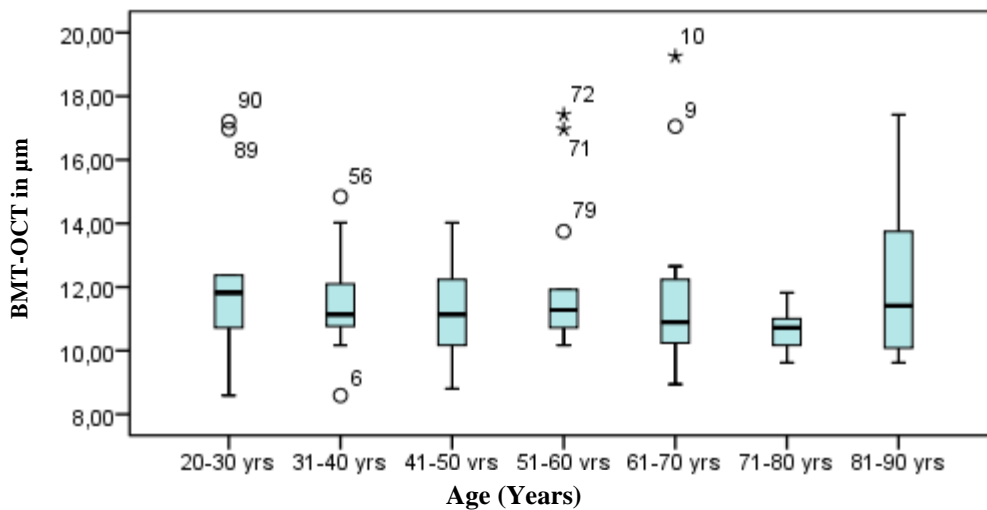


Fig. 17: Box-and-Whisker diagram shows the distributions of BMT-OCT in different age groups.

It has been found no correlation between the Bowman’s membrane thickness measured by SD-OCT (BMT-OCT) and the age (Person correlation $r = 0$, $P = 0.9$).

The mean epithelial thickness (BMT-OCT) and standard deviation values (mean \pm SD) in male/female and right eye/ left eye measured with SD-OCT are shown in the table 6 and figures 18 and 19.

Table 6: BMT-OCT (mean \pm SD) in μm both sexes and both eyes.

| | Male | Female | Right eye | Left eye |
|---|----------------|----------------|----------------|-----------------|
| BMT-OCT in μm (mean \pm SD) | 11.5 \pm 2.2 | 11.7 \pm 1.9 | 11.8 \pm 1.9 | 11.5 \pm 2.11 |

It has been found no association between the BMT-OCT and sex ($r = 0.031$, $P = 0.7$) and right or left eye ($r = 0.065$, $P = 0.5$).

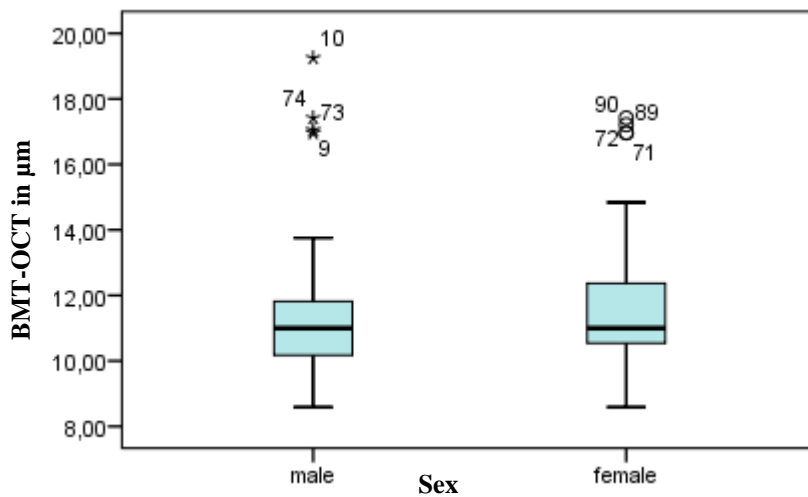


Fig. 18: Box-and-Whisker diagram shows the BMT-OCT distributions of both sexes.

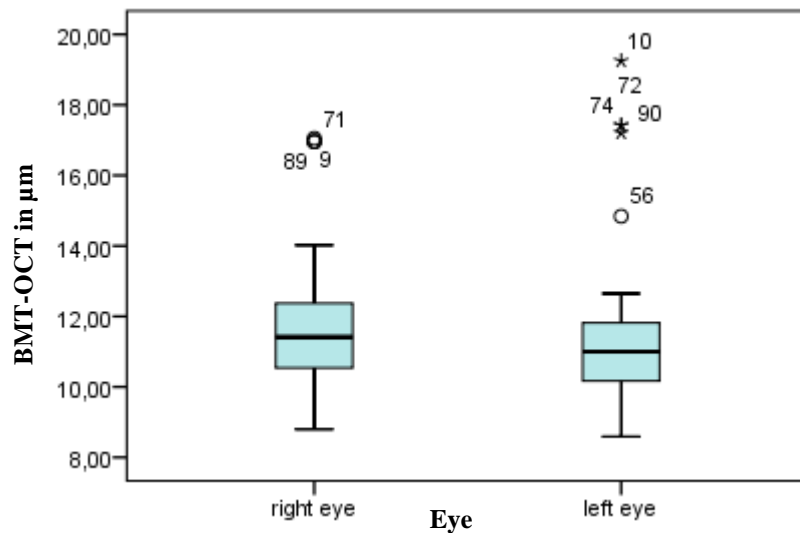


Fig. 19: Box-and-Whisker diagram shows the BMT-OCT distributions in both eyes.

5.1.3.3 THE STROMA

The mean stromal thickness values (ST-OCT) and standard deviation (mean ± SD) measurements with SD-OCT in 100 eyes are shown in table 7 and figure 20.

Table 7: Stromal thickness (mean ± SD) in different age group (N ≥ 10) measured by SD-OCT.

| ST-OCT (Mean ± SD) in μm | |
|---------------------------------|--------------|
| 20-30 y | 503.4 ± 34.9 |
| 31-40 y | 489.6 ± 28.8 |
| 41-50 y | 490.3 ± 29.6 |
| 51-60 y | 487.3 ± 35.6 |
| 61-70 y | 505.7 ± 45.7 |
| 71-80 y | 503.9 ± 34.6 |
| 81-90 y | 496.3 ± 32.6 |

The comparison between the mean ST-OCT in different age group using a Kruskal-Wallis-Test showed no significant statistical difference in the thickness of the stroma (P Value = 0.8).

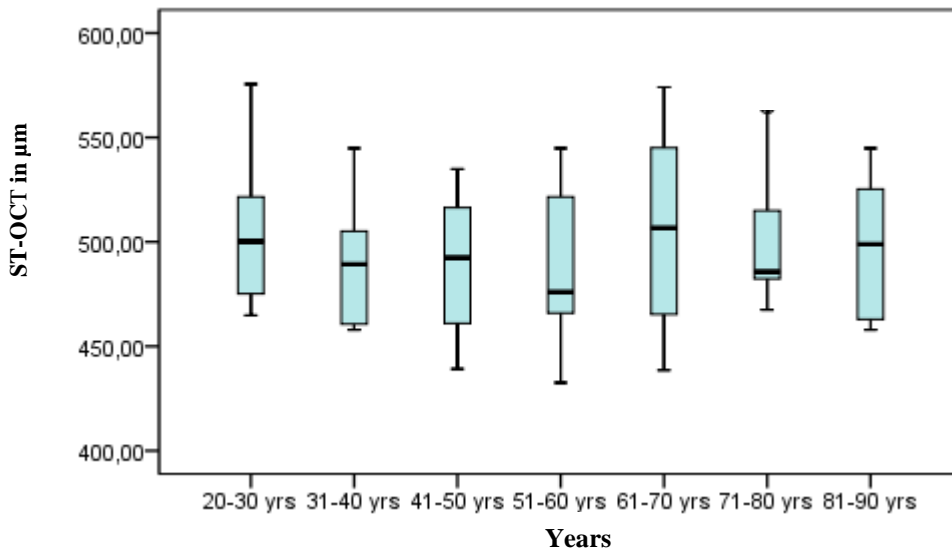


Fig. 20: Box-and-Whisker diagram shows the distributions of ST in different age groups by SD-OCT instrument.

It has been found no correlation between the stromal thickness measured by SD-OCT (ST-OCT) and the age (Pearson correlation $r = 0.038$, $P = 0.7$). The mean stromal thickness (ST-OCT) and

standard deviation values (mean \pm SD) in male/female and right eye/ left eye measured with SD-OCT are shown in the table 8 and figures 21 and 22.

Table 8: ST-OCT (mean \pm SD) in both sexes and both eyes.

| | Male | Female | Right eye | Left eye |
|--|------------------|------------------|------------------|------------------|
| ST-OCT in μm (mean \pm SD) | 489.5 \pm 35.9 | 495.1 \pm 34.2 | 497.9 \pm 36.2 | 495.2 \pm 33.7 |

It has been found no association between the ST-OCT and sex ($r = 0.049$, $P = 0.6$) and right or left eye ($r = 0.391$, $P = 0.7$).

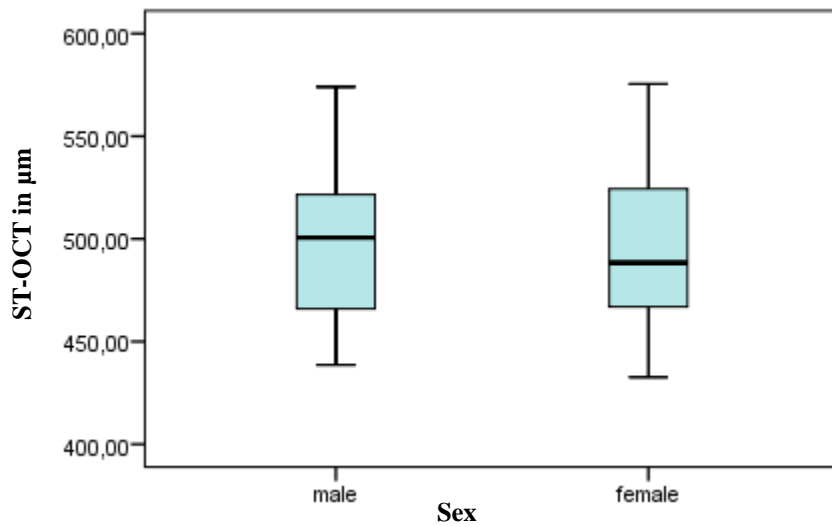


Fig. 21: Box-and-Whisker diagram shows the distributions of ST in both sexes by SD-OCT instrument.

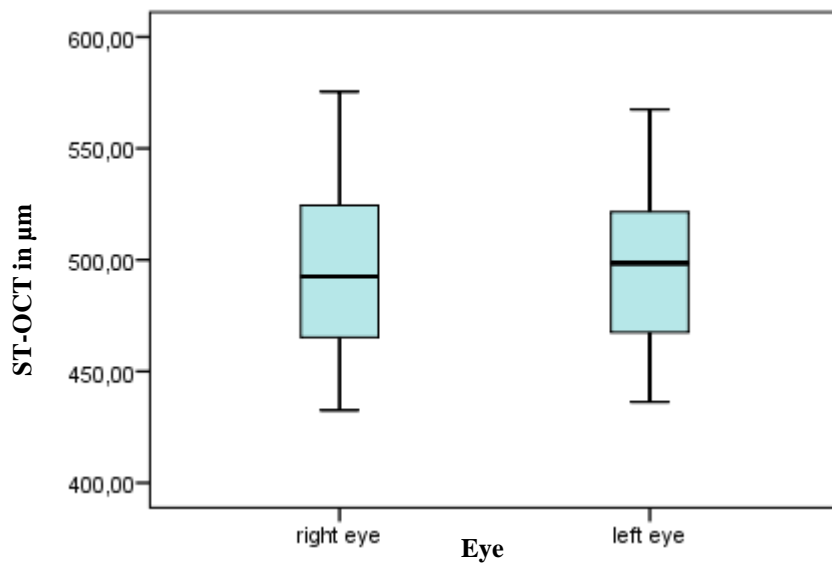


Fig. 22: Box-and-Whisker diagram shows the distributions of ST in both eyes by SD-OCT instrument.

The relationship between the central corneal thickness measured by SD-OCT and the age, gender and right/left eye will be discussed below.

5.1.4 ANALYSIS OF CENTRAL CORNEAL THICKNESS BY DEVICES

The mean central corneal thickness (CCT) ± SD measured by SD-OCT (CCT-OCT), Scheimpflug camera (CCT-SCH) and AC Master (CCT-ACM) are presented in table 6 and figure 23.

Table 9: Central corneal thickness values (mean ± SD) measured by the 3 devices.

| | CCT-OCT | CCT-SCH | CCT-ACM |
|------------------------|---------------|---------------|---------------|
| Mean ± SD in μm | 545.6 ± 34.9 | 553.7 ± 32.3 | 531.1 ± 33.7 |
| Range in μm | 492.7 - 621.8 | 492.7 - 622.6 | 469.3 - 600.4 |

Pairwise comparisons of the mean CCT by Wilcoxon-Test revealed that the mean CCT measurement obtained with SD-OCT was significantly thinner than the mean CCT obtained by Scheimpflug camera (P value < 0.001), while it was significantly thicker than the mean CCT obtained by AC Master (P-Value < 0.001). The box-and-whisker diagram is plotted to show the CCT distribution between the 3 instruments.

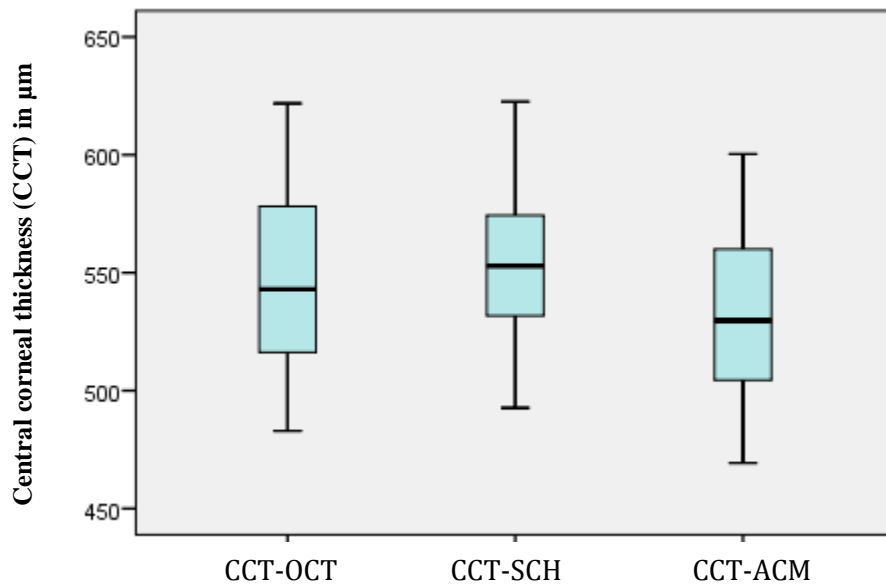


Fig. 23: Box-and-Whisker diagram shows the distributions of CCT for the 3 different devices.

5.1.5 CORRELATION IN CCT MEASUREMENT BETWEEN SD-OCT, SCHEIMFLUG CAMERA AND AC MASTER

Significant linear correlation coefficient values with a level of significance of < 0.05 were found in CCT measurement between SD-OCT and Scheimflug camera (Pearson correlation coefficient $r = 0.938$, $P < 0,001$), SD-OCT and AC Master ($r = 0.958$, $P > 0.001$) and Scheimflug camera and AC Master ($r = 0.943$, $P < 0.001$). (Fig. 15)

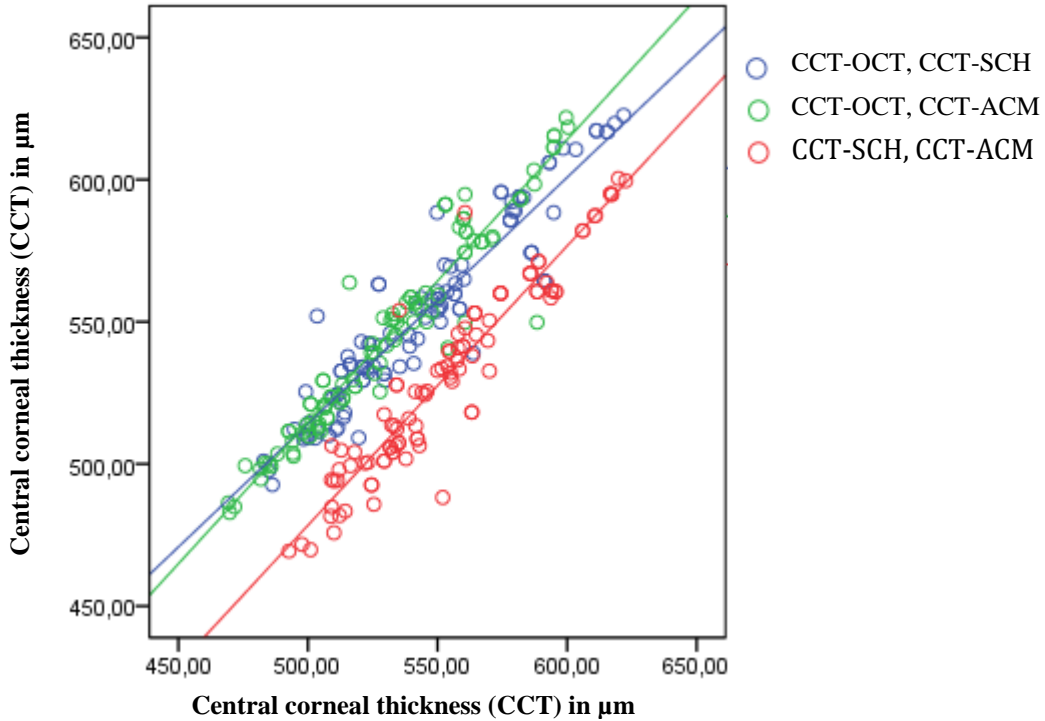


Fig. 24: significant linear correlation between the CCT measurement obtained with SD-OCT, Scheimpflug camera and AC Master.

5.1.6 AGREEMENT IN CCT MEASUREMENTS BETWEEN SD-OCT, SCHEIMPFLUG AND AC MASTER

The respective Bland-Altman plots between each pair of the three methods are described in the figures 25-27. The plots showed that CCT measured by SD-OCT was significantly thinner than that obtained with Scheimpflug camera (mean difference $8 \mu\text{m}$) (Fig. 25). CCT measured by SD-OCT measurement was significantly thicker than CCT measured by AC Master with a mean difference of $14 \mu\text{m}$ (Fig. 26). Meanwhile the CCT measured by AC Master was significantly thinner than that obtained with Scheimpflug camera with mean difference of $22.5 \mu\text{m}$ (Fig. 27). The 95% limits of agreement (LOA) for SD-OCT - Scheimpflug camera was $-8.0 \pm 23.8 \mu\text{m}$, for

SD-OCT - AC Master was $24.5 \pm 19.7 \mu\text{m}$ and for Scheimpflug camera - AC Master were 22.5 ± 22.0 . Therefore the greater acceptable agreement was between between the SD-OCT and AC Master although SD-OCT may give readings $34.2 \mu\text{m}$ above or $5.2 \mu\text{m}$ below those obtained with AC Master. Regarding the agreement between Scheimpflug - AC Master, the results showed that Scheimpflug camera may gives readings $44.5 \mu\text{m}$ above or $0.5 \mu\text{m}$ below the reading obtained from AC Master. The least acceptable agreement was between SD-OCT - Scheimpflug camera, whereby the results indicate that the SD-OCT may give readings $15.8 \mu\text{m}$ above or 31.8 below the readings obtained with Scheimpflug camera. Table 10 summarizes the results of agreement between each pair from the 3 devices.

Table 10: Agreement results between the 3 instruments.

| Device | Mean difference $\pm S$ | Coefficient of agreement COA | Upper limit of 95% of agreement | Lower limit of 95% of agreement | Magnitude of LOA |
|--------------------|-------------------------|------------------------------|---------------------------------|---------------------------------|------------------|
| SD-OCT-Scheimpflug | -8.0 ± 12.1 | 23.8 | 15.8 | -31.8 | 47.6 |
| SD-OCT-ACM | 14.5 ± 10.1 | 19.7 | 34.2 | -5.2 | 39.4 |
| Scheimpflug-ACM | 22.5 ± 11.2 | 22.0 | 44.5 | 0.5 | 45.0 |

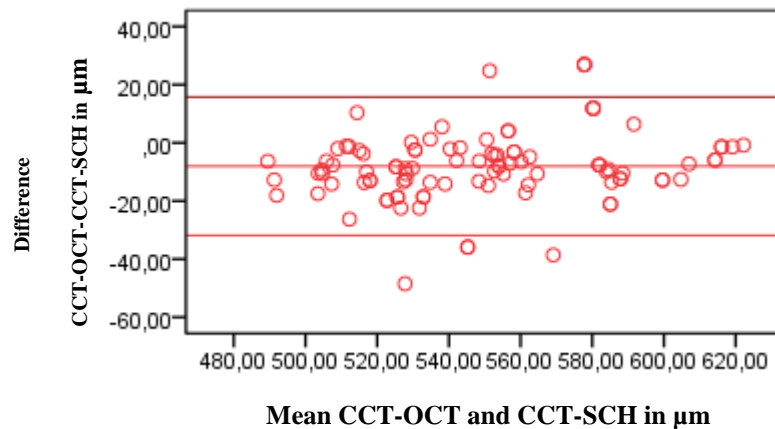


Fig. 25: Bland-Altman plot compares the CCT measurements obtained using SOCT and Scheimpflug camera.

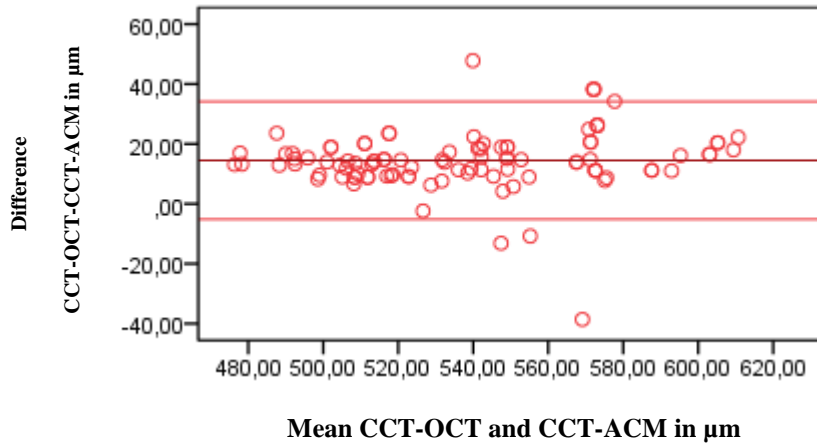


Fig. 26: Bland-Altman plot compares the CCT measurements obtained using SD-OCT and AC Master

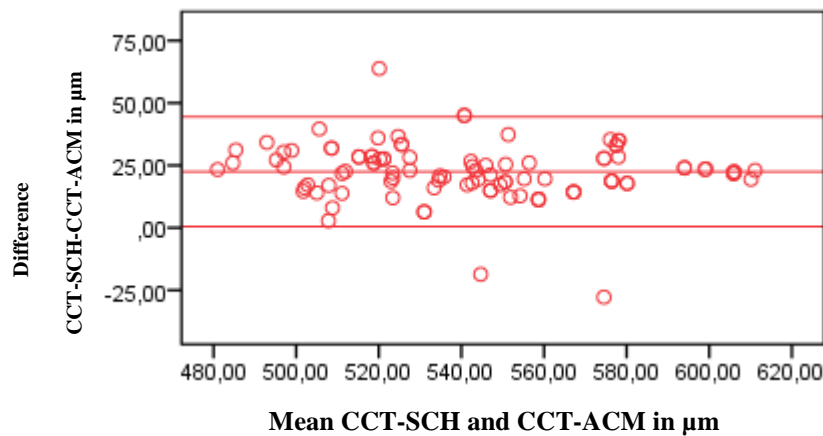


Fig. 27: Bland-Altman plot compares the CCT measurements obtained using Scheimpflug camera and AC Master

5.1.7 ANALYSIS OF THE RELATIONSHIP BETWEEN THE CCT AND GENDER

The mean CCT \pm SD measurements using SD-OCT, Scheimpflug camera and AC Master in male and female subjects are depicted in table 11 and figure 28.

Table 11: CCT values (mean \pm SD) in both sexes by the 3 instruments.

| | CCT-OCT | CCT-SCH | CCT-ACM |
|--|------------------|------------------|------------------|
| Male (mean \pm SD) in μm | 549.1 \pm 36.8 | 558.0 \pm 31.8 | 536.1 \pm 36.3 |
| Female (mean \pm SD) in μm | 543.3 \pm 33.9 | 550.7 \pm 32.6 | 527.9 \pm 31.8 |

Mann-Whitney-U-Test revealed no statistical significant difference when comparing the mean CCT in central corneal thickness between both sexes regardless of the device used in the measurement (Fig. 28).

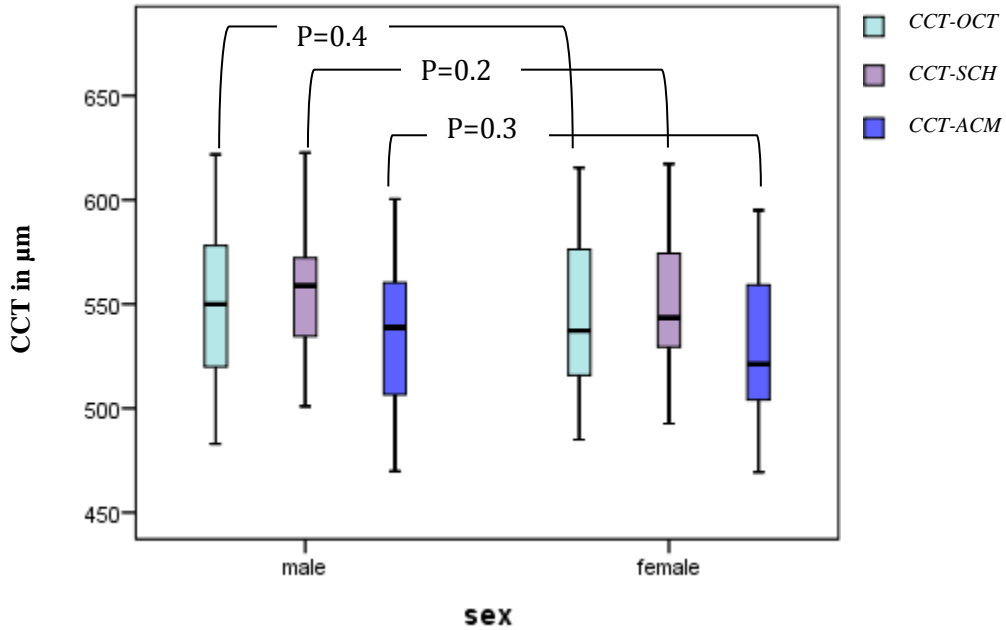


Fig. 28: Box-and-Whisker diagram shows the CCT distribution between both sexes by SD-OCT, Scheimpflug and AC Master.

5.1.8 ANALYSIS OF THE RELATIONSHIP BETWEEN CCT AND BOTH EYE

Mean CCT \pm SD measurements using SD-OCT, Scheimpflug camera and AC Master in male and female subjects described in table 12 and figure 29.

Table 12: shows the CCT values in both eyes by the 3 instruments.

| | CCT-OCT | CCT-SCH | CCT-ACM |
|--|------------------|------------------|------------------|
| OD (mean \pm SD) in μm | 545.3 \pm 34.4 | 553.8 \pm 31.8 | 531.4 \pm 33.5 |
| OS (mean \pm SD) in μm | 546.0 \pm 35.9 | 553.5 \pm 33.2 | 530.9 \pm 34.2 |

Mann-Whitney-U-Test showed no statistical significant difference in CCT in both sexes and both eyes during the comparison between mean CCT (Fig. 29).

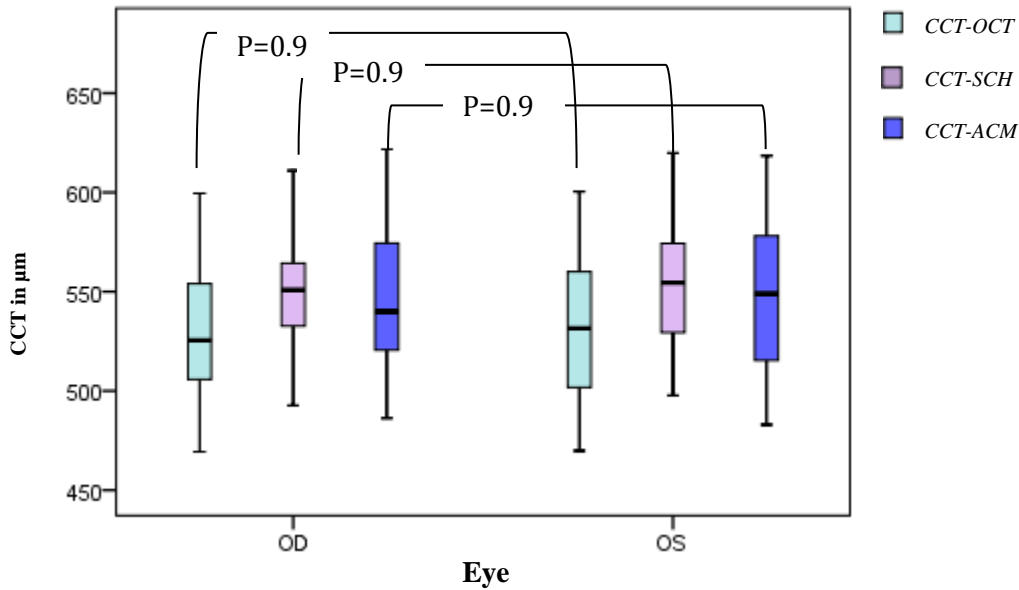


Fig. 29: Box-and-Whisker diagram shows the CCT distribution between both sexes by SD-OCT, Scheimpflug and AC Master

5.1.9 ANALYSIS OF THE RELATIONSHIP BETWEEN THE CCT AND AGE

The mean CCT and standard deviation values measured with SD-OCT, Scheimpflug camera and AC Master in different age groups are depicted in table 13 and figures 30, 31 and 32.

Table 13: Central corneal thickness (mean ± SD) in µm measured by 3 devices in different age groups (N ≥ 10).

| | CCT-OCT in µm | CCT-SCH in µm | CCT-ACM in µm |
|--------------------------|---------------|---------------|---------------|
| Age group 20-30 y | 547.5 ± 33.7 | 553.1 ± 27.5 | 531.2 ± 29.8 |
| Age group 31-40 y | 538.9 ± 30.3 | 542.9 ± 27.9 | 524.0 ± 24.9 |
| Age group 41-50 y | 543.7 ± 32.9 | 552.8 ± 33.2 | 527.5 ± 33.9 |
| Age group 51-60 y | 535.4 ± 34.5 | 540.6 ± 29.9 | 522.9 ± 35.9 |
| Age group 61-70 y | 555.8 ± 45.3 | 571.6 ± 39.1 | 543.0 ± 43.7 |
| Age group 71-80 y | 551.8 ± 36.5 | 561.1 ± 33.0 | 538.6 ± 34.1 |
| Age group 81-90 y | 546.1 ± 31.3 | 551.7 ± 27.9 | 532.4 ± 30.2 |

Kruskal-Wallis-Test was used to compare the mean CCT measured by SD-OCT, Scheimpflug camera and AC and showed no significant statistical difference in CCT in different age groups (P Value for all comparisons >0.05). There was no significant correlation detected between the CCT and age in all the 3 devices used in the measurement.

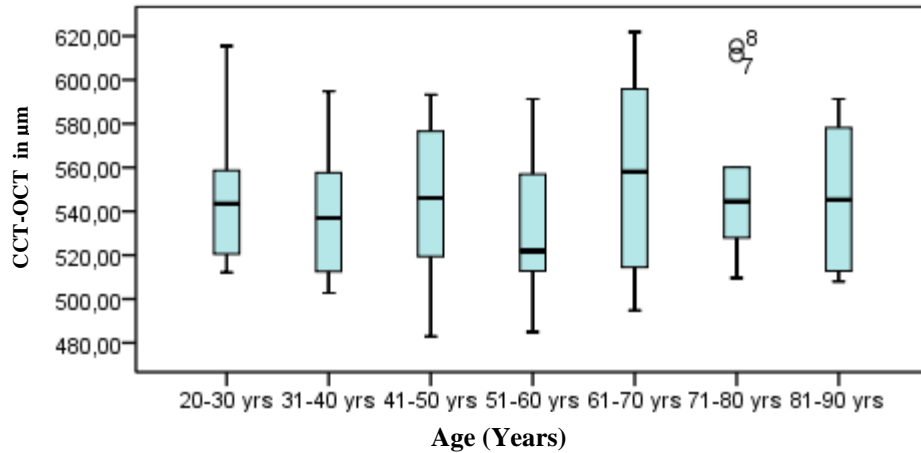


Fig. 30: Box-and-Whisker diagram shows the CCT-OCT distribution in different age groups.

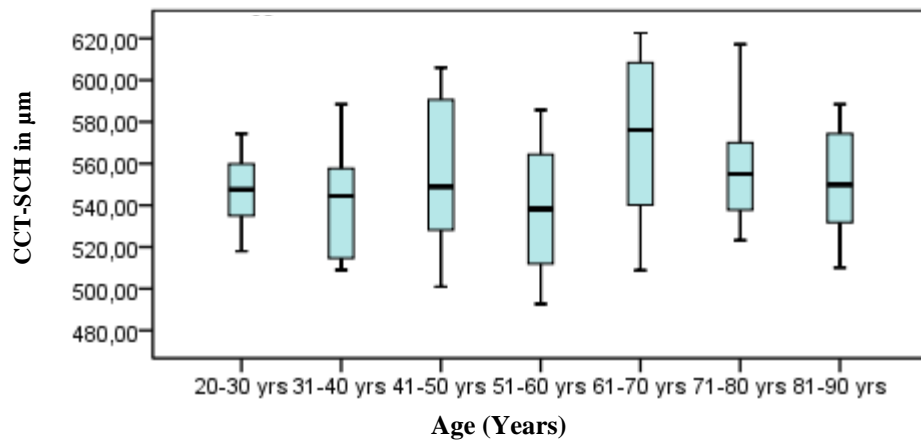


Fig. 31: Box-and-Whisker diagram shows the CCT-SCH distribution in different age groups.

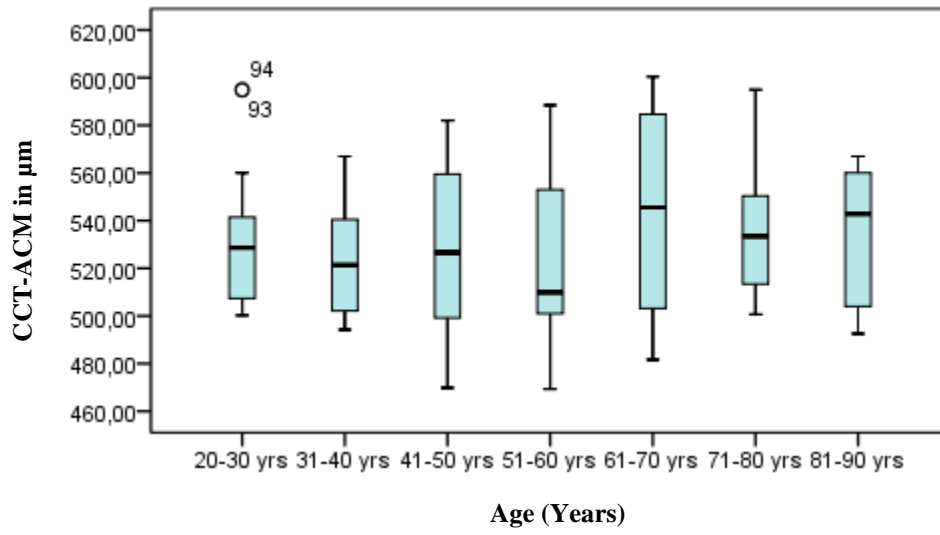


Fig. 32: Box-and-Whisker diagram shows the CCT-ACM distribution in different age groups

5.2 CORNEAL PATHOLOGIES

Seventy eyes with various corneal diseases were examined by SD-OCT device. For each disease we present only an image as an example. A complete ophthalmological examination for the patients led to the diagnosis of:

Epithelial diseases:

- Corneal degeneration unclear dignity.
- Perforated corneal ulcer.
- Recurrent epithelial erosions.
- Epithelial edema caused by acute angle closure glaucoma.
- Dry eye syndrome.
- Soft contact lens.
- Hard contact lens.

Stromal diseases:

- Keratitis associated with contact lens wear.
- Fungal keratitis.
- Stromal keratitis.
- Corneal foreign body.
- Corneal scar.
- Granular corneal dystrophy.
- Keratoconus.

Endothelial diseases:

- Endothelitis, Keratitis.
- Descemet's membrane detachment.
- Fuchs' endothelial dystrophy.
- Assessment of wound profile after penetrating keratoplasty (PKP).
- Bullous keratopathy.

5.2.1 EPITHELIAL DISEASES

5.2.1.1 CORNEAL DEGENERATION UNCLEAR DIGNITY

A 53 years old male patient sought treatment for subjective visual reduction since 6 months.

Slit-lamp examination (Fig. 33 A) revealed a prominent paracentral grayish oval corneal opacity with no evident signs of infection or inflammation.

SD-OCT scan (Fig. 33 B) demonstrated a prominent epithelial lesion with thickness of 247.0 μm (arrow 1) and intact Bowman's membrane (arrow 2) with an increases in the corneal thickness (CT) at the site of the lesion (900 μm), while the central corneal thickness (CCT) was 624 μm . Normal stroma and descemet's membrane-endothelium complex was detected. Confocal microscopy showed hyperreflective structure in the basal epithelial layer (Fig. 33 D) and superficial stroma (Fig. 33 E) similar to scar tissue.

Because of good visual acuity and peripheral location of the lesion no therapy was recommended for this patient.

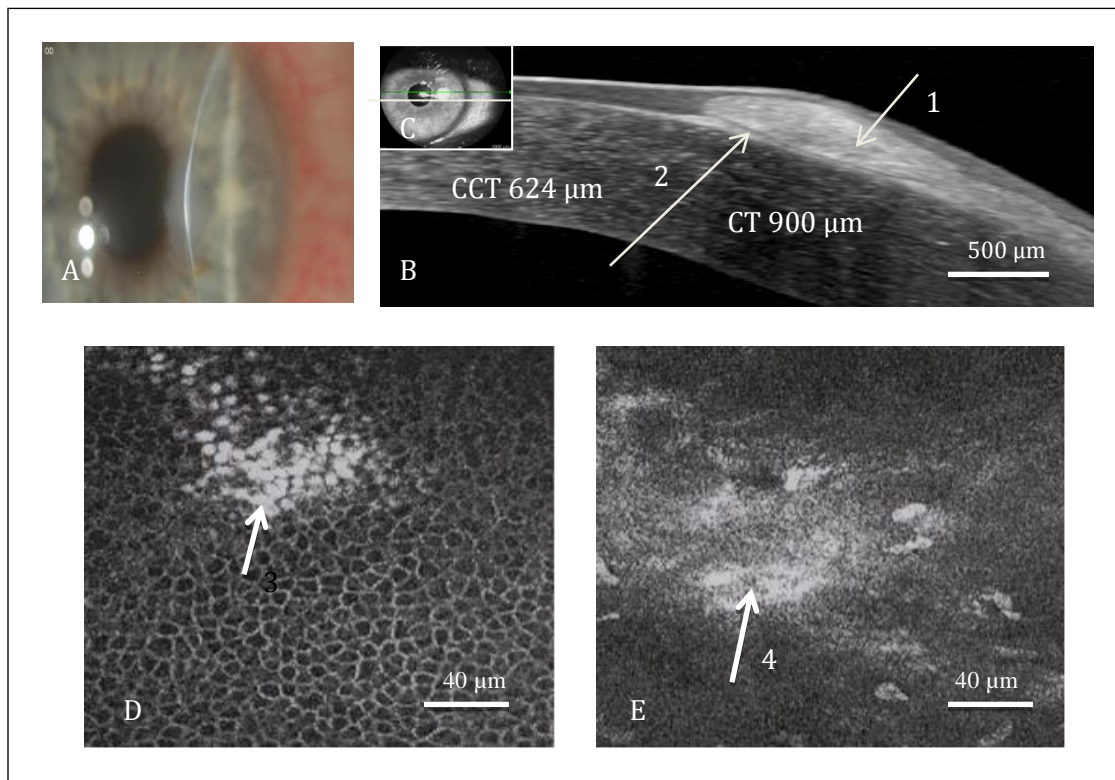


Fig. 33 (A) slit-lamp photograph of the cornea demonstrates grayish corneal lesion. (B) SD-OCT image shows epithelial lesion (arrow 1) with intact Bowman's membrane (arrow 2). (C) The scan orientation. (D) Confocal microscopy illustrates hyperreflective structure in the basal epithelial layer (arrow 3). (E) Confocal microscopy shows hyperreflective structure in the superficial stroma (arrow 4).

5.2.1.2 PERFORATED CORNEAL ULCER

A 55 years old female patient sought treatment for red painful left eye since 1 week.

Slit-lamp examination (Fig. 34 A) showed a paracentral perforated corneal ulcer with iris tamponed and corneal opacity and vascularization surrounding the corneal perforation.

SD-OCT scan (Fig. 34 B) revealed hyporeflective round structure in the middle of the cornea corresponding to corneal perforation (arrow 1) with hyperreflective bowl-shaped structure (arrow 2) which blocked the perforation from the bottom that could to be the iris. Additionally band shaped structure was attached to the posterior corneal surface (arrow 3) corresponding to iridocorneal touch (arrow 3) with obliteration of the anterior chamber at this area and stick-like structure on top of the perforation which was diagnosed as most probably an epithelial bridge (arrow 4) and precorneal tear film (arrow 5).

The next day multi-layered (5 layers) amnion membrane transplantation was performed to seal the corneal perforation and restore the globe integrity.

Two days postoperatively, slit-lamp examination (Fig. 34 D) and SD-OCT scan (Fig. 34 E) showed a complete filling of the corneal perforation with the multi-layered amnion membrane transplant (arrow 6). The therapeutic contact lens was in place (arrow 7) and a regular anterior chamber.

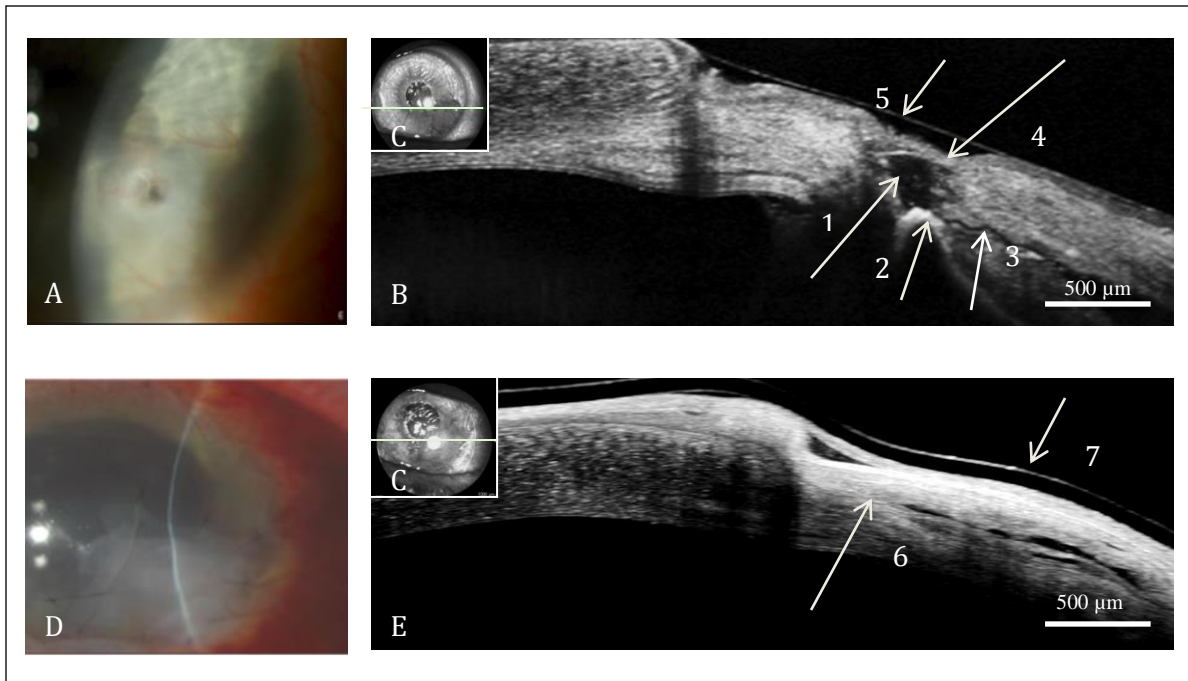


Fig. 34: (A) Slit-lamp photograph at presentation of the cornea with perforated corneal ulcer. (B) SD-OCT image at presentation of the cornea shows hyporefective round structure corresponds to the perforation (arrow 1), hyperreflective bowl-shaped structure blocked the perforation which could be the iris (arrow 2), band shaped structure attach to the posterior corneal surface corresponding to iridocorneal touch (arrow 3), stick-like structure sealed the perforation from the top which thought be an epithelial bridge (arrow 4) and precorneal tear film (arrow 5). (C) The scan orientation. (D) Postoperative slit-lamp photograph of the perforated corneal ulcer after multi-layered amnion transplantation. (E) Postoperative SD-OCT image illustrates multi-layered amnion membrane graft (arrow 6) closing the corneal perforation and therapeutic contact lens in place (arrow 7).

5.2.1.3 RECURRENT EPITHELIAL EROSIONS

A 45 year old male patient sought treatment of red painful left eye since 3 days.

Slit-lamp examination (Fig. 35 A) showed a moderate conjunctival injection and epithelial erosion with epithelial folds.

SD-OCT scan (Fig 35 B) demonstrated a defect in the epithelial layer of the cornea (arrow 1), epithelial folds (arrow 2) and partial detachment of the epithelium (arrow 3) from the underlying intact Bowman’s membrane at the site of the folds (arrow 4). Intact corneal stroma and Descemet’s membrane-endothelium complex (arrow 5) was observed. Debridement of corneal epithelium was done, therapeutic contact lens was placed and topical antibiotic was recommended. Postoperative slit-lamp examination (Fig. 35 D) and SD-OCT scan (Fig. 35 E) showed therapeutic contact lens (arrow 6), no corneal epithelium (arrow 7) and intact Bowman’s membrane, stroma and Descemet’s membrane-endothelial complex (arrow 8).

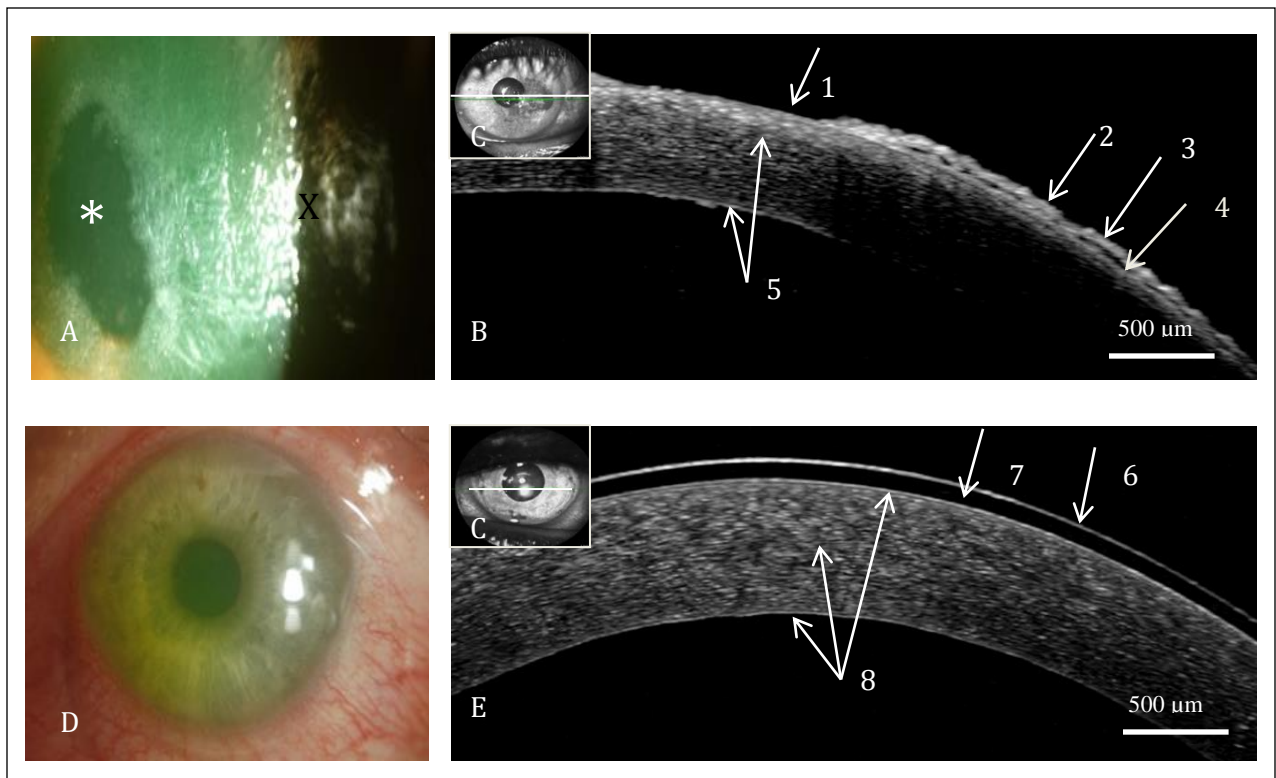


Fig. 35: (A) Slit-lamp photograph at presentation shows epithelial erosion (*) and epithelial wrinkles (x). (B) SD-OCT image at presentation reveals a defect in the epithelial layer of the cornea (arrow1), folds of the epithelium. (C) scan orientation. (D) slit-lamp photograph performed after debridement of corneal epithelium with therapeutic CL. (E) SD-OCT image after debridement of the epithelium shows cornea without epithelium (arrow 7) and therapeutic CL (arrow 6).

5.2.1.4 EPITHELIAL EDEMA CAUSED BY ACUTE ANGLE CLOSURE GLAUCOMA

A 55 years old male patient presented to our clinic with severe headache, ocular pain and visual halos.

Slit-lamp examination (Fig. 36 A) showed mild conjunctival injection, epithelial edema, shallow anterior chamber. The intraocular pressure (IOP) was 70 mmHg.

SD-OCT scan (Fig. 36 B) illustrated hyporeflective ovale structures (arrow 1) in the epithelial layer of the cornea which corresponds to epithelial edema with an increase in the epithelial thickness (ET) of 80 μm . Central corneal thickness (CCT) was 640 μm .

Intravenous acetazolamide 500 mg and topical antiglaucomal therapy was given. On the following day surgical Iridotomy was performed.

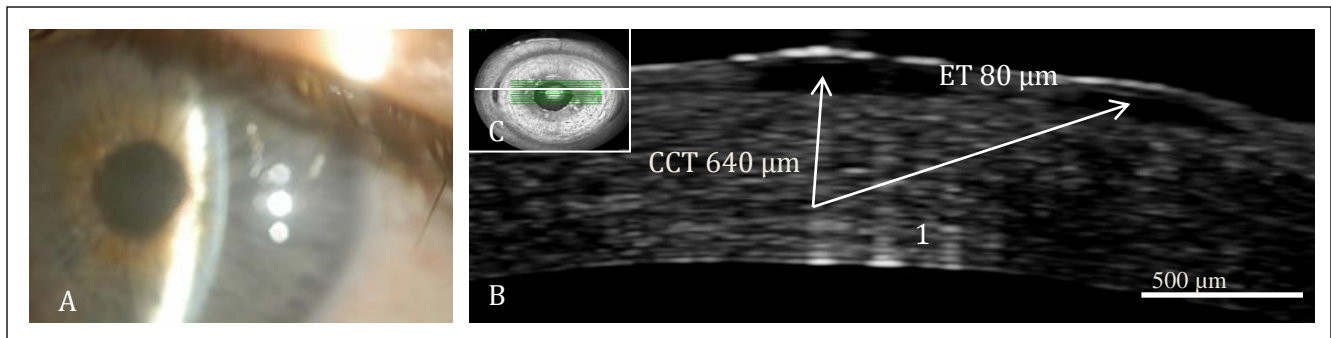


Fig. 36: (A) slit-lamp photograph at presentation shows epithelial edema with shallow anterior chamber. (B) SD-OCT image reveals hyporeflective oval structure in the epithelium (arrow 1), ET-OCT was 80 μm and CCT-OCT was 640 μm . (C) The scan orientation

5.2.1.5 DRY EYE SYNDROME

A 65 years old female patient sought treatment for watery eye since 3 months.

Slit-lamp examination (Fig. 37 A) showed punctate epithelial erosion which stained with fluorescein.

SD-OCT scans (Fig. 37 B) revealed irregular epithelial surface of the cornea (arrow 1), without the normally hyperreflective precorneal tear film layer. Bowman's membrane, stroma and Descemet's membrane-endothelial complex were normal (arrow 2).

The patient was subjected to a treatment with artificial tears.

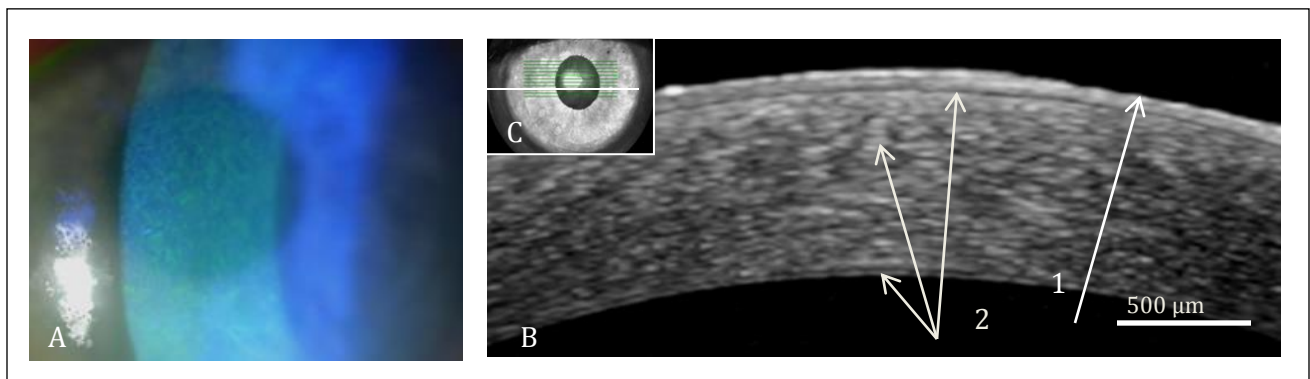


Fig. 37: (A) slit-lamp photograph shows punctate epithelial erosions due to dryness of the eye. (B) SD-OCT image reveals irregular epithelial surface (arrow 1) with intact Bowman's layer, stroma and descemet's-endothelial complex (arrow 2). (C) showed the scan orientation.

5.2.1.6 SOFT CONTACT LENS

A 36 years old healthy volunteer with normal visual acuity and normal ocular finding.

Slit-lamp examination (Fig. 38 A) showed normal cornea with contact lens in place.

SD-OCT scan (Fig. 38 B) showed proper adherence of soft contact lens to the corneal surface (arrow 1). Pre- and post-lens tear film (arrow 2) was detected and could be exactly measured. Pre-lens tear film thickness was 22 μm , post-lens tear film thickness was 14 μm . Intact epithelium, Bowman's membrane, stroma and descemet's membrane-endothelial complex (arrow 3) was demonstrated. Contact lens thickness was 85 μm , Central corneal thickness (CCT) was 570 μm .

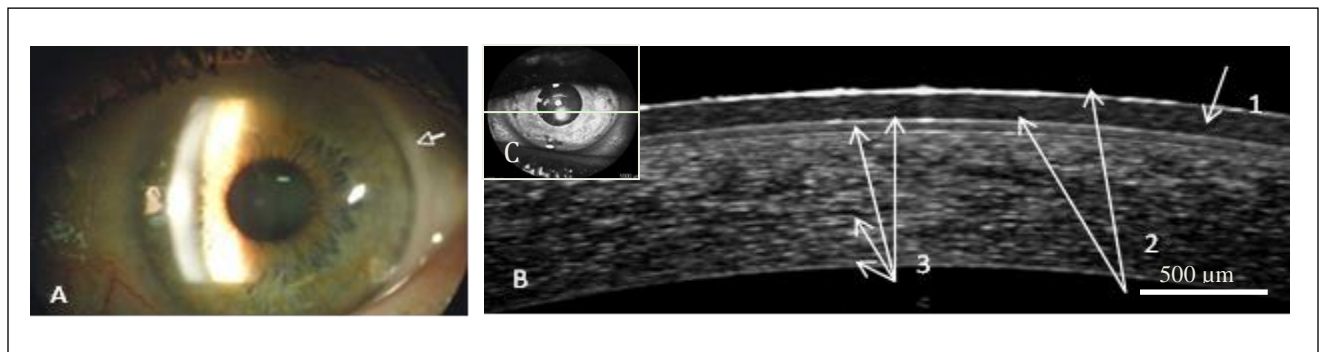


Fig. 38: (A) slit-lamp photograph of cornea with soft contact lens. (B) SD-OCT image shows normal cornea with soft contact lens in place (arrow 1), pre- and post-lens tear film layer (arrow 2), intact epithelium, Bowman's layer, stroma and descemet's-endothelial complex (arrow 3). (C) the scan orientation.

5.2.1.7 HARD CONTACT LENS

A 35 years old male patient presented to our clinic for a regular follow up of keratoconus of the left eye. The visual acuity was 0.3.

Slit-lamp examination (Fig. 39 A) showed opaque structure in the cornea with a hard contact lens in place.

SD-OCT scan (Fig. 39 B) demonstrated hard contact lens (arrow 1) with apical touch (arrow 2) and peripheral clearance (arrow 3), hyperreflective irregular-shaped structure in the superficial, middle and deep stroma up to the Descemet's membrane-endothelial layer (arrow 4) which corresponds to formation of scar tissue in the cornea and destruction of Bowman's membrane (arrow 5) was observed. The thickness of the contact lens (CL) was 125 μm , the central corneal thickness was 380 μm .

A difference in the reflectivity pattern in the SD-OCT images of soft and hard contact lenses was observed.

Due to presence of scar tissue in the cornea, poor visual acuity and the corneal thickness at the thinnest point of the cornea was less than 400 μm , penetrating keratoplasty was recommended.

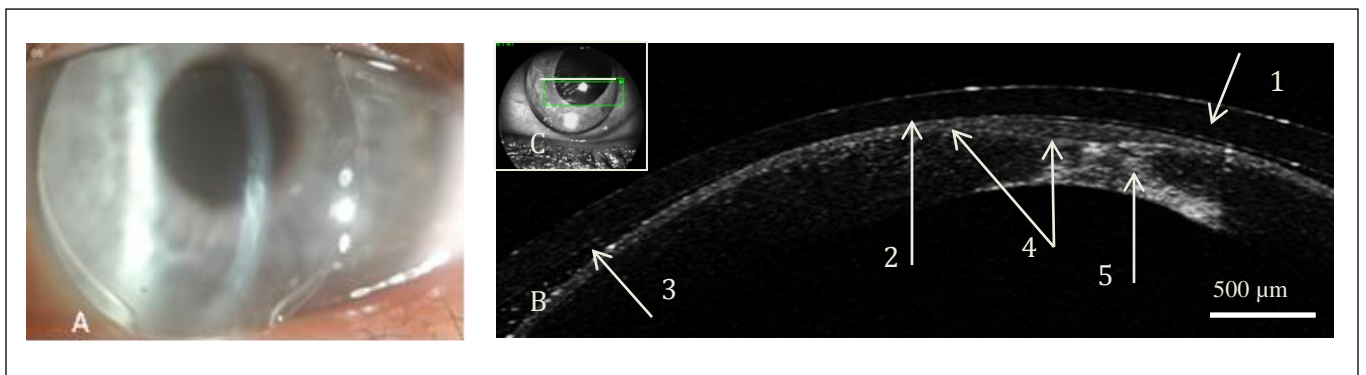


Fig. 39: (A) slit-lamp photograph of cornea in patient with keratoconus and hard contact lens wear. (B) SD-OCT image shows hard contact lens (arrow 1) with apical touch (arrow 2) and peripheral clearance (arrow 3), hyperreflective irregular-shaped structure in the stroma up to the descemet's – endothelial complex corresponds to scar tissue (arrow 4) with destruction of Bowman's membrane layer (arrow 5). (C)The scan orientation.

5.2.2 STROMAL DISEASES

5.2.2.1 KERATITIS ASSOCIATED WITH CONTACT LENS WEAR

A 26- years old male contact lens wearer patient sought treatment for a painful red right eye since 3 days. Slit lamp examination (Fig. 40 A) showed moderate conjunctival injection with epithelial defect that was associated with paracentral whitish, round corneal infiltration.

SD-OCT scan (Fig. 40 B) at presentation showed prominent, rounded hyperreflective lesion in the epithelium and stroma reaching middle stroma (arrow 1) corresponds to corneal infiltration with shadowing of deep corneal layers posterior to it (arrow 2). The infiltration parameters were: infiltrate thickness (IT) 415 μm with an infiltrate width (IW) 230 μm . Increase in the central corneal thickness due to corneal edema was demonstrated. Central corneal thickness (CCT) was 948 μm .

After six weeks of intensive topical treatment with antibiotics there was a complete clinical resolution of the corneal infiltrate (Fig. 40 D). SD-OCT (Fig. 40 E) scan demonstrated a hyperreflective plate-shaped structure in the anterior and middle stroma which corresponded to a corneal scar (arrow 3) with an associated destruction of Bowman’s membrane at this area (arrow 4). The central corneal thickness was 553 μm .

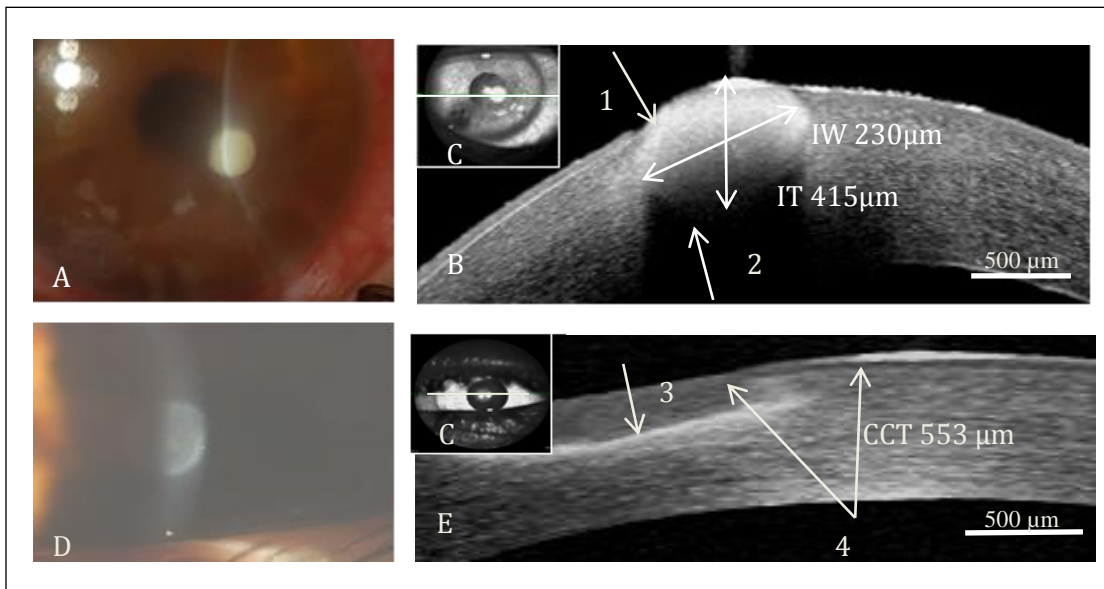


Fig .40: (A) slit-lamp photograph at presentation shows round, whitish corneal infiltration. (B) SD-OCT image at presentation reveals a prominent, rounded hyperreflective corneal lesion (arrow 1) with shadowing of deep corneal layers (arrow 2). (C) showed the scan orientation. (D) Slit lamp photograph six weeks after treatment demonstrates paracentral round corneal opacity. (E) SD-OCT image illustrates hyperreflective plate-like structure in the anterior and middle stroma corresponds to the corneal scar (arrow 3) with destruction of Bowman’s membrane (arrow 4).

5.2.2.2 FUNGAL KERATITIS

A 65 years old female patient sought treatment of painful right eye since one week.

Slit-lamp examination (Fig. 41 A) showed central corneal clouding with epithelial erosions and descemet's membrane folds.

SD-OCT scan (Fig 41 B) revealed defects in the epithelium (arrow 1) and Bowman's membrane (arrow 2), milde hyperreflective structure in the superficial stroma which corresponds to the area of the corneal clouding (arrow 3) and ruffles in descemet's membrane-endothelial complex (arrow 4). The central corneal thickness here is 1050 μm .

In vivo confocal microscopy (IVCM) (Fig. 41 D) revealed multiple, hyperreflective, well-delineated filamentous structures with branches in the middle stroma, which thought to be fungal hyphae.

Topical antifungal and antibiotic treatment was advised.

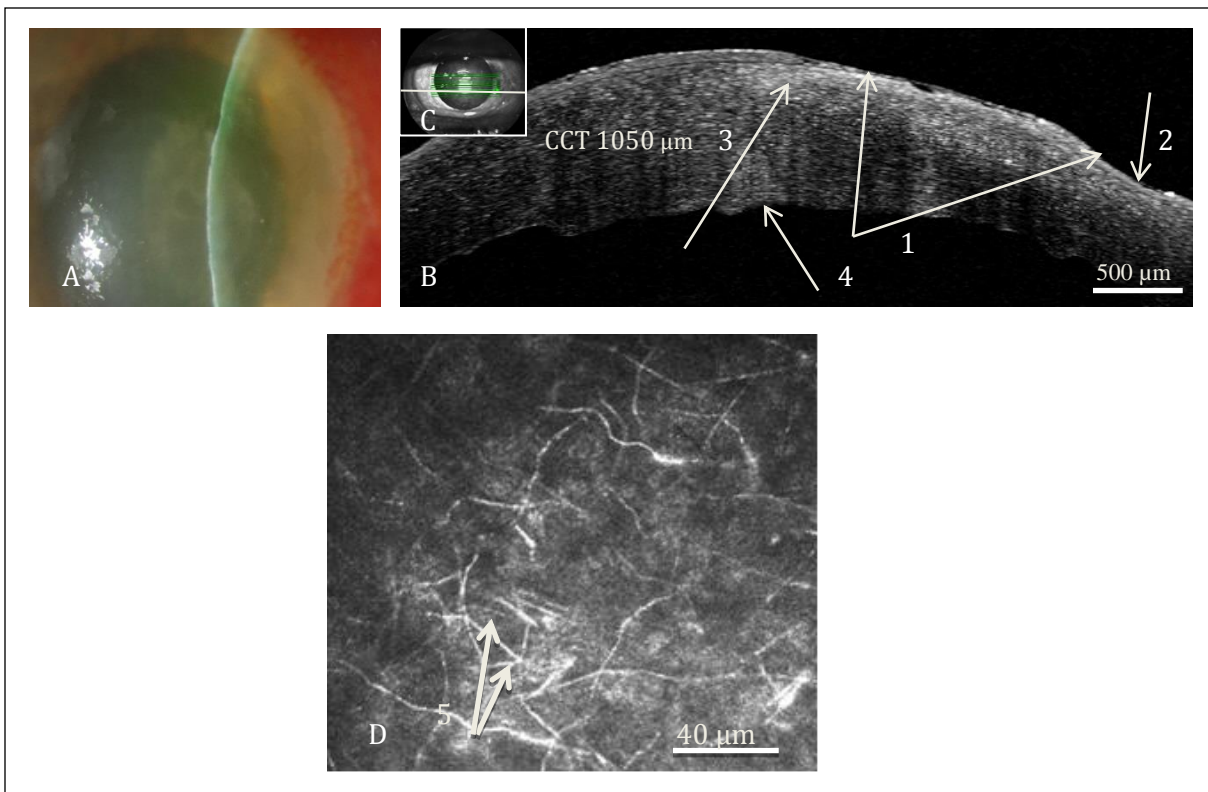


Fig. 41: (A) Slit-lamp photograph shows corneal clouding and descemet's membrane folds. (B) SD-OCT image illustrates epithelial defects (arrow 1), destruction of Bowman's membrane layer (arrow 2), hyperreflective structure in the superficial stroma corresponding to the area of the clouding. (C) shows the scan orientation. (D) IVCM shows multiple hyperreflective filamentous structures in the corneal stroma.

5.2.2.3 STROMAL KERATITIS

A 35 years old male complained of blurred vision with discomfort of the right eye since 2 days.

Slit-lamp examination (Fig. 42 A) revealed a central zone of stromal opacity with endothelial deposits.

SD-OCT scan (Fig. 42 B) showed multiple central hyperreflective rings (arrow1) in the epithelium, superficial and middle stroma corresponds to the corneal opacity and hyperreflective irregular descemet's membrane-endothelial complex (arrow 2). Destruction of Bowman's membrane was demonstrated.

Topical steroids treatment was recommended.

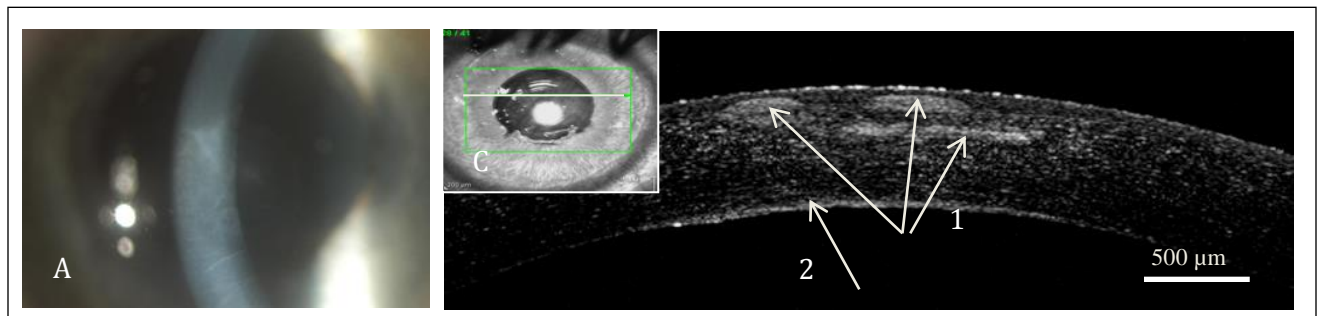


Fig. 42: (A) Slit-lamp photograph shows central stromal opacity. (B) SD-OCT image of the cornea demonstrates epithelial and superficial hyperreflective structures correspond to the corneal opacity (arrow 1) and irregular hyperreflective descemet's -endothelial complex (arrow 2). (C) shows the scan orientation.

5.2.2.4 CORNEAL FOREIGN BODY

A 25 years old male patient presented at our clinic following a partial removal of corneal foreign body from the left cornea and was symptomatically free.

Slit-lamp examination (Fig. 43 A) showed a paracentral remnant of foreign body embedded in the cornea with no evident signs of infection or inflammation.

SD-OCT scan (Fig. 43 B) revealed hyperreflective structure corresponding to the location of the foreign body up to more than half of the corneal stroma (arrow 1). Foreign body depth (FBD) was 380 μm , corneal thickness (CT) was 643 μm . Shadowing of the deep corneal layers (arrow 2) posterior to the foreign body was observed. Initially many trails to remove the foreign body from the cornea revealed unsuccessful results. Finally the decision undertaken was against the complete removal of the foreign body due to free optical axis and the existing risk of corneal perforation.

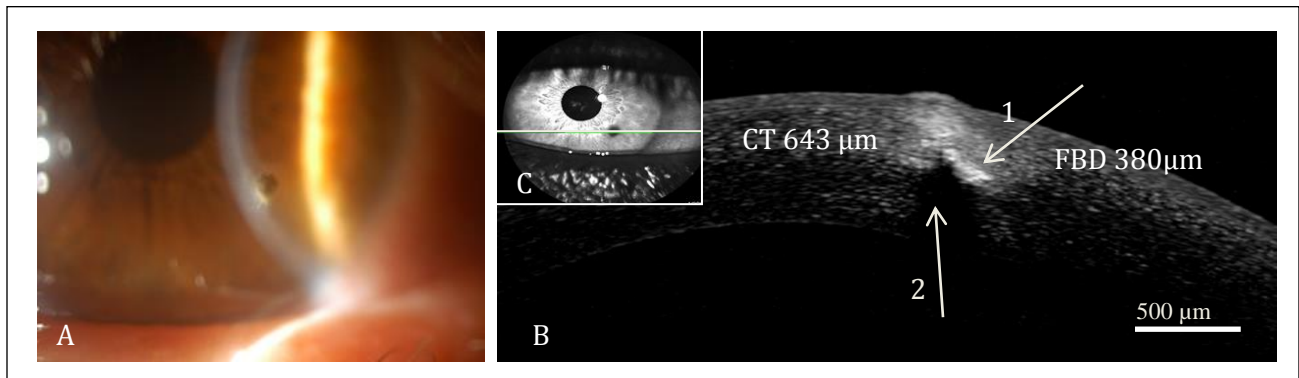


Fig. 43: (A) Slit-lamp photograph shows a paracentral remnant of corneal foreign body. (B) SD-OCT image reveals hyperreflective structure corresponds to the remnant of 1 foreign body (arrow 1) and shadowing of deep corneal layers (arrow 2). (C) shows the scan orientation.

5.2.2.5 CORNEAL SCAR

A 55 years old female patient complained of a decrease the visual acuity of the left eye.

Slit-lamp examination (Fig. 44 A) revealed a central corneal opacity.

SD-OCT scan (Fig. 44 B) showed hyperreflective irregular shaped structure in the corneal stroma up to descemet's-endothelial complex (arrow 1) corresponding to the scar tissue, destruction of the Bowman's membrane in the scar area (arrow 2) was detected. There was also a remarkable distortion of the posterior surface of the cornea (arrow 3). A decrease in the corneal thickness at the scar area was detected (CT 336 μm) while the corneal thickness of the neighboring area of the cornea was 530 μm .

Penetrating keratoplasty was recommended.

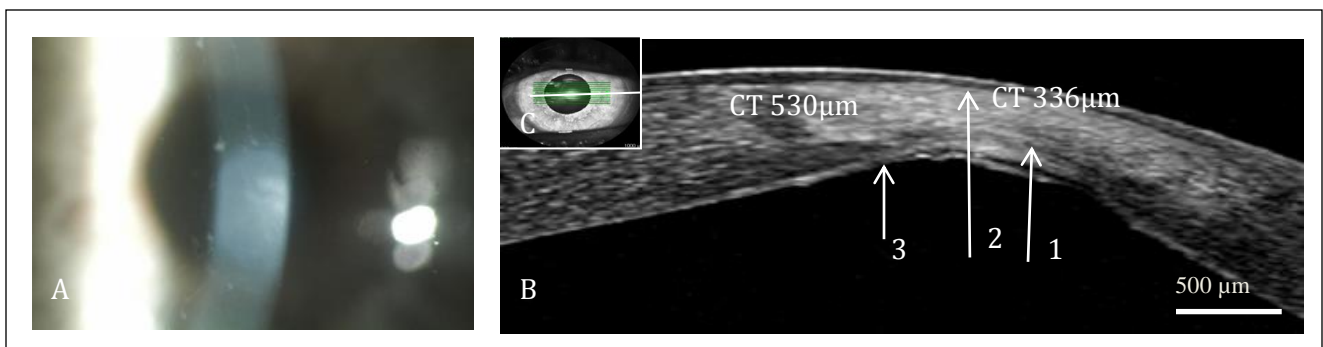


Fig. 44: (A) slit-lamp photograph shows central corneal opacity. (B) SD-OCT image demonstrates hyperreflective irregular structure in the stroma up to descemet's-endothelial complex (arrow 1), destruction of Bowman's layer (arrow 2) as well as distortion of the posterior border of the cornea (arrow 3). (C) The scan orientation.

5.2.2.6 GRANULAR CORNEAL DYSTROPHY

A 25 years old female patient referred to our clinic for Re- Phototherapeutic keratectomy (PTK) for both eyes, with the first PTK done before 5 years by granular corneal dystrophy. She was complaining of progressive visual loss since 1 month.

Slit-lamp examination (Fig. 45 A) showed small size gray stromal opacities.

SD-OCT scan (Fig. 45 B) showed small hyperreflective structures in the superficial stroma (arrow 1). Intact epithelium was detected (arrow 2). The depth of the stromal deposit was 80 μm . The central corneal thickness was (358 μm).

In vivo confocal microscopic (ICVM) examination (Fig. 45 D) revealed hyperreflective irregular material depositions in the level of Bowman's membrane and in the superficial stroma (Fig. 45 E).

Penetrated keratoplasty was recommended.

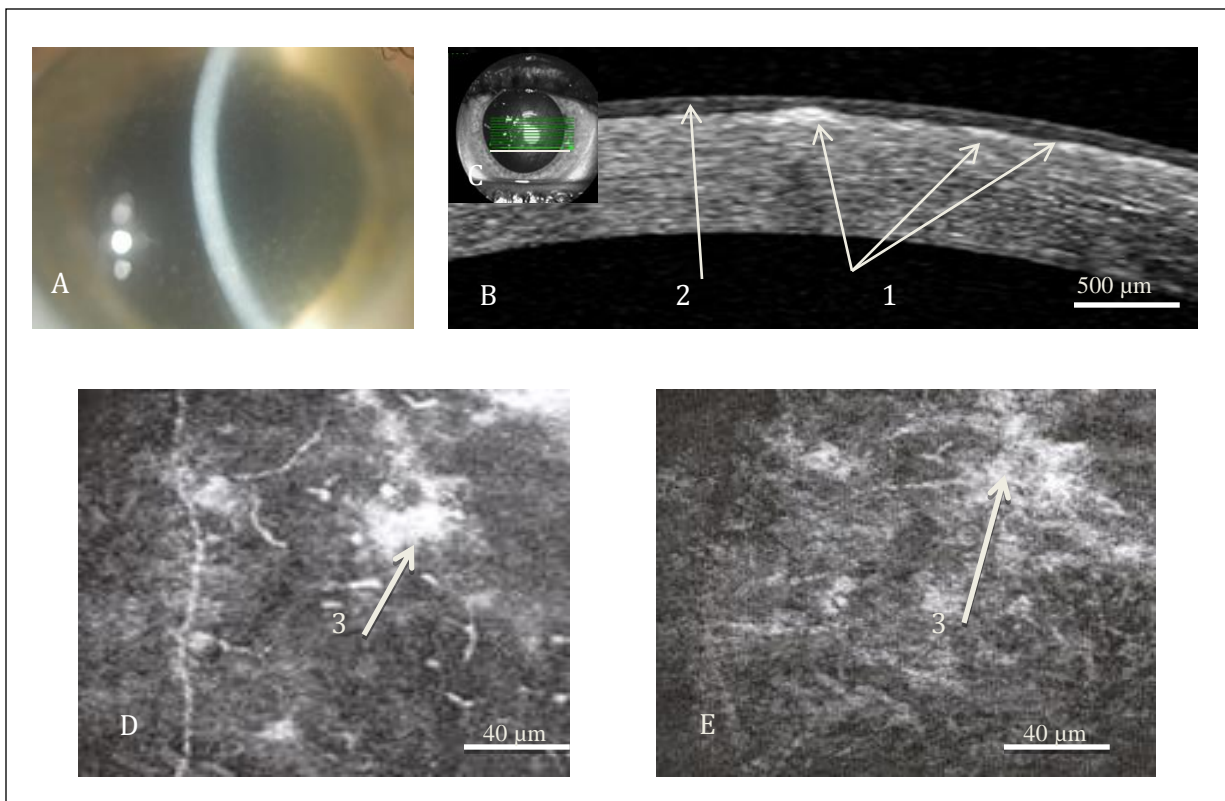


Fig. 45: (A) slit-lamp photograph shows small grayish stromal opacities. (B) SD-OCT image reveals superfascial stromal opacities (arrow 1) with intact epithelium (arrow 2). (C) The scan orientation. (D) ICVM illustrates hyperreflective star-like deposits in the Bowman's membrane (arrow 3). (E) ICVM shows highly reflective ill-shaped superficial stromal deposits.

5.2.2.7 KERATOCONUS

A 45 years old male patient presented to our clinic for planted follow-up of keratoconus of the left eye.

Slit-lamp examination (Fig. 42 A) showed positive both Munson's sign and Vogt's striae.

SD-OCT scan (Fig 42 B) revealed hyperreflective linear structure in the middle and deep stroma (arrow 1) which thought to be Vogt's striae with a decrease in the central corneal thickness (CCT 412 μm). Intact epithelium, Bowman's membrane, stroma and Descemet's membrane-endothelium complex was observed.

Corneal Cross-linking was advised.

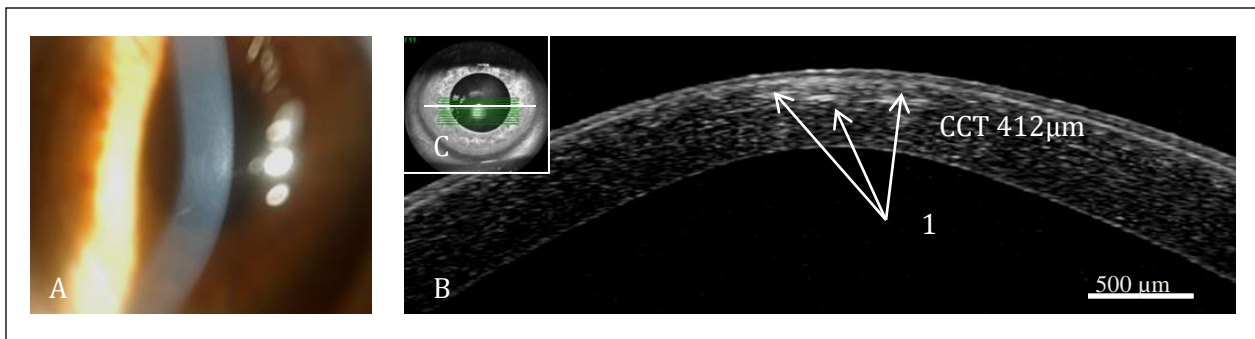


Fig. 46: (A) slit-lamp photograph shows Vogt's striae. (B) SD-OCT image demonstrates hyperreflective lines in the middle and deep stroma which could be Vogt's striae. (C) The scan orientation.

5.2.3 ENDOTHELIAL DISEASES

5.2.3.1 KERATITIS, ENDOTHELITIS

A 45- years old male patient sought treatment for a painful red right eye since 2 days. Slit-lamp examination (Fig. 47 A) showed moderate conjunctival injection, epithelial erosion, stromal edema, descemet’s membrane folds and endothelial deposits. .

SD-OCT scan (Fig. 47 B) revealed dot-like endothelial deposits which corresponds to keratic deposits (arrow 1) and ruffles of descemet’s-endothelial complex (arrow 2). Defect of the corneal epithelium and destruction of Bowman’s membrane was observed (arrow 3). Corneal thickness was (CT) (959.00 μm).

In vivo confocal microscopic examination (Fig. 47 D) illustrated hyperreflective star-shaped keratocytes in the superficial and middle stroma (arrow 4) and in (Fig. 47 E) multiple hyperreflective dots seemed to be clumped together in the endothelium (arrow 5). Topical antibiotics were recommended.

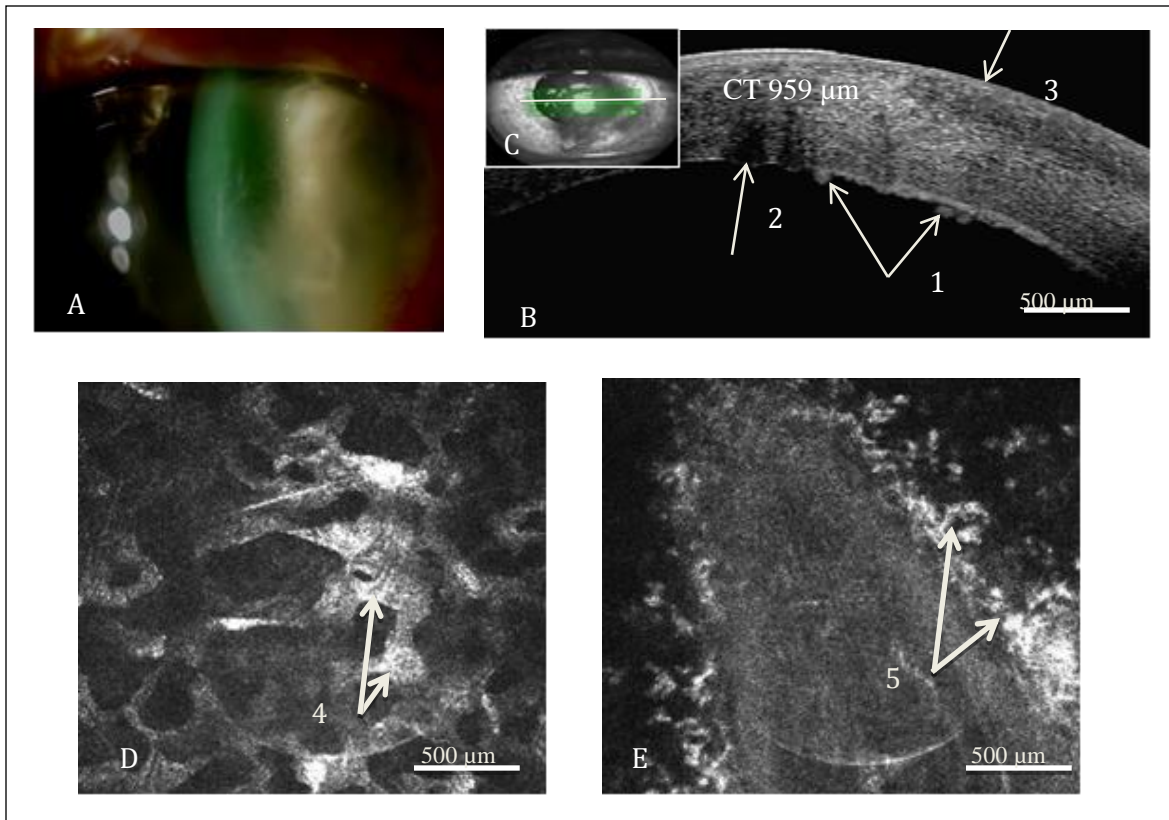


Fig. 47: (A) Slit-lamp photograph shows epithelial erosions with stromal edema and descemet’s folds. (B) SD-OCT image demonstrates dot-like endothelial deposits (arrow 1) with ruffles in the descemet’s-endothelial complex (arrow 2) and defect of the epithelium and destruction of Bowman’s layer (arrow 3). (C) shows the scan meridian. (D) IVCM reveals hyperreflective star-shaped keratocytes in the stroma (arrow 4). (E) IVCM demonstrates hyperreflective multiple dot-like endothelial deposits (arrow 5).

5.2.3.2 DESCemet'S MEMBRANE DETACHMENT

A 73 years male patient complained of no clinical improvement of visual acuity following a cataract surgery of the right eye since 1 week.

Slit-lamp examination (Fig. 48 A) showed stromal corneal edema and Descemet's membrane folds with no signs of infection.

SD-OCT scan (Fig. 48 B) showed a thread -like structure in the inferior cornea (arrow 1) which was diagnosed to be detachment of descemet's membrane with an increase in the central corneal thickness (CCT) (1055 μm).

On the following day the patient was subjected to intracameral air bubble injection. Postoperative slit-lamp examination (Fig. 48 D) demonstrated resolution of the corneal edema and a partially absorbed air bubble in the anterior chamber. Postoperative SD-OCT scan (Fig.48 E) showed a complete regression of the detachment of the descemet's membrane (arrow 2) and a remarkable decreased in the central corneal thickness (CT 704 μm).

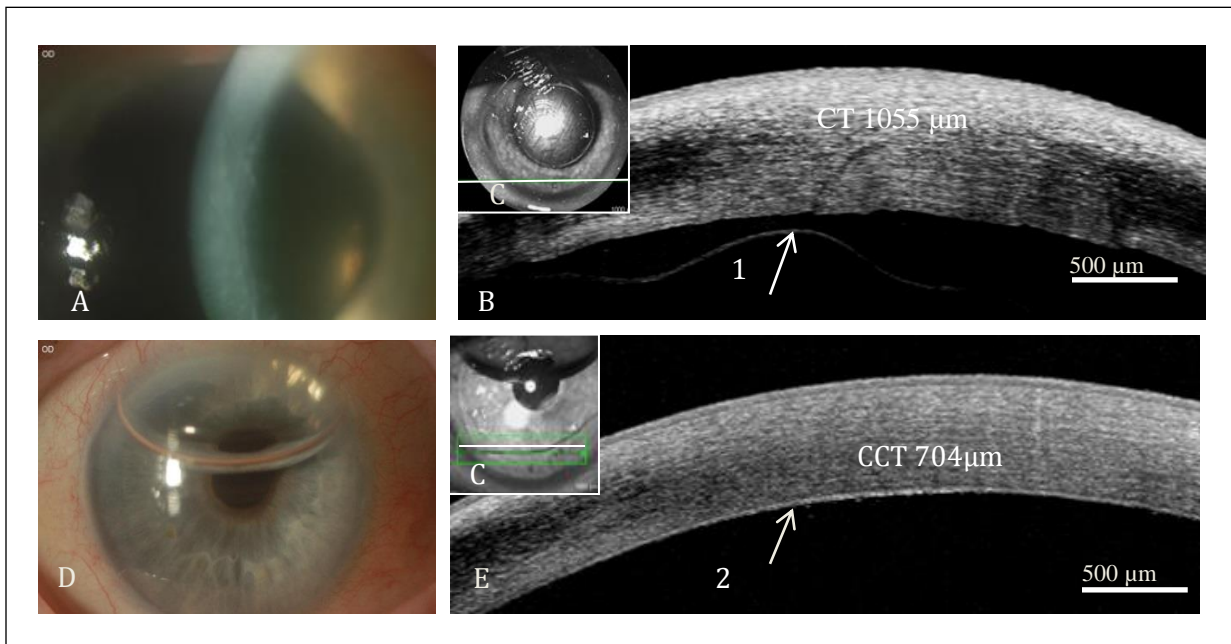


Fig. 48: (A) Slit-lamp photograph at presentation shows corneal stromal edema and Descemet's membrane folds. (B) SD-OCT image at presentation reveals a thread -like structure in the inferior cornea corresponding to detachment of Descemet's membrane (arrow 1). (C) shows the scan orientation. (D) Postoperative slit-lamp photograph illustrates incomplete resorbed air bubble in the anterior chamber. (E) Postoperative SD-OCT image shows a reattachment of descemet's membrane (arrow 2).

5.2.3.3 FUCHS' ENDOTHELIAL DYSTROPHY

A 55 years old male patient complained of reduction of visual acuity of both eyes.

Slit-lamp examination (Fig. 49 A) showed bilateral epithelial edema, stromal edema, descemet's membrane folds and cornea guttata, right eye more severe than left eye.

SD-OCT scan of right eye (Fig. 49 B) demonstrated hyporeflective elongated structure in the epithelial layer of the cornea (arrow 1) corresponding to epithelial edema, thickened Descemet's membrane-endothelial complex as well as ruffles of Descemet's membrane (arrow 2). Thickness of descemet's membrane-endothelium complex was 35 μm . An increase in the central corneal thickness (CCT 865 μm) was detected.

Penetrated keratoplasty was recommended.

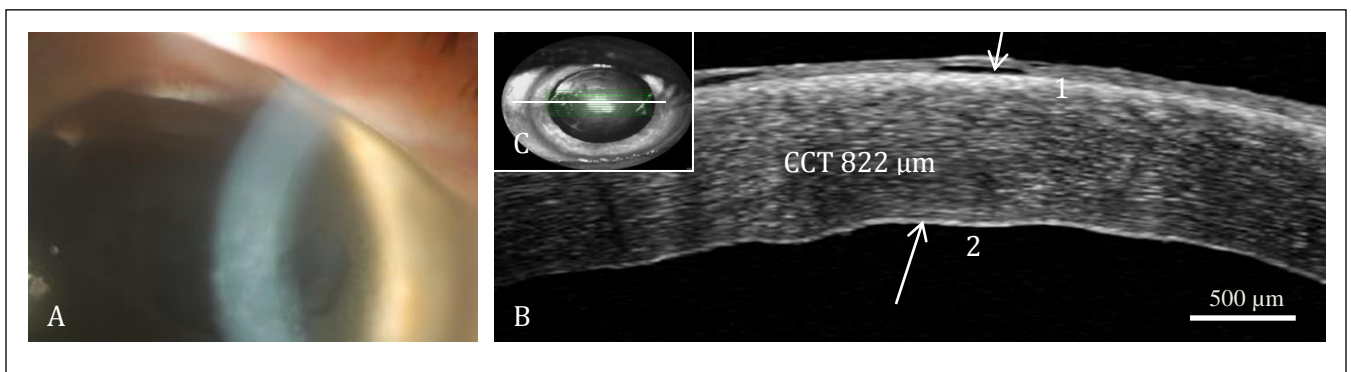


Fig. 49: (A) slit-lamp photograph of epithelial bullae and cornea guttata in patient with Fuchs's endothelial dystrophy. (B) SD-OCT image shows hyporeflective elongated structure in the epithelium (arrow 1) and ruffles in the Descemet's-endothelial complex and increase of the thickness of the descemet's-endothelial complex (arrow 2). (C) The scan orientation.

5.2.3.4 ASSESSMENT OF WOUND PROFILE AFTER PENETRATING KERATOPLASTY (PKP)

A 73 years old male patient presented to our clinic for a regular follow-up giving a history of a penetrating keratoplasty of the left eye for the past 15 years.

Slit-lamp examination (Fig. 50 A) demonstrated opacities of the corneal transplant with superfascial and deep vascularization of the left eye.

SD- OCT scan (Fig. 50 B) showed keratoplastic incision with endothelial wound gape (arrow 1), and epithelial wound alignment (arrow 2) and hyperreflective structure in the superficial stroma corresponding to corneal scar (arrow 3). Destruction of Bowman's membrane was observed. Corneal thickness in the wound area was 423 μm .

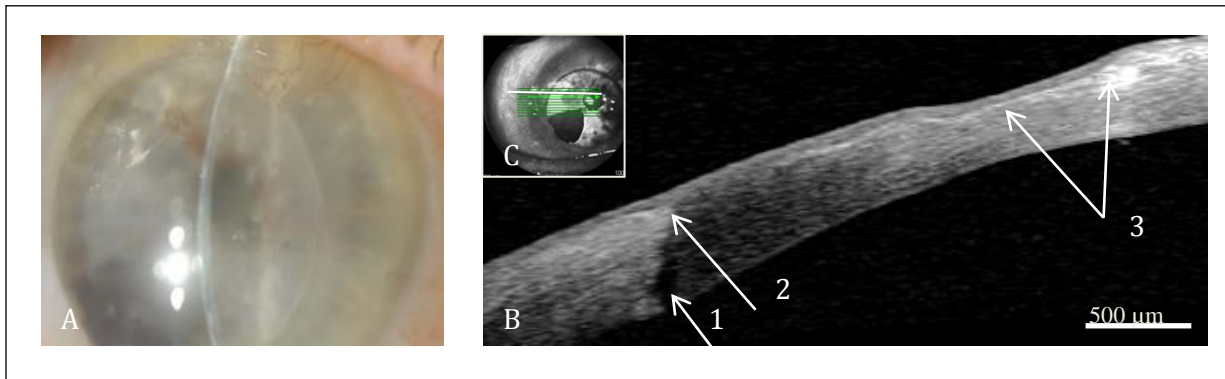


Fig. 50: (A) slit-lamp photograph shows opacified corneal transplant. (B) SD-OCT image reveals wound malapposition at the endothelial side (arrow 1), proper alignment of the wound at the epithelial side (arrow 2) and hyperreflective structure in the superficial stroma (arrow 3). (C) shows the scan orientation.

5.2.3.5 BULLOUS KERATOPATHY

A 55 years old male patient presented to our clinic with decrease in the visual acuity of the left eye for the past 3 years.

Slit-lamp examination (Fig. 41 A) showed epithelial edema with epithelial bullae associated with stromal edema.

SD-OCT scan (Fig. 41 B) illustrated hyporeflective elongated structure in the epithelial layer of the cornea (arrow 1) corresponding to epithelial edema and irregularity of the Descemet's membrane-endothelial complex (arrow 2). Intact stroma was observed (arrow 3) and intact precorneal tear film (arrow 4). Epithelial thickness was 60 μm and central corneal thickness was 720 μm .

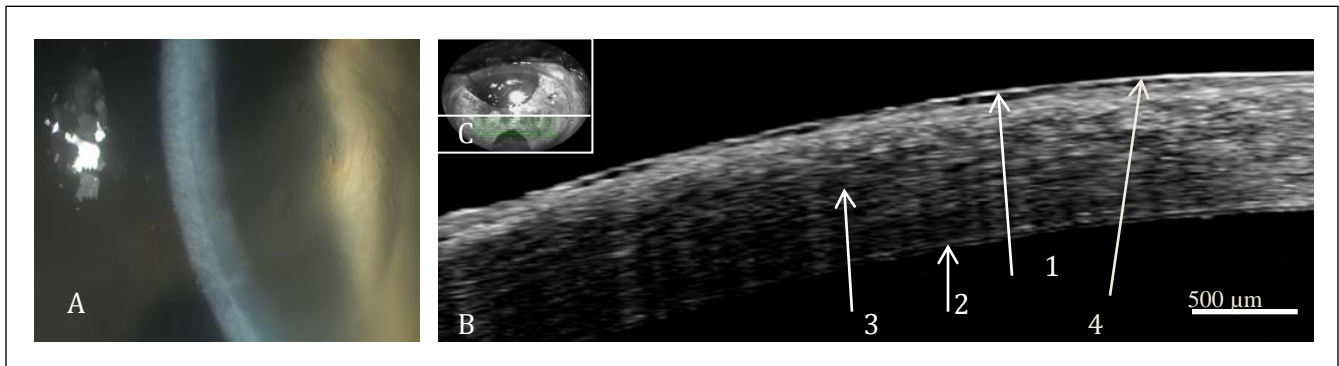


Fig. 51: (A) slit-lamp photograph shows stromal and epithelial edema with epithelial bullae (B) SD-OCT image demonstrates hyporeflective elongated structure in the corneal epithelium (arrow 1), irregular Descemet's-endothelial complex (arrow 2), intact stroma (arrow 3) and intact precorneal tear film (arrow 4). (C) The scan orientation.

6 DISCUSSION

6.1 HEALTHY CORNEA

Recent advances in the imaging techniques of ophthalmology has improved considerably in the past few years, but only selected techniques allow high resolution imaging of the anterior segment of the eye. Spectral domain optical coherence tomography (SD-OCT) provides high resolution cross-sectional imaging of the cornea in vivo and allows distinguishing the layered structure of the cornea for anterior segment morphometry as well as the objective quantification, localization and documentation of corneal pathologies. In contrast to other techniques, such as ultrasound biomicroscopy and confocal microscopy, SD-OCT as a non invasive and non contact technique, which does not require direct contact with the eye or immersion in saline solution usually provide detailed examination of the cornea. In the present study the SD-OCT was initially applied practically to obtain the OCT characteristics of healthy corneas prior to its use in the study of the diseased cornea.

The cornea is composed of 5 layers. Each layer reflects light differently according to variable indices of refraction. Findings from time-based corneal OCT images were found to be in good agreement with those of histologic sections.³³ Our SD-OCT images delineated 3 layers of the cornea (epithelium, Bowman's membrane and stroma) as separate entities, showed good correlation with well-known histologic and anatomical corneal norms and provided substantially improved detailed information when compared with the commercially available time-domain OCT images. The results in this study are comparable with those of Kaluzny *et al* who examined various corneal abnormalities using SD-OCT.³⁴

The measurement of central corneal thickness (CCT) is clinically important when assessing corneal disease because the corneal thickness varies with the endothelial cell health and function.³⁵ Furthermore, the central corneal thickness (CCT) is a widely used diagnostic parameter for planning refractive surgery, monitoring corneal ectasia like keratoconus, complementing intraocular pressure (IOP), calculating the risk of progression from ocular hypertension to glaucoma³⁶⁻³⁸, and studying corneal endothelial cell function after contact lens use.³⁹ CCT is also taken into consideration when collagen cross-linking treatment is performed for progressive keratoconus.⁴⁰ Hence, the accurate measurement of CCT is essential for

diagnosis and treatment of ophthalmic diseases. Several pachymetry devices are recently available for use in the ophthalmologic field such as ultrasonic pachymetry (USP)⁴¹, noncontact specular microscopy, scanning slit topography⁴², the rotating Scheimpflug camera⁴³ and optical coherence tomography (OCT)⁴¹ are recently available. Despite the fact that the common technique for measuring CCT is USP because of its established reliability and utility, but the direct contact with the cornea induces patient discomfort, increases the risk of infection, corneal epithelial damage and additionally introduces errors because of corneal compression or misplacement of the probe. Furthermore, the usage of topical anesthesia in the measurement of CCT with USP may induce chemical and mechanical changes in the CCT.⁴⁴ Thus; we may possibly reach to the conclusion that the usage of noncontact pachymetry devices has a greater likelihood of being advantageous.

Recently, anterior segment optical coherence tomography (AS-OCT) has been developed to image the anterior segment of the eye and provided noninvasive pachymetry as well as corneal mapping. Some comparative studies have been performed using commercially available types of AS-OCTs, namely, Visante-OCT (Carl Zeiss Meditec, Dublin, CA)⁴⁵, slit-lamp-OCT (Heidelberg Engineering, Dossenheim, Germany)⁴⁶ and RTVue-100-OCT (Optovue, Inc, Fremont).⁴⁷

Spectralis OCT is a spectral domain optical coherence tomography (SD-OCT) (Heidelberg Engineering, Heidelberg, Germany) which scans faster (40000 A-scans per second) and provides higher resolution (depth of resolution 7 μm , transvers resolution is 20 μm)² when compared with both time domain OCT (Visante OCT) (scan 2000 A scans/second , depth resolution 18 μm , Transvers resolution 60 μm)⁴⁵ and Fourier domain OCT (RTVue-100-OCT) (scan 260000 A-scan per second, depth resolution 5 μm and transvers resolution 15 μm).⁴⁸ SOCT has been recently introduced commercially in the clinical ophthalmologic practice. Therefore it is important to undertake research studies to compare this pachymetry device with the other established non contact methods for measuring the corneal thickness.

In this study, a comparison of the measurement of central corneal thickness (CCT) was undertaken with the relatively new method (SD-OCT) and also with those established methods (rotating Scheimpflug Pentacam camera and AC Master). The correlation and agreement between the three devices as well as the estimation of the thickness of different corneal layers was

analyzed and discussed. In table 14 we summarized and compared the results of the thickness of different corneal layers assessed by SD-OCT and other different devices in the previous studies.

Table 14: Summary of various studies on different corneal layers thickness (mean \pm SD) in μm

| Literature | CCT | ET | BMT | ST | Technique |
|-------------------------|------------------|----------------|----------------|------------------|------------------------|
| Our study | 545.6 \pm 34.9 | 39.9 \pm 6.0 | 11.7 \pm 2.1 | 496.6 \pm 34.8 | SD-OCT |
| Prakasam [37] | 538.0 \pm 21.7 | 48.2 \pm 2.3 | 10.4 \pm 0.7 | - | SD-OCT |
| Li [49] | - | 52.3 \pm 3.6 | - | - | FD-OCT |
| Germundsson [50] | - | - | 9.1 \pm 1.4 | - | Confocal microscopy |
| Tao [51] | - | 52.5 \pm 2.4 | 17.7 \pm 1.6 | - | Ultra-high SD-OCT |
| Ou [52] | 563.6 \pm 35.8 | - | - | - | Orbscan |
| Park [53] | 535.8 \pm 40.7 | - | - | - | Orbscan |
| Park [53] | 544.5 \pm 30.7 | - | - | - | Pentacam |
| Park [53] | 541.8 \pm 31.3 | - | - | - | Ultrasound pachymetry |
| Al-Mezaine [54] | 516.2 \pm 40.6 | - | - | - | Ultrasound pachymetry |
| Al-Mezaine [54] | 522 \pm 42.2 | - | - | - | Pentacam |
| Hashemi [55] | 555 | - | - | - | Ultrasound. Pachymetry |
| Wong [56] | 555.9 \pm 32.4 | - | - | - | Orbscan |
| Muscat [57] | 526 \pm 28 0 | - | - | - | OCT |
| Bechmann [1] | 530 \pm 32 | - | - | - | OCT |
| Bechmann [1] | 581 \pm 34 | - | - | - | Pachymetry |
| Li [58] | 538.8 \pm 26.2 | - | - | - | AS-OCT |
| Li [58] | 553.2 \pm 25.5 | - | - | - | Orbscan |
| Li [58] | 553.5 \pm 30.3 | - | - | - | Ultrasound pachymetry |

Our results of Bowman's membrane thickness (BMT-OCT), stroma thickness (ST-OCT) and central corneal thickness (CCT-OCT) was found to be compatible with the thickness values using the different measurement techniques^{1, 29, 49-58}, but on the contrary our epithelial thickness (ET) was documented to be lower than those reported in the literature. In the all previous literature reports used OCT instrument for CCT measurement, the CCT was taken from the front boundary to the back boundary curves of the cornea on a delineated cross-sectional image which includes the precorneal tear film layer.⁴⁸ Our measurement software program (MATLAB) enables us to take accurate measurement of corneal layers thickness by exclusion of the precorneal tear film layer, thus minimizing the overestimation of corneal thickness or the subjective error which results from using the caliber tools of the device in the thickness measurements. Therefore we can probably explain that our low epithelial thickness value may be due to the fact of this exclusion of the tear film layer. Prakasam *et al*²⁹ reported that the values of ET was 48.2 μm . Although the same OCT device (SD-OCT) and the same measurement's program (MATLAB) was used, they obtained higher ET values than the ones recorded in our study. In Prakasam's report the ET was measured between the inflection point on the descending peak of the first maximum and inflection point on the descending peak of the second maximum and the BMT was measured between the inflection point on the ascending peak of the second maximum and inflection point on the descending peak of the second maximum. This clearly explains the fact that the Bowman's membrane was included in their epithelial thickness measurement, and consequently accounts for the observed differences between the two values of the ET of both studies.

We found a high correlation between the SD-OCT and Scheimpflug camera in CCT measurements ($r = 0.938$) taking into account the reference to the correlation between the different devices. Although the CCT measured by SD-OCT was statistically significantly lower than that obtained by Scheimpflug camera with a mean difference of 8.03 μm ; but several studies reported compatible results with our findings. Ishibazawa *et al*⁴⁸ reported that the FD-OCT underestimated the CCT in comparison with Pentacam with a mean difference of 22 μm . Gorgun *et al*⁵⁹ also reported that the CCT measured by both Visante-OCT and Slit-lamp-OCT was lower than that obtained by Pentacam. On the contrary Ponce *et al*⁶⁰ demonstrated that, there was no significant difference in CCT measurement between Pentacam and Visante-OCT. On the contrary O'Donnell *et al*⁶¹ reported that the Pentacam gave higher values of CCT than Visante-

OCT. These conflicting results in the literature reports of Pentacam and AS-OCT in CCT measurement requires further future research to be undertaken to solve these problems.

The rotating Scheimpflug camera measures the corneal thickness between the air–tear film interface and the posterior corneal surface.⁶² This could be explained by the fact that the high resolution of the SD-OCT has lead to better identification of corneal edges and may probably have resulted in the underestimation of the CCT measured by SD-OCT when compared with the CCT obtained by Scheimpflug camera.

Although ultrasound pachymetry considered as the standard technique for CCT measurement, some noncontact techniques such as AS-OCT, Scheimpflug camera, AC Master and Orbscan have become available in the in the ophthalmologic field. Several published studies compared the CCT measurements between Pentacam and Ultrasonic Pachymetry⁵⁵, Pentacam with different models of AS-OCT⁴⁶, Ultrasonic pachymetry with AS-OCT⁵⁹, AS-OCT with Orbscan⁵⁶ and Pentacam with AC Master⁶⁴ with different levels of agreement between the methods. But to our knowledge, there are no previous reports conducted on the comparison of the CCT that assess the agreement between the AS-OCT system and AC Master in normal eyes. To the best of our knowledge, this is the first baseline study conducted to assess the comparison of the CCT and to estimate the agreement between the AS-OCT system and AC Master in normal eyes where the results revealed also a high correlation between both devices ($r = 0.958$), although there was an underestimation of the CCT by AC Master when compared with that measured by SD-OCT (mean difference of 14.0 μm). The AC-Master measures corneal thickness (CT), anterior chamber depth (ACD), and lens thickness (LT) from a single point of the cornea (usually the centre) in one step by the PCI method.³⁸ The measurement with AC Master turned out to be more complicated, time consuming and needs expert examiner when compared with the SD-OCT or the Scheimpflug camera. It is not yet obvious until this current time whether the statistically significantly low CCT value measured by AC Master was due to the results of the different measurement principles or erroneous measurements with the AC Master.

The results of agreement in the current study assessed by Bland-Altman plots showed that the SD-OCT and AC Master instruments tended to have the best agreement for the CCT with 95% limits of agreement (LOA) from -5.2 to 34.2 μm and magnitude of 95% LOA of 39.4 μm . The Scheimpflug tended to provide higher readings for CCT compared with the SD-OCT and AC

Master with 95% LOA from -31.8, to 15.8 μm , 0.5 to 44.5 μm and span of the 95% LOA of 47.4 μm and 45 μm for SD-OCT-Scheimpflug and Scheimpflug-AC Master respectively.

O'Donnell *et al*⁶³ reported a wider 95% limits of agreement (LOA) and found that the 95% LOA between Visante-OCT and Pentacam were 25.61 μm to -49.11 μm with magnitude of the LOA of 74 μm , while Chen *et al*⁶⁵ documented a narrower 95% LOA and found that the 95% LOA between FD-OCT and Pentacam were -0.7 to 22.5 μm with magnitude of 95% LOA of 23.2 μm . Until this current study there are no previous reports that studied the assessment and the correlation between the SD-OCT and AC Master.

To determine the CCT on the corneal cross-sections obtained from AS-OCT, it is very important to take the AS-OCT cross sections in the centre of the cornea. If the sections do not pass through the centre of the cornea, CCT values will be overestimated. Thus, we did make the assurance that our SD-OCT cross sections passed through the centre of the pupil. The variations between studies are also likely to be affected by variability in the identification of the corneal epithelium and endothelium and during measurement and exclusion of the precorneal tear film from the measurement, as all studies that used AS-OCT to estimate the CCT measured the thickness by using the calibre tools of the software program of the device. The developed software program with MATLAB conducted in the present study enabled us to determine exactly point to point distance measurement of the different corneal layers and CCT and resulted in the reduction of subjective error in thickness estimation.

We found some discrepancies in the agreement results between the methods that could be due to the use of different models of anterior segment optical coherence tomography (AS-OCT) in the CCT measurement. This discrepancy could be of clinically relevance during the evaluation of patients. Doughty *et al*⁶⁶ reported that a 10% difference in CCT would result in a 3.4 mmHg difference in intraocular pressure. On other hand overestimation of the CCT may lead to serious complications in patients undergoing refractive surgeries, whereas underestimation could lead to exclusion of patients from refractive procedures. Consequently, these discrepancies indicate that CCT measurement with these devices are advised not be used interchangeably in the clinical practise in spite of the existence of a high correlation coefficient.

Aging generates structural and functional changes in the cornea including changes in the shape, optical and physical properties, degenerative changes, cellular and innervation density changes.^{67,68} Steepening of the keratometry, shift from with to against the rule of astigmatism and increase in the Descemet's membrane thickness was reported by Faragher *et al.*⁶⁷ Corneal wound healing has been observed to decline with age and age affects the refractive outcomes and visual acuity following laser refractive surgery.⁶⁹ Niederer *et al.*⁶⁸ observed a decrease in the keratocyte density, nerve fiber density and endothelial cell density with age. He also reported no significant alteration in the epithelial cell density with age. The association between the CCT and the thickness of different corneal layers measured by SD-OCT instrument was analysed with age. There was no significant correlation between the ET-OCT ($r = 0.11$, $P = 0.2$), BMT-OCT, ($r = 0$, $P = 0.9$), ST-OCT ($r = 0.03$, $P = 0.7$) and CCT-OCT ($r = 0.06$, $P = 0.5$), with the age. Similar results reported by Faragher *et al.*⁶⁷, Wong *et al.*⁵⁶, Bechmann *et al.*¹, who found no significant association between the CCT and the age. In contrast Alsbirk *et al.*⁷⁰, Nissen *et al.*⁷¹ and Lam *et al.*⁷² reported negative correlation between the CCT and the age using ultrasound pachymetry. Several researchers studied the relationship between the CCT and age using different measurement techniques. To the best of our knowledge, this is the first time to study the association of the thickness of the different corneal layers and the age.

In this study, there was also no significant correlation between the thickness of different corneal layers and CCT measured by SD-OCT and gender and the right or left eye. Regarding the association between the CCT measured by Scheimpflug camera and AC Master with age, gender and left / right eye, there was no statistical significant difference in the CCT measurements in the age, sex and right / left eye regardless the device which we was used and these findings were similarly reported by Wong *et al.*⁵⁶, Alsbirk *et al.*⁷⁰, Nissen *et al.*⁷¹ and Lam *et al.*⁷²

6.2 CORNEAL PATHOLOGIES

Slit-lamp examination is the standard technique for corneal examination, but it is highly subjective and depends on the experience of the examiner, therefore many technologies were recently introduced to improve the clinical evaluation of the cornea.

Confocal microscopy is the most powerful *in vivo* imaging modality which resolve the structure and the cellular level of the corneal tissue.⁷³ The examination with confocal microscopy is non invasive, but patient's preparation includes the use of topical anaesthesia, coupling immersion technique and the examination is somewhat complicated requiring an expert examiner. In addition, confocal microscopy cannot generate cross-sectional images for the clinical analysis.

SD-OCT is a non invasive and non contact technique that provides rapid, high resolution, detailed cross-sectional images of the cornea and anterior segment of the eye. In our study we showed that the SD-OCT device possessed several characteristics that support the diagnosis of different corneal pathologies, facilitate the decision-making, allow the successful planning of refractive procedures and improve the postoperative follow up.

The SD-OCT scan in the patient with corneal degeneration unclear dignity (case 5.2.1.1) provides the opportunity to analyse *in vivo* the morphologic properties of the cornea with high resolution similar to histologic images as it importantly revealed an intraepithelial lesion with an intact Bowman's membrane underneath. By using slit-lamp biomicroscopy, this picture may lead to the diagnosis of Salzmann nodular degeneration. Salzmann nodular degeneration is a non-inflammatory progressive corneal degeneration characterized by elevated, whitish-gray subepithelial nodules.⁷⁴ Although Salzmann nodular degeneration can be asymptomatic, it can cause severe pain, irritation, irregular astigmatism, and significant decrease in visual acuity.⁷⁵ Histologically, it was reported that, the destruction of Bowman's membrane layer is the most significant morphologic properties of Salzmann nodular degeneration⁷⁶ which was unfortunately not detected in our case. Because of the good visual acuity and the peripheral location of the lesion the patient did not require surgical intervention.

Other important feature of the SD-OCT was its usefulness when the corneal epithelium is injured that creates a difficulty for the practical application of the direct contact with the cornea. In this study SD-OCT was practically applied safely and comfortably in patients with corneal keratitis,

epithelial erosions and perforated corneal ulcer. In the patient with perforated corneal ulcer (case 5.2.1.2) the corneal perforation and the iris tamponed were obviously observed by the slit-lamp examination but the epithelial bridge and the area with iridocorneal touch were obscured. In this aspect, the SD-OCT provides detailed visualization and high-resolution documentation without contact with the ocular surface. Postoperatively the slit-lamp and fluorescein staining were previously used to evaluate the epithelial healing after amnion membrane transplantation,^{77, 78} but this method of examination provides very limited information. SD-OCT examination was valuable in the postoperative follow up as shown in this case after multilayered amnion membrane transplantation for postoperative monitoring the corneal healing process, corneal stroma-amniotic membrane tissue modification and integration of amniotic membrane with the corneal tissue as well as the recovery of a stable and regular anterior chamber.

In the cases of keratitis SD-OCT scan provided a vast range of qualitative and quantitative informations which allow the objective assessment of the keratitis severity, monitoring the course of the disease and the response to the treatment. SD-OCT images the stromal infiltrations as hyperreflective area, so the infiltration's parameters such as thickness and width can be measured as shown in the case of keratitis associated with contact lens wear (case 5.2.2.1) and the case of stromal keratitis (case 5.2.2.3). Stromal edema is visualized in the SD-OCT image as a diffuse thickening of the corneal stroma that leads to increase in the corneal thickness. Also Descemet's membrane folds can be imaged as ruffles in the normally smooth Descemet's-endothelial complex. When the infection and inflammation were resolving, a reduction in the corneal thickness was observed and formation of permanent opaque corneal scar, as detected in case of keratitis associated with contact lens wear after treatment (case 5.2.2.1), was resulted. In the case of fungal keratitis (case 5.2.2.2), the patient was initially treated with antibiotics as he was diagnosed as bacterial keratitis. Reiterative scans with SD-OCT demonstrated increase in the corneal thickness prior to its detection by slit-lamp examination and before the deterioration become clinically apparent. In vivo confocal microscopic (IVCM) examination for this patient revealed multiple hyperreflective filamentous structures in the superficial and deep stroma, which was consistent with fungal element. Then the patient was treated with topical antifungal eye drops.

Additional quantitative information which could be helpful in the assessment of keratitis could be provided by SD-OCT was the imaging of the deeper corneal layer changes. SD-OCT imaged the inflammatory cells as aggregation on the endothelial surface of the cornea forming keratic precipitates. This pathologic feature was detected in the patient with Endothelitis (case 5.2.3.1) suggesting that the source of inflammation was the endothelium. In vivo confocal microscopic examination of this patient confirmed this information as it revealed multiple, hyperreflective, greasy, dot-like deposits in the endothelial layer of the cornea that was highly suggestive of endothelial inflammation.

The unique depth measurement ability of the SD-OCT device was clinically important for planning the therapeutic method in removal of the corneal foreign body as in case 5.2.2.4. Corneal foreign bodies have been reported to be the second most common type of eye injury; comprising approximately 30.8% of ocular injuries.⁷⁹ In our case the exact estimation of corneal thickness and the depth of corneal foreign body were the reason of not removing the corneal foreign body completely because of the existent of the high risk of corneal perforation, asymptomatic patient and the free optical axis. Although this clinical information could be given by high-frequency ultrasound biomicroscopy (UBM),⁸⁰ it would be not be preferable in to use UBM in a patient with perforated eye injury, because of the risk of contamination. Additionally, the examination with SD-OCT was faster and with better resolution than UBM. In other cases with ocular trauma Wylegala *et al*⁸¹ founded that the AS-OCT may reveal unexpected lesions that are invisible to recognize in routine slit-lamp examination.

Granular corneal dystrophy (GCD) is a rare bilateral, non inflammatory, progressive, autosomal-dominant corneal disease characterized by discrete, gray-white, irregular-shaped opacities between the lamellae of the corneal stroma.⁸² The number and the size of these gray-white opacities gradually increase over the life time of the patient resulting in visual impairment.⁸³ Diffuse corneal infiltrates may obscure the clinical differentiation between anterior and deeper stromal opacities in advanced corneal dystrophies, making the decision for penetrating keratoplasty (PK) or phototherapeutic keratectomc (PTK) difficult. The scars or opacities within the optical zone are well known to generally respond effectively to ablative laser treatment such as phototherapeutic keratectomy (PTK), but only if they can be removed while maintaining a minimal corneal thickness of 300 μm including the epithelium.⁸⁴

In our patient with granular corneal dystrophy (case 5.2.2.6) the SD-OCT assessed the anatomic morphology of the cornea, visualized deposits in the corneal stroma, and measured exactly the depth of these intrastromal infiltrates (80 μm) as well as the total corneal thickness which was 318 μm . In another case with corneal scar (case 5.2.2.5) was the corneal thickness 358 μm . In both cases because of the exact estimation of the corneal thickness estimated around 300 μm was the principal reason of choosing the penetrating keratoplasty as alternative therapeutic option to the phototherapeutic keratectomy.

Although corneal topography is the standard method for early diagnosis and control assessment of keratoconus, it has significant limitations as it requires regular corneal surface.⁸⁵ SD-OCT technique is a reliable method in the evaluation and assessment of the pachymetrical profile of the corneal cross-sections of patient with different stages of keratoconus before exposing patients to lamellar keratoplasty and cross-linking. This has given the authors the opportunity to measure the exact corneal thickness as shown in the patients with keratoconus (case 5.2.2.7 and case 5.2.1.7) which is the most important value in exclusion of patients who exhibit corneal thickness less than 400 μm at the thinnest point of the cornea from the cross linking. Doors *et al*⁸⁶ demonstrated the usefulness of AS-OCT to detect the corneal cross-linking demarcation line that could be found within the first month after the treatment and could be related to the effectiveness of the treatment.

The most useful information obtained from SD-OCT imaging was for the deep corneal layers as in the patient with descemet's membrane detachment (case 5.2.3.2). Descemet's membrane detachment (DMD) is a rare but potentially vision threatening complication of intraocular surgeries usually in relation to cataract, glaucoma and corneal surgeries such as penetrating keratoplasty (PKP), and deep anterior lamellar keratoplasty (DALK).⁸⁷ DMD with mild corneal edema could be observed by slit-lamp biomicroscopy. However, it is difficult for clinicians to find direct evidence for DMD when obvious corneal edema exists. Once DMD is confirmed, swift action is imperative so as to avoid irreversible vision impairment due to endothelial pump failure.⁸⁸ Repair techniques for treating DMD include injecting air or other gases such as SF₆ and C₃F₈ in the anterior chamber, repositioning with viscoelastic substances, manual repositioning and suturing the DM to the corneal stroma.⁸⁹ In our case SD-OCT imaging proved its usefulness in detecting the position and the extent of DMD which allows us to prepare the surgical plan more appropriately, and monitor the outcomes of the treatment.

Fuchs' endothelial dystrophy is characterized by cornea guttata, an accelerated loss of endothelial cells resulting in corneal edema and finally loss of visual acuity.⁹⁰ The disease is clinically diagnosed by slit-lamp examination and confirmed by corneal thickness measurement which reveals increase in the corneal thickness by corneal edema, additionally endothelial cell evaluation by confocal microscopy could be done.⁹¹ Histologically, the endothelium in Fuchs' dystrophy produces excessive amount of abnormal basement membrane resulting in a thickened Descemet's membrane (DM).⁹² Thus the study of the characteristics and the thickness of DM in vivo could be essential to understanding better the role it plays in the pathogenesis and progression of Fuchs' endothelial dystrophy. SD-OCT in our study revealed an increase in the Descemet's membrane-endothelium complex thickness in all patients with Fuchs' endothelial dystrophy (case 5.2.3.3). This finding was in agreement with Abou Shousha M. *et al*⁹³ who reported a highly significant thickening of DM in Fuchs' endothelial dystrophy patients compared with normal subjects by using Ultra-High-Resolution OCT. This result could provide new insights into the disease and a method to start exploring the natural history and perhaps generating a treatment based on a better ability to predict the prognosis of the disease.

Penetrating keratoplasty (PKP) has enjoyed a relatively high success rate compared with transplantation of other tissue. The visual outcome is compromised by high resultant spherical ametropia and high regular or irregular astigmatism.⁹⁴ This could be the result of incorrect graft-host matching or imprecise wound apposition. In an earlier study that analysed the graft-host junction was found that 60.8% of all the graft-host junctions had internal graft-host malappositions.¹⁰² Until recently, the ability to clinically determine the graft-host apposition was based on the clinical examination of the epithelial side of the wound which is usually not indicative of the amount of wound malapposition and consequently the wound strength. In the present study we assessed the wound profile of a patient who underwent full thickness corneal transplantation (case 5.2.3.4). SD-OCT scan detected internal graft-host malapposition, while external graft-host apposition was observed. This is most probably due to the alignment of the anterior surface during intraoperative suture placement, while the posterior surface remained mismatched. Jhanji *et al*⁹⁵ reported that the intraocular pressure (IOP), final refraction and final visual outcome were all significantly correlated with the presence and the size of the wound malapposition. In addition, AS-OCT proved its usefulness in the new generation of corneal transplantation procedures such as full-thickness penetrating keratoplasty with incisions shaped

by femtosecond lasers, Descemet stripping endothelial keratoplasty (DSEK) and deep lamellar endothelial keratoplasty (DLEK). It can further image the creation of donor flap and measure the corneal layers thickness profile prior to DESK and DELK. Moreover it can detect the interface abnormality, verify the graft detachment and visualize the donor button dislocation postoperatively.¹⁰⁴

The relationship between the ocular surface and contact lenses (CL) is of primary relevance for researchers and clinicians as it plays a significant role in lens comfort and safety of the ocular surface. Traditional methods to evaluate such a relationship rely mainly on fluorescein staining of the tears.⁹⁷ However, a recent study demonstrated that only 61–67% of experienced practitioners can correctly identify the static fluorescein pattern of an ideally fitted contact lens.⁹⁸ Currently, there are three technologies that could potentially be used for visualization of contact lens-ocular surface relationship. The first one is high-frequency ultrasound imaging. The main disadvantage of this technique is essential use of the immersion bath, which can change examination conditions.⁹⁹ The second possibility is the Scheimpflug camera¹⁰⁰, however it was reported that it is not capable for visualizing a contact lens on the ocular surface, probably due to the very low scattering of lens material.³⁴ The third technique that might be considered is AS-OCT. It is analogous to conventional ultrasonic imaging, except that AS-OCT does not require direct contact with the investigated tissue. We found that the SD-OCT is a very useful tool in contact lens practise as it can investigate the contact lens-cornea relationship as shown in the patients with soft and hard contact lens (case 5.2.1.6 and 5.2.1.7) where the areas in which the lens touches the cornea and the lens shows clearance with the cornea were evident. Also it allowed us to measure accurately post-lens tear film thickness as in the case 5.2.1.6. This is particularly important in modern complex lens designs for advanced treatment of corneal abnormalities and correction of refractive error by corneal refractive therapy through the application of contact lens overnight. Furthermore, SD-OCT can measure in vivo the CL parameter changes such as lens thickness, diameter, and radius that can change the fitting relationships with the ocular surface when subjected to the physiological conditions of tears compared with the in vitro evaluation.¹⁰¹ Also in several applications such as the use of therapeutic contact lens or when assessing the effect of contact lens on the corneal physiology, SD-OCT provides the possibility of measuring the corneal response without need to remove the lens.¹⁰² Other interesting issue related to the properties of the contact lens materials is the

difference in the reflectivity profile. It was documented that the hard contact lens material provides a lower reflectivity pattern than the soft contact lens material. Moreover, SD-OCT could also be helpful in diagnosis, evaluation and documentation of contact lens complications as in the case of keratitis associated with contact lens wear (case 5.2.2.1). There is a greater likelihood that the SD-OCT technology will have a positive impact on the understanding and CL fitting will improve the customization specially in corneas with complex geometries as in keratoconic, traumatic, and ectatic eyes.

When the scanning beam is perpendicular to the tissue structure, reflectivity is very high. The tissue orientation combined with the large difference in refractive index between air and the tear film creates a high level of reflectivity observed centrally in the tear film.⁹⁶ An increase in the light reflectivity in the SD-OCT images corresponds to surgical incisions, corneal scarring, dens infiltration, deposition of hyalinized or basal membrane material and corneal edema. A decrease in the light reflectivity was due to fluid accumulation in the potential spaces as in bullous keratopathy (case 5.2.3.5), epithelial edema (case 5.2.1.4) and Fuchs' endothelial dystrophy (case 5.2.3.3) or shadowing such as in keratitis associated with contact lens (case 5.2.2.1) and corneal foreign body (5.2.2.4).

Our SD-OCT device was also beneficial for the digital documentation for patients with recurrent epithelial erosion (case 5.2.1.3), epithelial edema (case 5.2.1.4) and dry eye syndrome (case 5.2.1.5).

Recently Kieval et al¹⁰³ reported that the AS-OCT may have potential in the non invasive diagnosis and surveillance of patients with ocular surface squamous neoplasia, as it showed an excellent correlation with the histopathologic examination. It could be also used as a non invasive technology to monitor for the recurrence after surgical exision or medical treatment. The application of AS-OCT in evaluation of ocular diseases in paediatric population has been reported by Byauduro *et al*¹⁰⁴, who found that the AS-OCT instrument was feasible technique to applicable in children and useful to clarify the diagnosis, clinical and surgical follow-up of anterior segment disorders in children.

Although this prototype of SD-OCT technology has successfully captured high-quality cross-sectional corneal images, but it still does have limitations. One of the limitations of our SD-OCT

device was its inability to resolve the Descemet's membrane and endothelial cell layers as separate entities. This is most probably because of the fact that the refractive index of the Descemet's membrane or endothelium is very close to the stroma, thus the backscattered light from those layers is subtle enough to make them undetectable. Also the endothelium, 5 to 6 μm thick, approaches the image resolution of the prototype SD-OCT, which makes it difficult to differentiate as a separate entity. However, we were able to possibly detect the increase in the thickness of the Descemet's membrane-endothelial complex in all cases of Fuchs' endothelial dystrophy. Another limitation of our instrument was that, the dense hyperreflective corneal lesions result in shadowing of corneal layers posterior to it, and therefore may obscure a clear diagnosis of underlying pathologic features.

7 CONCLUSION

In conclusion, SD-OCT device serves as non contact and non invasive technology that provides rapid, high resolution, in vivo detailed cross-sectional images of the cornea. The anatomical layers of the cornea can be well delineated and SD-OCT scan revealed structural landmarks, allowing assignment of corneal structures with changes in the reflectivity. Thus the thickness of the epithelium, Bowman's membrane, stroma and central corneal thickness can be easily measured.

The CCT measurement with SD-OCT showed a very good correlation with both Scheimpflug camera and AC Master. Based on our presented data and statistical analysis, SD-OCT device appears to give a good agreement with AC Master in measurement of CCT, although it gives CCT readings slightly but significantly higher than the CCT values obtained with AC Master device. SD-OCT instrument seems to have a relatively poor agreement with Scheimpflug camera, as it gives CCT values significantly higher than those obtained with SD-OCT device.

The correlation between the central corneal thickness and thickness of different corneal layers with age, sex and right / left eye, showed no statistical significant correlation between the CCT or the different corneal layers thickness measured with SD-OCT or with the Scheimpflug or AC Master with age, gender or right / left eye.

We suggest that the SD-OCT device could be used as an alternative in the CCT and different corneal layers thickness measurement. Despite of their high correlation the SD-OCT, Scheimpflug camera and AC Master devices should not be used interchangeably in the clinical practice.

Being a non-contact instrument, SD-OCT examination can be performed in a short time without contact and discomfort to the patients with epithelial problems, perforated eye injury, postoperative patient and patients with infectious corneal diseases. In such cases the direct contact with the cornea cannot be made due to the extreme pain resulting from the contact and the high risk of contamination. In this study, we were able to measure exactly the different corneal lesions parameters as the thickness and width of these lesions which provides more objective assessment of the progression or the regression of the disease. In some cases, this was the diagnostic clue in choosing the therapeutic option to treat the patient and then monitoring the disease after treatment. Another advantage of SD-OCT is the possibility to evaluate the deeper

corneal layers that cannot be assessed by slit-lamp biomicroscopy. It was valuable in detecting the position and extent of the Desemet's membrane detachment, planning of the surgical procedure and postoperative follow up. In this study we were also able to highlight on the benefits of SD-OCT technology in the contact lens practice, as it opens a wide range of applications in the contact lens researches and clinical activity and will improve the customization of the contact lens especially in the distorted corneas. Despite of the low resolution of SD-OCT device when compared with confocal microscopy and its inability to provide the cellular level resolution, it was sufficiently sensitive to detect relatively small lesions in the different corneal layers. In summary, our SD-OCT is a completely non invasive imaging method that allowed high-resolution, descriptive morphological evaluation of the corneal structure and a wide range of corneal pathologies without requiring ocular anesthesia, water bath or direct contact with the eye. Our study strongly suggests that the SD-OCT technologies has a valuable role in the clinical evaluations, facilitation and enhancement of the diagnosis, making the therapeutic decisions, planning of the surgical procedures and postoperatively follow up of the patients with different corneal diseases and it can be also used in conjunction with other diagnostic tools.

8 THESES

- Spectral domain optical coherence tomography (SD-OCT) as a non invasive and non contact technique primates high resolution cross-sectional imaging of the cornea in vivo and allows distinguishing the layered structure of the cornea for anterior segment morphometry, objective quantification, localization and documentation of corneal pathologies.
- Central corneal thickness (CCT) and different corneal layers thickness of 100 eyes from 50 healthy volunteers were measured by spectral domain optical coherence tomography and only CCT measured with a rotating Scheimpflug camera and AC Master.
- Various corneal pathologies from 70 eyes were scanned by SD-OCT and all SD-OCT scans were compared with slit-lamp biomicroscopy.
- The mean epithelial-, Bowman's membrane-, Stromal- and central corneal thickness and standard deviation in μm measured by SD-OCT were 39.9 ± 6.0 , 11.7 ± 2.1 , 496.6 ± 34.8 and 545.6 ± 35.0 respectively.
- The comparison between the mean epithelial thickness values measured by SD-OCT revealed no significant statistical difference in the thickness of the epithelium in different age groups (P Value = 0.6), both sexes (P = 0.6) and both eyes (P = 0.7).
- It has been found no significant statistical difference in the Bowman's membrane thickness measured by SD-OCT in different age groups (P = 0.5), both sexes (P = 0.7) and both eyes (P = 0.5).
- It also showed that there is no significant statistical difference in the stromal thickness measured by SD-OCT in different age groups (P = 0.8), both sexes (P = 0.6) and both eyes (P = 0.7).
- It was not found a significant statistical difference in the central corneal thickness measured by SD-OCT in different age groups (P = 0.5), both sexes (P = 0.4) and both eyes (P = 0.9).
- The mean CCT and standard deviation in μm measured by SD-OCT, Scheimpflug camera and AC Master in 100 healthy eyes were 545.6 ± 34.9 , 553.7 ± 32.3 and 531.1 ± 33.7 respectively.

- Pairwise comparisons of the mean CCT measured by the SD-OCT, Scheimpflug camera and AC Master revealed that the mean CCT measurement obtained with SD-OCT was significantly thinner than the mean CCT obtained by Scheimpflug camera (P value < 0.001), while it was significantly thicker than the mean CCT obtained by AC Master (P-Value < 0.001).
- Significant linear correlation coefficient values were found in CCT measurement between SD-OCT and Scheimpflug camera (Pearson correlation $r = 0.938$, $P < 0.001$), SD-OCT and AC Master ($r = 0.958$, $P < 0.001$) and Scheimpflug camera and AC Master ($r = 0.943$, $P < 0.001$).
- Based on our presented data and statistical analysis, SD-OCT device appears to give a good agreement with AC Master in measurement of CCT with 95% limits of agreement (LOA) from -5.2 to 34.2 μm and magnitude of 95% LOA 39.4 μm and a relatively poor agreement with Scheimpflug camera with 95% LOA from -31.8 to 15.8 μm and magnitude of 95% LOA 47.6.
- The SD-OCT device could be used as an alternative in the CCT measurement. The SD-OCT, Scheimpflug camera and AC Master devices should not be used interchangeably in the clinical practice, despite of their high correlation
- In corneal pathologies SD-OCT scan provides the opportunity to analyse in vivo the morphologic properties of the cornea with high resolution similar to histologic images as in the patient with corneal degeneration unclear dignity.
- Also we were able to measure exactly the different corneal lesions parameters as the thickness and width of these lesions and the total corneal thickness which provide more objective assessment of the progression or the regression of the disease and gives the diagnostic clue in choosing the therapeutic option to treat the patient and then monitoring the disease after treatment such in cases with keratitis, corneal foreign body, granular corneal dystrophy and corneal foreign body.
- Being a non-contact instrument, SD-OCT examination can be performed in a short time without contact and discomfort to the patients with epithelial problems, perforated eye injury, postoperative patient and patients with infectious corneal diseases such in patients with perforated corneal ulcer, keratitis and recurrent epithelial erosions.

- Another advantage of SD-OCT is the possibility to evaluate the deeper corneal layers that cannot be assessed by slit-lamp biomicroscopy. It was valuable in detecting the position and extent of the Descemet's membrane detachment, planning of the surgical procedure and postoperative follow up. Also it provides valuable information in assessment of posterior wound profile in a patient who underwent a full thickness keratoplasty as well as measurement of the thickened Descemet's membrane-endothelial complex as shown in the patients with Fuchs' endothelial dystrophy.
- In this study we were also able to highlight on the benefits of SD-OCT technology in the contact lens practice, as it opens a wide range of applications in the contact lens researches and clinical activity and will improve the customization of the contact lens especially in the distorted corneas.
- Our study strongly suggests that the SD-OCT technologies has a valuable role in the clinical evaluations, facilitation and enhancement of the diagnosis, making the therapeutic decisions, planning of the surgical procedures and postoperatively follow up of the patients with different corneal diseases and it can be also used in conjunction with other diagnostic tools.

9 REFERENCES

1. Bechmann M, Thiel M and Neubauer et al. Central corneal thickness measurement with a retinal optical coherence tomography Device Versus Standard Ultrasonic Pachymetry. *Cornea* 2001; 20(1): 50-54.
2. Kaluzny B, Kaluzny J and Szkulmowska A et al. Spectral Optical Coherence Tomography: A Novel Technique for Cornea Imaging. *Cornea* 2006; 25(8): 960-965
3. Lincoff H, Kreissing I. Optical coherence tomography of pneumatic displacement of optic disc pit maculopathy. *Br. J. Ophthalmol.* 1998; 82:367–72.
4. Izatt JA, Hee MR and Swanson MS et al. Micrometer-scale resolution imaging of the anterior eye in vivo with optical coherence tomography. *Arch. Ophthalmol.* 1994; 112:1584–9.
5. Hoerauf H, Wirbelauer C and Scholz C et al. Slit-lamp-adapted optical coherence tomography of the anterior segment. *Graefes Arch. Clin. Exp. Ophthalmol.* 2000; 238:8–18.
6. Li H, Leung CK and Wong L et al. Comparative study of central corneal thickness measurement with slit-lamp optical coherence tomography and Visante optical coherence tomography. *Ophthalmology* 2008;115:796-801.
7. Wojtkowski M, Bajraszewski T and Gorczynska I et al. Ophthalmic imaging by spectral optical coherence tomography. *Am. J. Ophthalmol.* 2004;138:412-419
8. Stephen D, Klyce and Roger w. Beuerman. Structure and function of the cornea. Herbert E. Kaufman, Bruce A. Barron. *The Cornea* 2nd edition Maryurite B. McDonald, 1997 USA. Page 3-72.
9. Farjo A, McDermott M and Soong H. Corneal anatomy, physiology and wound healing Duker Js (Eds) *ophthalmology*. 3rd edition Mosby. 2009. Page 203-208.
10. Beuerman R W, Pedroza: Ultrastructure of human cornea, *Microscopy Research and technique*.1996;33:320-335.
11. Estill S, Primo EJ and Wilson G. Apoptosis in shed human Corneal cells. *Invest Ophthalmol Vis Sci* 2000;41:3360-3364.
12. Pfister RR: The normal structure of corneal epithelium: a Scanning electron microscopic study. *Invest Ophthalmol* 1973;12:654-668.

13. Hanna C, Bicknell DS and O'Brien J. Cell turnover in adult human eye. *Arch Ophthalmology* 1961;65: 695-8.
14. Suzuki K, Tanaka T and Enoki M et al. Coordinated reassembly of the basement membrane and junctional proteins. *Invest Ophthalmol Vis Sci* 2000;41:2495-2500.
15. Madri JA, Pratt BM and Yurchenco PD et al. The ultrastructural organization and architecture of basement membrane. P.6. in Porter R, Whelan J(eds): *Basement Membrane and Cell Movement*. CIBA Foundation Symposium. Vol 108. Pitman Press, London, 1984.
16. Tervo K, Tervo T and Van Setten G-B et al. Integrins in human corneal epithelium. *Cornea* 1991;10:461-5.
17. Smolek M K, Klyce S D. *Cornea*. Duaen's foundations of clinical ophthalmology. ed. Tasman W and Jaeger EA 5th ed USA :Williams and Wilkins 2001; 1-19.
18. Boote C, Dennis S and Newton, et al. Collagen fibrils appear more closely packed in the prepupillary cornea: optical and biochemical implications. *Invest Ophthalmol Vis Sci*. 2003;44:2941-2948.
19. Meek KM, Boote C. The organization of collagen in the corneal stroma. *Exp Eye Res* 2004;78:503-12.
20. Maurice DM. The cornea and sclera. P 1. in Davidson H (ed): *The Eye*. Vol. 1B. *Vegetative Physiology and Biochemistry*. 3rd Ed. Academic Press, Orlando, FL, 1984.
21. Yue BYJT, Sugar J and Schrode K: Collagen staining in corneal tissue. *Curr Eye Res* 1986;5:559-564.
22. Muller LJ, Pels E and Vrensen GFJM. The specific architecture of the anterior stroma accounts for maintenance of corneal curvature. *Br J Ophthalmology* 2001;85:437-43.
23. Borcharding MS, Blacik LJ and Sitig RA et al: Proteoglycans and collagen fiber organization in human corneoscleral tissue. *Exp, Eye Res* 1975;21:59-70.
24. Johnson DH, Bourne WM and Campbell RJ: The ultrastructure of Descemet's membrane. I. Change with age in normal corneas, *Arch Ophthalmol* 1982;100:1942-1947.
25. Bourne WM, Johnson DH and Campbell RJ: The ultrastructure of Descemet's membrane. III. Fuchs dystrophy. *Arch Ophthalmol* 1982;100:1952-1955.

26. Watsky MA, McCarney MD and McLaughlin et al. Corneal endothelial junctions and the effect of ouabain. *Invest Ophthalmol Vis Sci* 1990;31:933-941.
27. Laing RA, Sandstrom MA, Liebowitz HM. In vivo photomicrography of corneal endothelium. *Arch Ophthalmol* 1975;93:143-5.
28. McCartney MD, Robertson DP and Wood TO et al. ATPase pump site density in human dysfunctional corneal endothelium. *Invest Ophthalmol Vis Sci* 1987;28:1955-62.
29. Prakasam R, Schwiede M, and Hütz W et al. Corneal responses to eye rubbing with Spectral Domain Optical Coherence Tomography. *Curr Eye Res* 2012 Jan;37(1):25-32.
30. Buehl W, Stojanac D and Sacu S et al. Comparison of Three Methods of Measuring Corneal Thickness and Anterior Chamber Depth. *Am J Ophthalmol* 2006;141:7–12.
31. W.Drexler, Findl O and Menapace R et al. Partial coherence interferometry: a novel approach to biometry in cataract surgery. *Am J Ophthalmol* 126 (1998), 524-534.
32. Bland M and Altman D G. Statistical methods for assessing agreement between two methods of clinical measurement. *Lancet*; 1986: 307-310.
33. Wirbelauer C, Winkler J and Bastian GO et al. Histopathological correlation of corneal diseases with optical coherence tomography. *Graefes Arch Clin Exp Ophthalmol*. 2002;240(9):727-734.
34. Kaluzny BJ, Kaluzny JJ and Szkulmowska A et al. Spectral optical coherence tomography: a new imaging technique in contact lens practice. *Ophthalmic Physiol Opt*. 2006;26(2):127-132.
35. Waring GO, Bourne WM and Edelhauser HF et al. The corneal endothelium. Normal and pathologic structure and function. *Ophthalmology*.1982;89:531-590.
36. Copt RP, Thomas R and Mermoud A. Central corneal thickness in ocular hypertension, primary open-angle glaucoma, and normal tension glaucoma. *Arch Ophthalmol*. 1999;117:14–16.
37. Gordon MO, Beiser JA and Brandt JD et al. The Ocular Hypertension Treatment Study: baseline factors that predict the onset of primary openangle glaucoma. *Arch Ophthalmol*. 2002;120:714–720.

38. Brandt JD, Beiser JA and Gordon MO et al. Central corneal thickness and measured IOP response to topical ocular hypotensive medication in the ocular hypertension treatment study. *Am J Ophthalmol.* 2004;138:717–722.
39. Leem HS, Lee KJ and Shin KC. Central corneal thickness and corneal endothelial cell changes caused by contact lens use in diabetic patients. *Yonsei Med J* 2011;52:322-5.
40. Ashwin PT and McDonnell PJ. Collagen cross-linkage: a comprehensive review and directions for future research. *Br J Ophthalmol* 2010;94:965-70.
41. Zhao PS, Wong TY and Wong WL et al. Comparison of central corneal thickness measurements by Visante anterior segment optical coherence tomography with ultrasound pachymetry. *Am J Ophthalmol.* 2007;143:1047–1049.
42. López-Miguel A, Nieto JC and Díez-Cuenca M et al. Agreement of non-contact pachymetry after LASIK: comparison of combined scanning-slit/Placido disc topography and specular microscopy. *Eye (Lond).* 2010 Jun;24(6):1064-70.
43. Ponce CMP, Rocha KM and Smith SD et al. Central and peripheral corneal thickness measured with optical coherence tomography, Scheimpflug imaging, and ultrasound pachymetry in normal, keratoconus-suspect, and post-laser in situ keratomileusis eyes. *J Cataract Refract Surg.* 2009;35: 1055–1062.
44. Hong JP, Nam SM, and Kim TI et al. Reliability of RTVue, Visante, and slit-lamp adapted ultrasonic pachymetry for central corneal thickness measurement. *Yonsei Med J.* 2012 May;53(3):634-41.
45. Li EY, Mohamed S and Leung CK et al. Agreement among 3 methods to measure corneal thickness: ultrasound pachymetry, Orbscan and Visante anterior segment optical coherence tomography. *Ophthalmology.* 2007; 114:1842–1847.
46. Li H, Leung CK and Wong L et al. Comparative study of central corneal thickness measurement with slit-lamp optical coherence tomography and Visante optical coherence tomography. *Ophthalmology.* 2008;115: 796–801.
47. Prakash G, Agrwal A and Jacob S et al. Comparison of Fourier-domain and time-domain optical coherence tomography for assessment of corneal thickness and intersession repeatability. *Am J Ophthalmol.* 2009;148: 282–290.

48. Ishibazawa A, Igarashi S and Hanada K et al. Central Corneal Thickness Measurements With Fourier-Domain Optical Coherence Tomography Versus Ultrasonic Pachymetry and Rotating Scheimpflug Camera *Cornea* 2011;30:615–619.
49. Li Y, Tan O and Weiss JL et al. Corneal Epithelial Thickness Mapping by Fourier-Domain Optical Coherence Tomography in Normal and Keratoconic Eyes. *Ophthalmology*. 2012 Aug 20.
50. Germundsson J, Fagerholm P and Koulikovska M et al. An accurate method to determine Bowman's layer thickness in vivo in the human cornea. *invest Ophthalmol Vis Sci*. 2012 Apr 30;53(4):2354-9.
51. Tao A, Wang J and Chen Q et al. Topographic thickness of Bowman's layer determined by ultra-high resolution spectral domain-optical coherence tomography. *Invest Ophthalmol Vis Sci*. 2011 Jun 1;52(6):3901-7.
52. Ou TH, Lai IC and Teng MC. Comparison of central corneal thickness measurements by ultrasonic pachymetry, Orbscan II, and SP3000P in eyes with glaucoma or glaucoma suspect. *Chang Gung Med J*. 2012 May-Jun;35(3):255-62.
53. Park SH, Choi SK and Lee D. Corneal thickness measurement using orbscan, pentacam, galilei, and ultrasound in normal and post-femtosecond laser in situ keratomileusis eyes. *Cornea*. 2012 Sep;31(9):978-82.
54. Al-Mezaine HS, Al-Amro SA and Kangave D. Comparison of central corneal thickness measurements using Pentacam and ultrasonic pachymetry in post-LASIK eyes for myopia. *Eur J Ophthalmol*. 2010;20(5):852-7.
55. Hashemi H and Mehravaran S. Central corneal thickness measurement with Pentacam, Orbscan II, and ultrasound devices before and after laser refractive surgery for myopia. *J Cataract Refract Surg*. 2007;33(10):1701-7.
56. AC-M Wong, C-C Wong and NS-Y Yuen et al. Correlational study of central corneal thickness measurements on Hong Kong Chinese using optical coherence tomography, Orbscan and ultrasound pachymetry. *Eye* (2002); 16: 715–721.
57. Muscat S, McKay N and Parks S et al. Repeatability and Reproducibility of Corneal Thickness Measurements by Optical Coherence Tomography. *Invest Ophthalmol and Vis Sci* 2002; 43:1791-1795.

58. Li EY, Mohamed S and Leung CK. Agreement among 3 methods to measure corneal thickness: ultrasound pachymetry, Orbscan II, and Visante anterior segment optical coherence tomography. *Ophthalmology*. 2007;114(10):1842-7.
59. Gorgun E, Yenerel NM and Dinc UA et al. Comparison of non-contact methods for the measurement of central corneal thickness. *Ophthalmic Surg Lasers Imaging*. 2011 ;42(5):400-7.
60. Ponce CMP, Rocha KM and Smith SD et al. Central and peripheral corneal thickness measured with optical coherence tomography, Scheimpflug imaging, and ultrasound pachymetry in normal, keratoconus-suspect, and post-laser in situ keratomileusis eyes. *J Cataract Refract Surg*. 2009;35: 1055–1062.
61. O'Donnell C, Hartwig A and Radhakrishnan H. Comparison of Central Corneal Thickness and Anterior Chamber Depth Measured Using LenStar LS900, Pentacam, and Visante AS-OCT. *Cornea*. 2012;31(9):983-8.
62. Amano S, Honda N and Amano Y et al. Comparison of central corneal thickness measurements by rotating Scheimpflug camera, ultrasonic pachymetry, and scanning-slit corneal topography. *Ophthalmology*. 2006; 113:937–941.
63. O'Donnell C, MCOptom F and Maldonado-Codina C et al. Agreement and Repeatability of Central Thickness Measurement in Normal Corneas Using Ultrasound Pachymetry and the OCULUS Pentacam. *Cornea* 2005; 24(8): 920-924.
64. Buehl W, Stojanac D and Sacu S et al. Comparison of three methods of measuring corneal thickness and anterior chamber depth. *Am J of Ophthalmol* 2006 (141) 7-12.
65. Chen S, Huang J and Wen D et al. Measurement of central corneal thickness by high-resolution Scheimpflug imaging, Fourier-domain optical coherence tomography and ultrasound pachymetry. *Acta Ophthalmol*. 2012;(5):449-55.
66. Doughty MJ and Zaman ML. Human corneal thickness and its impact on intraocular pressure measures: a review and metaanalysis approach. *Surv Ophthalmol* 2000;44:367–408.
67. Faragher A, Mulhlland B and Tuft S et al. Aging and the cornea. *Br J Ophthalmol* 1997;81:814-7.

68. Niederer R L, Perumal D and Sherwin et al. Age-related differences in the normal human cornea: a laser scanning in vivo confocal microscopy study. *Br J Ophthalmol* 2007;1165-1169.
69. Chatterjee A, Shah SS and Doyle SJ. Effect of age on the final refractive outcome for 2342 patients following photorefractive keratectomy. *Inves Ophthalmol Vis Sci* 1996;37:S57.
70. Alsbirk P H. Corneal thickness: Age Variation, Sex Difference and Oculometric Correlations. *Acta Ophthalmol* 1978;56:95-104.
71. Nissen J, Hjortdal J and , Ehlers N et al. A clinical comparison of optical and ultrasonic pachometry. *Acta Ophthalmologica* 1991;69:659-663.
72. Lam, A K and Douthwaite, W A. The Corneal-Thickness Profile in Hong Kong Chinese. *cornea* 1998;17:384-388.
73. Cavanagh HD, El-Agha MS and Petroll WM et al. Specular microscopy, confocal microscopy, and ultrasound biomicroscopy: diagnostic tools of the past century. *Cornea* 2000;19:712–722.
74. Hurmeric V, Yoo SH, and Karp CL et al. In vivo morphologic characteristics of Salzmann nodular degeneration with ultra-high-resolution optical coherence tomography. *Am J Ophthalmol*. 2011 Feb;151(2):248-56.
75. Werner Leonardo P, Issid K and Werner Liliana P et al. Salzmann’s corneal degeneration associated with epithelial basement membrane dystrophy. *Cornea* 2000;19(1):121–123.
76. Das S, Link B and Seitz B. Salzmann’s nodular degeneration of the cornea: a review and case series. *Cornea* 2005;24(7):772–777.
77. Khokhar S, Natung T and Sony P et al. Amniotic membrane transplantation in refractory neurotrophic corneal ulcers: a randomized, controlled clinical trial. *Cornea* 2005;24(6):654–660.
78. Prabhasawat P, Tesavibul N and Komolsuradej W. Single and multilayer amniotic membrane transplantation for persistent corneal epithelial defect with and without stromal thinning and perforation. *Br J Ophthalmol* 2001;85(12): 1455–1463.
79. McGwin G and Owsley C. Incidence of emergency department-treated eye in the United States. *Arch Ophthalmol*. 2005;123:662–6.

80. Barash D, Goldenberg-Cohen N and Weinberger D et al. Ultrasound biomicroscopic detection of anterior ocular segment foreign body after trauma. *Am J Ophthalmol.* 1998;126:197–202.
81. Wylegala E, Dobrowolski D and Tarnawska D et al. Anterior segment optical coherence tomography in eye injuries. *Graefes Arch Clin Exp Ophthalmol.* 2009;247:451–5
82. Meyer H M and Sekund W. Evaluation of granular corneal dystrophy with optical coherent tomography. *Cornea* 2004;23:270–271.
83. Mannis MJ, De Sousa LB and Gross RH. The stromal dystrophies. In: Krachemer JH, Mannis MJ, Holland EJ, eds. *Cornea and External Disease: Clinical Diagnosis and Management.* St. Louis: Mosby; 1997:1043–1051.
84. Ramos J. S, Li. Y and Huang D. Clinical and research applications of anterior segment optical coherence tomography – a review. *Clinical and Experimental Ophthalmology* 2009; 37: 81–89.
85. Swartz T, Marten L and Wang M. Measuring the cornea: the latest developments in corneal topography. *Curr Opin Ophthalmol.* 2007;18:325–333.
86. Doors M, Tahzib N G and Eggink F A et al. Use of anterior segment optical coherence tomography to study corneal changes after collagen cross-linking. *Am J Ophthalmol* 2009;148:844-851.
87. Zhou S.Y, Wang C.X and Cai X. Y et al. Anterior Segment OCT-Based Diagnosis and Management of Descemet’s Membrane Detachment. *Ophthalmologica* 2012;227:215–222.
88. Kothari S, Kothari K and Parikh RS. Role of anterior segment optical coherence tomogram in Descemet's membrane detachment. *Indian J Ophthalmol* 2011;59:303-5.
89. Jeng BH and Meisler DM. A combined technique for surgical repair of Descemet’s membrane detachments. *Ophthal Surg Lasers Imaging* 2006; 37: 291–297.
90. Rodrigues MM, Krachmer JH and Hackett et al. Fuch’s corneal dystrophy: a clinicopathologic of variation in corneal edema. *Ophthalmology* 1986;93:789-96.
91. Chiou A G, Kaufman SC and Beuerman et al. Confocal microscopy in cornea guttata and fuch’s endothelial dystrophy. *Br J Ophthalmol* 1999;83:185-9.

92. Adamis AP, Filatov V and Tripathi BJ et al. Fuch's endothelial dystrophy of the cornea. *Surv Ophthalmol* 1993;38:149-68.
93. Abuo Shousha M, Perez VL and Wang J et al. Use of ultra-high-resolution optical coherence tomography to detect in vivo characteristics of descemet's membrane in fuchs' dystrophy. *Ophthalmology* 2010;117:1220-1227.
94. Kaiserman I, Bahar I and Rootman DS. Corneal wound malapposition after penetrating keratoplasty: an optical coherence tomography study. *Br J Ophthalmol*. 2008 Aug;92(8):1103-7.
95. Jhanji V, Constantinou M and Vajpayee RB et al. Evaluation of posterior wound profile after penetrating keratoplasty using anterior segment optical coherence tomography. *Cornea*. 2011;30(3):277-80.
96. Christopoulos V, Kagemann L and Wollstein G et al. In Vivo Corneal High-Speed, Ultra-High-Resolution Optical Coherence Tomography. *Arch Ophthalmol*. 2007;125(8):1027-1035.
97. Fink BA, Barr JT and Edrington TB et al. A comparison of two methods of evaluating cornea-to-contact lens base curve fluorescein patterns in keratoconus. *Optom Vis Sci*. 2001;78:589-598.
98. Mountford J, Cho P and Chui W. Is fluorescein pattern analysis a valid method of assessing the accuracy of reverse geometry lenses for orthokeratology. *Clin Exp Optom* (2005);88; 33-38.
99. Reinstein Z, Silverman H. and Rondeau M et al. Epithelial and corneal thickness measurements by high-frequency ultrasound digital signal processing. *Ophthalmology* (1994);101;140-146.
100. Holladay T, Belin M and Chayet A S et al. Next-generation technology for the cataract and refractive surgery. *Suppl Cataract Refract. Surg. Today* (2005);1; 1-11.
101. Gonzalez-Meijome M, Cervinõ A and Carracedo G et al. High-Resolution Spectral Domain Optical Coherence Tomography Technology for the Visualization of Contact Lens to Cornea Relationships. *Cornea* 2010;29:1359-1367.
102. Martin R, de Juan, V and Rodriguez G et al. Measurement of corneal swelling variations without removal of the contact lens during extended wear. *Invest Ophthalmol Vis Sci*. 2007;48:3043-3050.

103. Kieval J, Karp C and Abou Shousha M et al. Ultra-high Resolution optical coherence tomography for differentiation of ocular surface squamous neoplasia and pterygia. *Ophthalmology* 2012;119:481-486.
104. Cauduro R S, Ferraz C and Morales M. Application of anterior segment optical coherence tomography in pediatric ophthalmology. *J Ophthalmology*. 2012;2012:313120.

10 CAPTIONS FOR FIGURES AND TABLES

10.1 FIGURE

Fig. 1: Light micrograph of human cornea 9

Fig. 2: Light micrograph of corneal epithelium..... 9

Fig. 3: Schematic graph of the tight junction of corneal epithelium 10

Fig. 4: Electric microscopic graph of Bowman’s membrane 11

Fig. 5: Electric microscopic graph of Bowman’s membrane 12

Fig. 6: Light micrograph of corneal stroma 13

Fig. 7: Electron micrograph of corneal stroma 13

Fig. 8: Electron micrograph of Descemet’s membrane 14

Fig. 9: Electron micrograph of corneal endothelium 15

Fig. 10: SD-OCT image and thickness analysis of healthy cornea by MATLAB program 18

Fig. 11: Photograph of Scheimpflug camera device 19

Fig. 12: Photograph of AC Master device 20

Fig. 13: Analysis of SD-OCT image of healthy cornea 23

Fig. 14: Boxplot diagram demonstrating the ET-OCT distribution in different age groups 24

Fig. 15: Boxplot diagram demonstrating the ET-OCT distribution in both sexes 25

Fig. 16: Boxplot diagram demonstrating the ET-OCT distribution in both eyes 25

Fig. 17: Boxplot diagram demonstrating the BMT-OCT distribution in different age groups ... 26

Fig. 18: Boxplot diagram demonstrating the BMT-OCT distribution in both sexes 27

Fig. 19: Boxplot diagram demonstrating the BMT-OCT distribution in both eyes 27

Fig. 20: Boxplot diagram demonstrating the ST-OCT distribution in different age groups..... 28

Fig. 21: Boxplot diagram demonstrating the BMT-OCT distribution in both sexes 29

Fig. 22: Boxplot diagram demonstrating the BMT-OCT distribution in both eyes 29

Fig. 23: Boxplot diagram demonstrating the CCT distribution among the 3 device 30

Fig. 24: Graph shows linear correlation between the 3 devices 31

Fig. 25: Graph showed Bland-Altman plot between CCT-OCT and CCT-SCH 32

Fig. 26: Graph showed Bland-Altman plot between CCT-OCT and CCT-ACM 33

Fig. 27: Graph showed Bland-Altman plot between CCT-SCH and CCT-ACM 33

Fig. 28: Boxplot diagram demonstrating the CCT distribution in both sexes by 3 devices 34

Fig. 29: Boxplot diagram demonstrating the CCT distribution in both eyes by 3 devices..... 35

Fig. 30: Boxplot diagram demonstrating the CCT-OCT distribution in different age groups .. 36

Fig. 31: Boxplot diagram demonstrating the CCT-SCH distribution in different age groups .. 36

Fig. 32: Boxplot diagram demonstrating the CCT-ACM distribution in different age groups . 37

Fig. 33: Photograph, SD-OCT imag and IVCM of corneal degeneration 39

Fig. 34: Photograph and SD-OCT imag of cornea with perforated corneal ulcer 41

Fig. 35: Photograph and SD-OCT imag of cornea with recurrent epithelial erosions 42

Fig. 36: Photograph and SD-OCT imag of cornea with acute angle closure glaucoma 43

Fig. 37: Photograph and SD-OCT imag of cornea with dry eye syndrome..... 44

Fig. 38: Photograph and SD-OCT imag of cornea with soft contact lens 45

Fig. 39: Photograph and SD-OCT imag of cornea with hard contact lens 46

Fig. 40: Photograph and SD-OCT imag of cornea with keratitis associated with contact lens . 47

Fig. 41: Photograph, SD-OCT imag and IVCM of cornea with fungal keratitis 48

Fig. 42: Photograph and SD-OCT imag of cornea with stromal keratitis..... 49

Fig. 43: Photograph and SD-OCT imag of corneal foreign body 50

Fig. 44: Photograph and SD-OCT imag of corneal scar 51

Fig. 45: Photograph, SD-OCT imag and IVCM of cornea granular corneal dystrophy 52

Fig. 46: Photograph and SD-OCT imag of cornea with keratoconus 53

Fig. 47: Photograph, SD-OCT imag and ICVM of Endothelitis 54

Fig. 48: Photograph, SD-OCT imag of Descemet’s membrane detachment..... 55

Fig. 49: Photograph and SD-OCT imag of Fuch’s endothelial dystrophy 56

Fig. 50: Photograph and SD-OCT imag of corneal wound after full thickness PK.....57

Fig. 51: Photograph and SD-OCT imag of bullous keratopathy..... 58

10.2 TABLE

| | | |
|-----------|--|----|
| Table 1: | Values of corneal parameters measured by the 3 instruments | 21 |
| Table 2: | Different corneal layers thickness measured by SD-OCT device | 23 |
| Table 3: | ET-OCT values in different age groups | 24 |
| Table 4: | ET-OCT values in both sexes and both eyes | 25 |
| Table 5: | BMT-OCT values in different age groups..... | 26 |
| Table 6: | BMT-OCT values in both sexes and both eyes | 27 |
| Table 7: | ST-OCT values in different age groups | 28 |
| Table 8: | ST-OCT values in both sexes and both eyes | 29 |
| Table 9: | Values of CCT measured by the 3 instruments | 30 |
| Table 10: | Results of agreement between the 3 instruments | 32 |
| Table 11: | Values of CCT in both sexes measured by the 3 instruments | 33 |
| Table 12: | Values of CCT in both eyes measured by the 3 instruments | 34 |
| Table 13: | CCT values in different age groups measured by the 3 instruments | 35 |
| Table14: | Values of different corneal layers thickness reported by previous studies..... | 61 |

10.3 LIST OF ABBREVIATIONS

| | |
|--|---------|
| Anterior chamber depth | ACD |
| Anterior segment optical coherence tomography | AS-OCT |
| Bowman's membrane | BM |
| Bowman's membrane thickness | BMT |
| Bowman's membrane thickness measured by optical coherence tomography | BMT-OCT |
| Central corneal thickness | CCT |
| Central corneal thickness measured by AC Master | CCT-ACM |
| Central corneal thickness measured by optical coherence tomography | CCT-OCT |
| Central corneal thickness measured by Scheimpflug camera..... | CCT-SCH |
| Coefficient of agreement | COA |
| Diopter | D |
| Deep anterior lamellar keratoplasty | DALK |
| Deep lamellar endothelial keratoplasty | DLEK |
| Descemet's membrane..... | DM |
| Descemet's membrane detachment | DMD |
| Descemet's stripping endothelial keratoplasty | DSEK |
| Endothelium | ENDO |
| Epithelium | EPI |
| Epithelial thickness | ET |
| Epithelial thickness measured by optical coherence tomography | ET-OCT |
| Fourier-Domain Optical Coherence Tomography | FD-OCT |
| Granular corneal dystrophy | GCD |
| Intraocular pressure | IOP |
| In vivo confocal microscopy | IVCM |
| Limits of agreement | LOA |
| Lens thickness | LT |
| Mean difference between 2 instruments..... | a |
| Optical coherence tomography | OCT |
| Penetrating keratoplasty | PK |
| Phototherapeutic keratoplasty | PKP |

| | |
|---|--------|
| Pearson correlation coefficient | r |
| Standard deviation of the mean difference between 2 instruments | s |
| Standard deviation | SD |
| Spectral domain optical coherence tomography | SD-OCT |
| Statistical Package for Social Sciences | SPSS |
| Time domain optical coherence tomography | TD-OCT |
| Ultrasound biomicroscopy | UBM |
| Ultrasonic pachymetry | USP |

11 CURRICULUM VITAE

Name: Riyam Alkadhi

Birthday: 26.5.1978

Place of birth: Aden, Jemen

Marital status: Married

Education:

- 2004-2008 Master's degree in Ophthalmology, medical faculty, Cairo University, Egypt
- 2003-2004 Practice year, medical faculty, Aden University, Yemen
- 1996-2002 Bachelor's Degree, medical faculty, Cairo University, Egypt
- 1993-1996 High School, Sana'a, Yemen
- 1990-1993 Preparatory School, Sana'a, Yemen
- 1984-1990 Elementary School, Aden, Yemen

Experience

- Resident in the department of ophthalmology at Rostock University in the period from 1.07.2010 -30.06.2012, Rostock, Germany.
- Demonstrator in the department of ophthalmology at Aden University, in the period 01.06.2008-30.09.2009, Aden, Yemen.
- Resident in the ophthalmology department, Kasr El Aini teaching and research hospital at Cairo University, in the period from 1.11.2004 - 30.04.2007, Cairo, Egypt.

12 DECLARATION

I hereby declare on my honor that I have this work at the Medical Faculty of the University of Rostock to doctoral work submitted under the supervision of Prof. Dr. R. F Guthoff independently conducted and not used other than those indicated in the dissertation tools and resources.

I did not submit this study to any domestic or foreign medical faculty as an application for admission to doctoral studies or presented this work as a doctoral thesis.

Rostock, in February 2013

Riyam Alkadhi

13 ACKNOWLEDGMENTS

First and foremost, I would like to offer my sincerest gratitude to my supervisor Prof. Dr. Rudolf F. Guthoff who supported me with great knowledge and continuous valuable supervision and also provided me with direction and technical advices throughout my PhD study.

My special thanks go to Prof. Dr. Oliver Stachs for the great efforts, enthusiasm and valuable comments in explaining things clearly and simply during the project analysis.

I would like to express my gratitude to my supervisor, Dr. Steffi Knappe whose expertise understanding and guidance added a great extent to my experience in this project.

Eventually I would also like to show my genuine appreciation and special gratitude to Dr. Iman Ali Ba-Saddik who took effort in proofreading my thesis and providing me with instructive interaction and valuable feedback.

I would like also to thank Mrs. R. Prakasam for the technical implementation of software MATLAB program and Prof. Dr. G . Kundt and Mrs. H. Krentz for the advice in the statistics.

Special gratitude is given to the staff of the department of ophthalmology at Rostock university, Germany who offered invaluable help and guidance in my work.

I owe thanks and gratitude to my dear parents, husband and sister for their endless love.

Lastly, I offer my regards and blessings to all of those who supported me in any respect and providing a stimulating and fun environment during the completion of the project.